◼ NTNU
Norwegian University of
Science and Technology

Analysis of Transportation and Installation of a Component of an Artificial Sea Bed

Camilla Kjelsaas

Analysis of Transportation and Installation of a Component of an Artificial Seabed

Camilla Kjelsaas

June 2016

MASTER THESIS

Department of Marine Technology

Norwegian University of Science and Technology

Supervisor 1: Professor Bernt J. Leira, IMT, NTNU

Supervisor 2: Martin Hasle, Deep Ocean

NTNU
Department of Marine Technology

MASTER THESIS IN MARINE STRUCTURES
SPRING 2016
for
Stud. Techn. Camilla Kjelsaas

Analysis of transportation and installation of mooring system components for a
Marine Bridge Concept

Analyse av transport og installasjon av forankringssystem for en marin bro-konstruksjon.

Marine bridges (i.e. floating bridges and submerged tunnels) are relevant for crossing of very deep and wide lakes or fjord systems. In order to compute the static and dynamic response of these bridges, the joint properties of the whole hydro-elastic system need to be accounted for. This applies both to the transportation, installation and operation phases.

The objective of the present project is to outline methods for response analysis and illustrate the calculation procedure for a particular bridge concept with focus on the transportation and installation phase of one of the components. The bridge consists of three main components: The mooring system (which is referred to as an artificial seabed), the floating bridge and the submerged tunnel. The concept is based on a tether system for the main part of the mooring, where a bundle of three pipes is pretensioned to around 40% of the yield stress. The mooring system components that are to be studied are the longitudinal bundles.

The following subjects are to be addressed as part of this work:

1. A review is to be made of existing marine bridges and future plans for such bridges. Similarities and differences between the different bridges are to be highlighted. Subsequently, the particular bridge concept to be focused upon is described in more detail.

2. The loads which are acting on the bundles during transportation and installation are to be described and associated structural models are discussed. For the transportation phase it is focused on submerged towing of the bundles, and this method is to be studied. Corresponding methods for both static and dynamic response analysis are elaborated and relevant numerical algorithms as implemented in relevant computer programs are described.

3. The bundle of three pipes and specific installation vessels are selected for the purpose of illustrating the modelling aspects and the calculation procedures. The details regarding the example structure is to be made based on discussion with the supervisor and the company Deep Ocean Group.

4. Parameter studies are performed (to the extent that time allows) with respect to variation of the towing and installation procedures as well as the environmental conditions (e.g. waves and current). It is relevant that the type and extent of such parameter variations are agreed upon with the supervisor during the course of the project study.
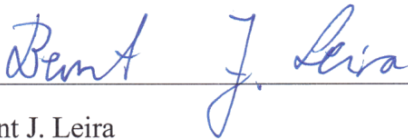
Start Date: 15.01.2016   **Due date:** 10.06.2016

Supervisor: Professor Bernt J. Leira

Contact person at Deep Ocean Group: Martin Hasle

Trondheim, 14.01.2016

Bernt J. Leira

Preface

This Master's Thesis is written at the Department of Marine Technology at NTNU in Trondheim, as the concluding work for the degree in Naval Architecture (MSc) with specialization in Marine Structures. The study and report was completed during the spring semester of 2016. The task for this study was provided by Martin Hasle from Deep Ocean Group, as a part of a project owned and developed by Reinertsen. The cooperation with the companies Deep Ocean Group and Reinertsen has given me valuable guidance in approaching the problems, as well as good understanding of the impact and complexity of the project. The report is written for readers with understanding and knowledge in Marine Technology and structures.

Trondheim, 2016-06-10

Camilla Kjelsaas

_____

Camilla Kjelsaas

Acknowledgment

I would like to thank my supervisor Bernt J. Leira for his guidance in my writing, as well as his important perspectives and deep knowledge on the relevant subject. His patience and guidance in making me understand the results has been of great help. I would also like to thank Martin Hasle from Deep Ocean Group, who has provided me with an exciting and challenging task for my Master's Thesis. He has also given me valuable viewpoints and guidance in approaching the problems of this Thesis, which I am very grateful for. Additionally I would like to thank Marit Reiso at Reinertsen for her enthusiasm regarding the Artificial Seabed Project. Her initiative for shared knowledge on this complex project have given me motivation to continue my work and understanding of the impact of the project. Finally, I would like to thank Xiaopeng Wu for his help and assistance with Sima Riflex.

C.K.

Summary and Conclusions

The purpose of this Master's Thesis was to study the transportation and installation of a bundle component to be used in an Artificial Seabed. The bundle, which is composed of three pipes and close to 4 km in length, is to be transported through the Sognefjord and installed as a connection between Lavik and Oppedal. The towing method that is to be used is the Controlled Depth Tow Method (CDTM). The CDTM involves towing an object in an immersed condition, which will avoid critical parts such as lift-off of deck and lowering of objects through the splash zone. The analyses in this study is divided into two parts, one for transportation and one for installation.The transportation over the North Sea is not included in this study, as it is a well known procedure used in the offshore industry. However, towing of long slender structures through a fjord has not been conducted before. The bundle length exceeds the width of the fjord, which makes the installation procedure challenging.

The computer program Sima Riflex is used for analyzing slender marine structures, and is utilized in this study. The finite element method is used for solving the structural analyses in Sima Riflex. For the dynamic analysis, the response of the system is found when it is exposed to a predefined sea state. Sima Riflex has different approaches for solving nonlinear systems, including nonlinear time domain analysis, linearized time domain analysis and frequency domain analysis. Finally an eigenvalue analysis is conducted for the different models as well, in order to show how the structure will behave when exposed to dynamic loading.

The bundle geometry is simplified to a circular pipe with properties corresponding to the original shape for the modeling in Sima Riflex. Both the towing and the installation models consist of the bundle with one towing wire and towing tug connected at each end point. Additional towing tugs have been applied as horizontal forces. The environmental conditions that are used are based upon studies of the Sognefjord conducted by SINTEF.

The transportation process is divided into three scenarios with different sea states, as to cover the towing through the different parts of the fjord. In order to maneuver the bundle through the turns of the fjord, it might be necessary to bend it. Therefore, two of the scenarios include a parameter study of the degree of bending of the bundle.

The installation process is also divided into three scenarios, where each represents a possible

installation approach. The first scenario conduct the installation by only curving the bundle using the horizontal plane. The second scenario do the same by only using the vertical plane for installation, thus lowering the bundle into the depth of the fjord. The final scenario utilizes a combination of both planes for the installation.

The active modes of the bundle during transportation in Sognefjord have eigenperiods of 2.8 s, which are inside the energetic wave period band. All wave motion is extinguished for the given towing depth, indicating that the responses are not caused by direct wave loads, but due to the motion of the tugs. The low periods indicate that the effect of fatigue damage should be studied closer for the towing operation. For towing through more severe sea states, direct wave loads are not avoided. This will increase the dynamic moments and displacements significantly. Furthermore it is found that the bundle can be curved during transportation, but within certain limits.

For the installation, the scenario that exploits both the horizontal and the vertical space will be the most suitable with respect to magnitude of responses in the bundle and feasibility of operation. Parameter studies of the immersion of the bundle is conducted, and it is found that an immersion of -75 m will give the smallest responses of dynamic displacement without significant increase in moment. Additionally the depth will leave a good distance between the bundle and the undersea borders of the fjord throughout the operation.

As a conclusion, it has been found that the towing through the fjord is feasible, but that direct wave loads should be avoided. An installation procedure that exploits both the horizontal and the vertical plane is found to be most suitable. The active modes during transportation and installation are in the energetic wave period band, and the responses are caused by the motion of the tugs. The sideways position of the bundle during installation will lead to increased responses, but as the active modes are far away from the vortex shedding frequency, VIV is possibly avoided. The responses both during transportation and installation remain below the critical limit, but fatigue damage is of concern and should be studied closer.

Sammendrag og konklusjoner

Hensikten med denne Masteroppgaven har vært å studere transport og installasjon av en bundelkomponent til bruk på en Kunstig Sjøbunn. Bundelen er sammensatt av tre rør og er 4 km lang, og vil bli transportert gjennom Sognefjorden til installasjonspunktet. Controlled Depth Tow Method (CDTM) er tauemetoden som vil bli benyttet for å transportere bundelen. Denne metoden går ut på å senke objektet som blir tauet, og transportere det ved denne dybden. En slik tauemetode unngår kritiske faser av en transportoperasjon, som å senke objektet gjennom vannflaten eller løfte det fra dekk. Analysen i denne studien er delt inn i to deler, en for transport og en for installasjon. Transport over Nordsjøen er ikke inkludert, da det følger en godt kjent prosedyre fra offshore industri. Tauing gjennom Sognefjorden er derimot ikke utført tidligere for denne typen objekt. Bundelens lengde er større enn bredden av fjorden, noe som gjør installasjonsprosessen utfordrende.

Sima Riflex er et dataprogram som brukes for å analysere slanke marine konstruksjoner, og blir brukt i denne oppgaven. Programmet baserer seg på elementmetoden. Den dynamiske analysen finner strukturens respons når den blir utsatt for en forutbestemt sjøtilstand. Sima Riflex har tre måter å løse ulineære systemer på, og disse inkluderer ulineær tidsdomeneanalyse, lineær tidsdomeneanalyse og frekvensområdeanalyse. Til slutt vil en egenfrekvensanalyse bli gjennomført, noe som vil bidra til å vise strukturens respons til dynamiske laster.

Geometrien til bundelen er forenklet til et sirkulært rør, men med egenskapene til den ekte bundelen. Både modellen for transport og installasjon består av bundelen og ett sett med slepetau og taubåt i hver ende. Dersom det har vært behov for flere taubåter har disse blitt modellert som horisontale krefter. Miljølastene benyttet i analysene er basert på studier om Sognefjorden gjennomført av SINTEF.

Transportfasen er delt inn i tre scenarioer med forskjellige sjøtilstander, for å dekke tauingen gjennom de forskjellige delene av fjorden. For å manøvrere bundelen gjennom svingene i fjorden, kan det være nødvendig å bøye den. Derfor vil to av scenarioene også inneholde en parameterstudie av grad av bøyning for bundelen.

Installasjonsprosessen er også delt inn i tre deler, der hver del representerer en mulig installasjonsmetode. Det første scenarioet gjennomfører installasjonen ved å bøye bundelen

kun det horisontale planet. Det andre scenarioet utfører installasjon ved å kun utnytte vertikalplanet, mens det siste scenarioet benytter seg av begge plan for installasjonen.

De aktive modene under transporten i Sognefjorden har egenperioder på 2.8 s, noe som er i bølgefrekvensbåndet. For den gitte sjøtilstanden er all bevegelse utryddet for en tauedybde på -30 m. Dette indikerer at responsen ikke kommer av direkte bølgelast, men på grunn av bevegelsen til taubåtene. Bevegelsen til bundelen under transport viser at effekten av utmatting burde bli studert nærmere. For mer alvorlige sjøtilstander er bundelen utsatt for direkte bølgelaster, noe som gir markant større bøyemoment og forflytninger. Videre er det blitt funnet at bundelen kan bli bøyd under transport, men at det er grenser for hvor stor bøyningen kan være.

For installasjonen viser det seg at scenarioet som utnytter både det horisontale og det vertikale planet er mest passende med hensyn til størrelse på responsene og operasjonens gjennomføringsevne. Parameterstudiene gjennomført viser at å senke bundelen -75 m ned i dypet under installasjon vil gi best resultater med tanke på moment og forflytning. I tillegg vil denne dybden gi god avstand til den undersjøiske fjellveggen gjennom operasjonen.

Som en konklusjon er det blitt funnet at transportetappen er gjennomførbar, men at direkte bølgelaster burde bli unngått siden det drastisk øker responsene i bundelen. Installasjonsscenarioet som utnytter både det horisontale og det vertikale planet vil være mest passende. De aktive modene under transport og installasjon er i bølgeperiodebåndet, noe som medfører at responsene er forårsaket av bevegelsene til taubåtene. Under installasjonen er bundelen plassert sidelengs i fjorden, noe som gjør at strømmen fører til større responser. Det er funnet at virvelavløsningsfrekvensen og den aktive egenperioden er langt fra hverandre, så virvelinduserte svingninger er derfor trolig unngått. Responsens både under transport og installasjon holder seg under den kritiske grenseverdien, men utmattingsskader er viktig å se nærmere på.

Acronyms and Abbreviations

CDTM Controlled depth tow method

CFD Computational fluid dynamics

DOF Degree of freedom

FEM Finite element method

JONSWAP Joint North Sea wave project

RAO Response amplitude operator

ROV Remotely operated underwater vehicle

SFT Submerged floating tunnel

TLP Tension leg platform

VIV Vortex induced vibrations

Contents

List of Figures

List of Tables

Chapter 1

Introduction

1.1 Background

Norway is famous for its high mountains and deep fjords, but these characteristics make it difficult to travel through Norway. The highway that goes through the west coast of Norway is extremely time consuming to travel, due to several fjord crossings by ferries. In 2010 the Norwegian Public Roads Administration created the project called "Ferry-free E39", which aims to reduce the travel time along the coast line. By eliminating the ferries on the route from Kristiansand to Trondheim, they wish to reduce the travel time from 21-22 hours to 12-13 hours (Skorpa, 2012).

Several concepts have been developed for extreme fjord crossings, and among them exist floating bridges, submerged floating tunnels, floating suspension bridges, and combinations of these.

One proposed solution for crossing the Sognefjord is to combine a floating bridge with a submerged floating tunnel. This project is owned by Reinertsen, but with cooperation with other companies, Deep Ocean Group being one of them(Engineering Department, Deep Ocean, 2014). The crossing site of the Sognefjord has an extremely large depth, which makes anchoring to the sea bottom unsuitable. Consequently, an "artificial sea bed" has been developed. This concept will create a stable system of wires imitating the sea bed, but at a less extreme depth. The combined floating bridge and floating tunnel can be moored to the artificial sea bed, and thus avoid mooring the structure to the actual sea bed. Figure 1.1 shows

the concept, including the submerged floating tunnel in the middle, the floating pontoon bridge on each side, and the artificial sea bed below the structure. Additionally, the ship barriers are seen connected to the submerged floating tunnel at both ends.
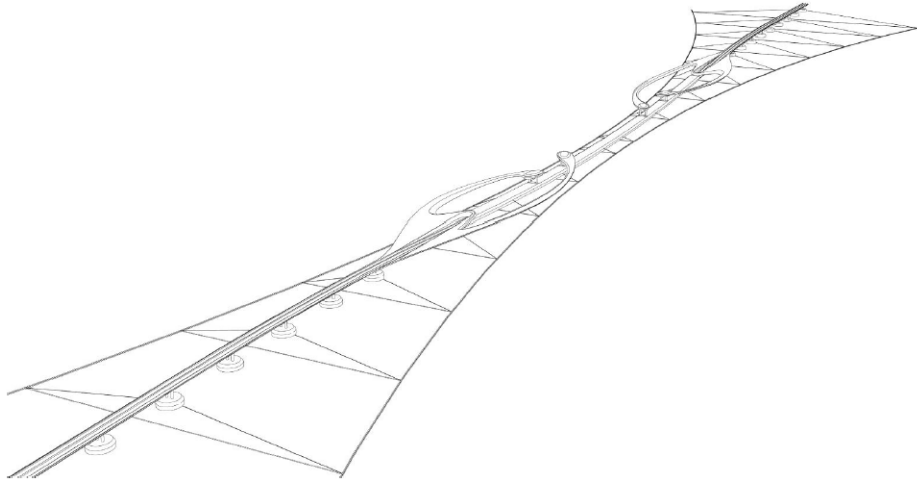
Figure 1.1: Concept by Reinertsen, called "Artificial Sea Bed" (Engineering Department, Deep Ocean, 2014)

In relation to this concept, this Master's Thesis will study the transportation and installation of the longitudinal bundles of the artificial sea bed. The aim is to find out if the towing through the Sognefjord is feasible by applying the controlled depth tow method (CDTM), and find the effects that influence the bundle during tow. For the installation of the bundle, possible approaches must be developed, modeled and analyzed, to find the most beneficial installation procedure.

The technology utilized for the concepts developed for fjord crossings often originate from offshore technology, and still the number of ideas and combinations of existing technology increase. This study aims to analyze one proposed concept for fjord crossings, by first dive into the existing ideas and concepts that are developed.

1.2 Objectives

The main objectives of this Master's Thesis are

1. Make a review of existing and planned marine bridges, including similarities and differences.

2. Make a review of the concept of controlled depth tow method, including usage.

3. Study the loads that act on the bundles during transportation and installation and discuss the associated structural models.

4. Describe the methods for both static and dynamic analysis used by the relevant computer program, Sima Riflex.

5. Model and analyze the transportation through the fjord and installation of the bundles in Sima Riflex.

6. Do a parameter study of the analyses with respect to variation of the transportation and installation procedures as well as environmental conditions.

7. Study the statistical responses of the transportation and installation procedures.

1.3   Scope and Limitations

The towing through the North Sea is excluded, due to this part being a well known procedure from offshore towing of pipelines. The main aspects of the analysis will be feasibility of the operation and structural responses of the bundle.

The limitations of this study are related to the extent of the analyses. It will for instance not be possible to analyze the towing through every part of the Sognefjord. Therefore a simplification is done by choosing three scenarios that are representative for the towing operation.

Furthermore, the towing tugs used for the towing operation in Sima Riflex might not be the same as intended used in the real operation. Thus can the vessels behave differently in the given sea states, and might give different structural responses in the bundle than for the real operation.

For the installation procedure, only one bundle will be simulated and analyzed. The installation procedure will be similar for both bundles, but the current will act differently on them due to the installation being mirrored versions of each other. This is a truth with modifications, as the current will move in or out of the fjord dependent on the tide. It is likely to believe that the responses in the bundles will be similar to each other, and mainly show

variations with respect to magnitude. Based on this, only the bundle installed with the current acting in the same direction as the curve of the bundle will be analyzed in this study.

For the statistical responses, only an extreme value distribution plot will be utilized to see if there are any consistency in the responses from the analyses.

1.4 Methodology

In order to accomplish the given objectives, the study started with a review of the existing reports and articles on the subject. This was to get an overview of the present research and methodologies developed. Next the relevant theories were studied to find which effects that were necessary to consider for modeling and understanding the analyses properly. Additionally, understanding of the computer program, Sima Riflex, is essential to get satisfactory results. Thus the theory of the program was an essential part of the study.

Eventually it was appropriate to model the case in Sima Riflex and run the relevant analyses. For both the installation and the transportation, the different models were first developed by drawing on paper, which is less time consuming than modeling in Sima Riflex.

Finally the discussion part was reached. As a consequence of it being several months in between the beginning of the study and the commissioning of the results, it was necessary to reread the report written during these months. This was done in order to manage to discuss the study as a whole, with relevant theories and parameters.

One could always argue that a more thorough assessment of the drawn installation approaches could have been done. Some of the suggestions was not possible to model at all, due to non-physical effects. In other words, a lot of time was spent on approaches that did not work. However, this was a very effective learning by doing approach, which clearly showed what did not work.

1.5 Structure of the Report

The report has nine chapters. The following chapter, Chapter 2, gives a detailed presentation about the fjord crossing concept that will be studied, as well as the relevant information about

the bundles. Chapter 3 contains the relevant theories that applies to slender marine structures in water. Chapter 4 goes through the relevant rules and regulations that apply for the marine operation that is studied. Next, Chapter 5 contains the theory of the computer program Sima Riflex. Then Chapter 6 gives the individual studies of this Thesis, with all the information and parameters that is utilized for modeling in Sima Riflex. Chapter 7 gives the results from the analysis, before Chapter 8 contains discussions of the results and methods. Finally, Chapter 9 gives the conclusions that are reached in this study.

1.6 Literature Review

The topics covered in this Literature Review include floating bridges, submerged floating tunnels (SFT's) and submerged towing methods. Floating bridges has been built several places in the world, and three important examples are covered in this section. The SFT's have not been built before, but there are thorough reports written on the subject, thus the theoretical aspects of the structure is covered. Some of these reports are studied closer in this literature review. The methods of submerged towing have been carefully studied by offshore companies and scientists, and it has been implemented for towing long slender pipelines for the offshore industry. However, in order to implement the method for other applications, the research and reports on the subject will be considered carefully in this literature review.

1.6.1 Floating Bridges

Fjords or straits that are either very deep or have a very soft seabed, will not be possible to cross using conventional bridges that are bottom supported (Watanabe and Utsunomiya, 2003). Instead, a floating bridge could be proper for these cases. This concept uses buoyancy from pontoons in order to support the bridge, instead of pillars into the ground. Thus will this method only require some sort of mooring system in order to keep the bridge still (Watanabe and Utsunomiya, 2003). The advantages with this bridge compared to conventional bridges will be large for these types of crossings.

Floating bridges have a long history. They were probably used already in year 2000 B.C (Watanabe and Utsunomiya, 2003). They have also been used in warfare throughout the

history, to cross the Dardanelles with boat bridges in year 480 B.C., and to this day for military missions (Watanabe and Utsunomiya, 2003).

For the very deep and wide fjords of Norway, it is likely that a traditional floating bridge must be combined with other concepts (Skorpa, 2012). For this Master's Thesis work, the concept of a combined floating bridge and submerged floating tunnel (SFT) will be studied. This solution makes it possible for large ships to pass the bridge over the SFT part.

Several pontoon bridges have been built around the world, and Bergsøysundet Bridge and Nordhordland Bridge in Norway and Evergreen Point Floating bridge in America are three important examples that will be covered here.

Bergsøysundet Bridge

Bergsøysundet bridge is located in Møre and Romsdal in Norway. This floating bridge is made of truss work and has 7 concrete pontoons (Øderud, 2009). It was completed in 1992 and the total length is 931 m. This bridge is only anchored at the end points. Together with the Nordhordland Bridge, these two bridges are the only ones with this unique anchorage technique (Øderud, 2009). Bergsøysundet Bridge can be seen in figure 1.2 below.

Figure 1.2: Bergsøysundet Bridge (Villoria, 2015)

Nordhordland Bridge

The Nordhordland Bridge was completed in 1994, and consists of a combination of a floating bridge and a cable-stayed bridge (Aas-Jakobsen, 2005). The floating bridge is the longest freely floating bridge with its 1245 m. It has 10 pontoons in concrete containing nine separate sections, where two can be filled with water without any damage to the structure (Aas-Jakobsen, 2005).

Nordhordland Bridge can be seen in figure 1.3 below.

Figure 1.3: Nordhordland Bridge (Villoria, 2015)

Evergreen Point Floating Bridge

The Evergreen Point Floating Bridge is situated in Seattle, USA, and is declared the longest floating bridge in the world (Chandler). It crosses Lake Washington and connects Seattle on one side, and Washington on the other side. The bridge was build due to the large workforce in Seattle, creating the fastest route across Lake Washington (Chandler). The bridge was completed in 1963. The total length is 2310 m and it has 33 pontoons and 58 anchor lines (Villoria, 2015). Figure 1.4 below show the Evergreen Point Floating Bridge.
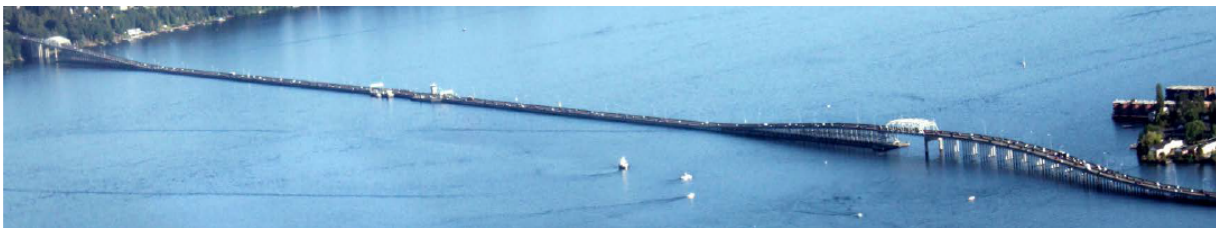
Figure 1.4: Evergreen Point Floating Bridge (Villoria, 2015)

1.6.2   Submerged Floating Tunnel

A SFT is a tube that is submerged in the water. It can consist of concrete or steel, be circular or square, and consist of one or two tubes (Skorpa, 2012). A structure like this can be moored

either to the sea bottom with mooring lines or to the sea surface with pontoons (Skorpa, 2012).

The first written papers about SFT's came from Sir Edward James Reed in 1882, where he proposed a SFT as concept for crossing the English Channel (Ingerslev, 2010). His plans was that a railway would use the SFT to cross the channel, but the English Parliament rejected him. Up to this day, there is still no SFT's built in the world, although thorough studies have been conducted (Skorpa, 2012). One of the studies that was almost fulfilled was the studies about a SFT crossing the Høgsfjord. This fjord, in addition to Bjørnafjord and Sognefjord, will be studied closer in this literature review, due to their relevancy in connection with SFT's.

Høgsfjord

The Høgsfjord is located in Rogaland in Norway and is 1400 m wide and 155 m deep. It was the location for political decisions in the 1980's, when the Norwegian Parliament encouraged the development of alternative fjord crossings. Due to large ship traffic in this area, tourists, and local politician's decisions, a feasibility study of a SFT as the desired concept was started (Skorpa and Østlid, 2001). This concept was researched throughout the 1980's and the 1990's, before the final decision fell on Ryfast, a rock tunnel below the seabed (Jøssang, 2005). The building of this concept was started shortly after the government decision in 2012 (ryf, 2015).

The result of the discussions about a SFT for crossing Høgsfjord, were several thorough studies that proved the concept to be feasible. Even new rules and specifications were developed during the process, and some state that the only thing remaining was the final decision (Skorpa and Østlid, 2001).

Bjørnafjord

Bjørnafjord is challenging to find a suitable bridge concept for, due to the crossing length of 5 km and depth up to 550 m (Gisvold, 2015a). The Public Roads Administration are leading the project for this fjord crossing, and they believe that the only options for crossing are floating bridges or SFT's, or rather a combination of both. The two main concepts that are developed for crossing the fjord, are a floating bridge with a middle part that is raised to enable ship crossings, and a submerged floating tunnel anchored to the sea surface (Gisvold, 2015a). Although the technology and the development on SFT's have come far, there are still some

work left. For example will it be necessary with better data from the crossing sites. However, if the work continue as planned, the first SFT in the world can be started on in five years (Gisvold, 2015b). An illustration of a SFT over Bjørnafjord is seen in figure 1.5 below.

Figure 1.5: Illustration of SFT over Bjørnafjord (Gisvold, 2015a)

Sognefjord

Thorough feasibility studies have been conducted for crossing of the Sognefjord. This fjord is among the widest and deepest fjords in Norway, and if a crossing method is found possible for this fjord, the method is likely to be implementable to other fjords. On behalf of the Public Roads Administration, Reinertsen Olav Olsen Group has conducted "Mulighetsstudie for kryssing av Sognefjorden" (Fjeld, 2013). In the report, the technical feasibility for a SFT crossing Sognefjorden is studied. The purpose is to create a basis for further investigation of possible crossings. The concept studied in this report consists of two circular tubes with transverse trusses in between. A cross section of the concept can be seen in figure 1.6 below. They conclude in the report that the concept is possible to implement.
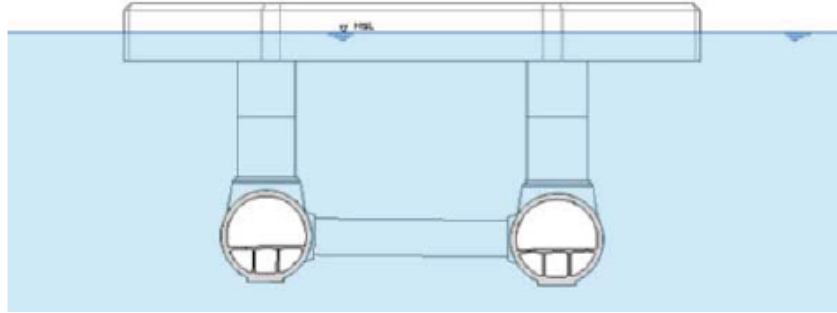
Figure 1.6: Concept of SFT over the Sognefjord (Fjeld, 2013)

1.6.3 Similarities and Differences Between the Marine Bridges

The difference between the Bergsøysundet Bridge, Nordhordland Bridge and Evergreen Point Floating Bridge is particularly the length of the bridges as well as the mooring method. The lengths are respectively 931 m, 1245 m and 2310 m. As a result of this, the first two bridges are moored only at the end points, while the last is moored with several mooring lines along the length of the bridge. The bridges moored only at the end points are of a curved shape. The curved shape give the necessary stiffness to avoid any more anchoring. As for similarities, all the floating bridges have pontoons made of concrete.

For the SFT's, most studies show that the concept is possible to build. Nevertheless, it has never been built before. A difference between the concepts proposed for a SFT is if two tubes should be used instead of one. However, this seems to be dependent on the length that is tested for the crossing. Relatively short crossings use one tube, while longer crossings use two tubes.

Altogether it seems like the length of both the floating bridge and the SFT will be the main aspect of developing these concepts.

1.6.4 Submerged Towing

Submerged towing is a concept developed in order to reduce the loads that act on the item being towed. It is a relatively newly developed concept, and was first used for transporting and installing pipelines. In the beginning, it was mostly used on pipelines that were short and light, which was explained in detail by E. G. Rooduyn during the conference "Subsea International '85" in London (Rooduyn, 1985). The later years, Subsea7 has studied the concept, and are now

using the method for pipelines up to 7.5 km of length (da Cruz and Davidson, 2006). They also use the method for transportation and installation of subsea structures (Jacobsen and Naess, 2014). Following is a thorough review of three important papers on the subject.

Deepwater Installation of Pipelines and Risers by Towing by I. C. P. da Cruz and J. D. Davidson, Subsea 7 (da Cruz and Davidson, 2006)

The paper is written in order to describe how the CDTM can be used for deep-water installations. The authors write that almost 60 pipeline bundles have been installed in the North Sea in depths up to 450 meters, by using CDTM. For installations on larger depths than this, new methods need to be developed. One of these methods are studied in this paper.

The authors explain how submerged towing is conducted. The pipelines that are to be transported and installed are within a carrier pipe that will cause some excess buoyancy. With even intervals, ballast chains with enough weight to exceed the excess buoyancy are secured to the pipe. This will cause some of the chain links to remain on the seabed. According to the authors, these chain links will create enough resistance to avoid movement of the bundle due to current, but without making the tow difficult for the tug. This configuration is called "off-bottom" mode. Furthermore, it is stated that the maneuvering speed is up to two knots, and that increasing speed will create forces that cause hydrodynamic lift. In order to use CTDM the minimum water depth is stated to be 60 meters.

Control of the pipeline during transportation can be achieved by modifying the speed of the towing tugs or by altering the tension caused by the trailing tug. They state that most of the weight is carried by buoyancy of the carrier pipe, leaving almost no weight to be carried by tension and curvature. The depth the pipeline is towed at must be such that wave motion is significantly reduced. A typical bundle tow in the North Sea would start with tow in off-bottom mode before increasing the speed and go into CDTM. Then the installation is performed in off-bottom mode.

The authors then study the possibilities of using CDTM for ultra-deep water depths. One possible solution is stated, consisting of three different phases. The first mode is the off-bottom tow, the second is CDTM, and finally the last mode is a catenary tow. The first two phases are identical to the method used for regular depths, while the catenary tow is especially for deep

water. At a water depth of 500-800 m, the pipeline is put down on the seabed. Then the buoys and chains are removed, before the tow continues in catenary tow mode.

They highlight the pipeline response to wave loading, and report that specific directions can cause resonance of the pipeline and thus large stresses. This is also important when considering fatigue. In addition, they find that the phase when the pipeline is the most subjected to excitation is in off-bottom mode. This is the consequence of towing closer to the sea surface. However, the pipe will also be subjected to vessel motion induced bending, but the response of this will be largest during steep catenary tow mode. The effect of this during off-bottom mode tow, the authors believe to be little.

Numerical and experimental studies of submerged towing of a subsea template by Tore Jacobsen and Bernt J. Leira, 2012 (Jacobsen and Leira, 2012)

The purpose of the paper is to take a closer look at submerged towing of a subsea template. The authors focus on the dynamics of the system, and test for different towing velocities and sea states. The background for this research is that the regular method of towing templates includes several critical phases. Amongst these are lift-off from the deck and immersion through the splash zone. These operations will also limit the operational window. A submerged tow through the moonpool of a vessel is believed to give a broader operational window. According to the authors, the hydrodynamic loading will cause the dynamic behavior of the template, and thus restrict the operational window. This is the issue studied in the paper.

In order to model and analyze the problem in a simplified way, the authors present the template-ship system by a one degree of freedom (DOF) system. By following the DNV Recommended Practice, they find found that the motion of the vessel will govern the motion of an object that is deeply submerged. The natural frequency of the system is found, and it is discovered that for short oscillation frequencies the oscillation of the system will be the same motion as for the wire and the vessel. In order to find the coefficients for damping and added mass in the equation of motion, the authors use a simplified approach. By only consider the suction anchors since these give the largest impact on the coefficients for added mass and damping, the coefficients can be found from the DNV Recommended Practice. The angle of

the wire that the template is connected to is of importance to avoid contact between the wire and the edges of the moonpool. The necessary calculations can then be completed in order to find the maximum force in the lifting wire, and the authors use a linear superposition of the quasistatic drag- and dynamic forces.

According to the paper, Morison's formula can be used to calculate the hydrodynamic loads acting on a slender structure if the diameter of it is much smaller than the wavelength. The problem is modelled using SIMO, and in order to model the template, long and slim elements are used. The dynamic equation of equilibrium is presented, with possible solution methods being solving by convolution integrals or solving by separation of motions.

The authors perform an experimental investigation in order to verify the analytical models. For the experiment, 12 different wave conditions are used, and the aim is to find the towing force in the wire, to observe the movements of the template and to measure the offset angle. Figure 1.7 shows the experiment of subsea towing of the template.
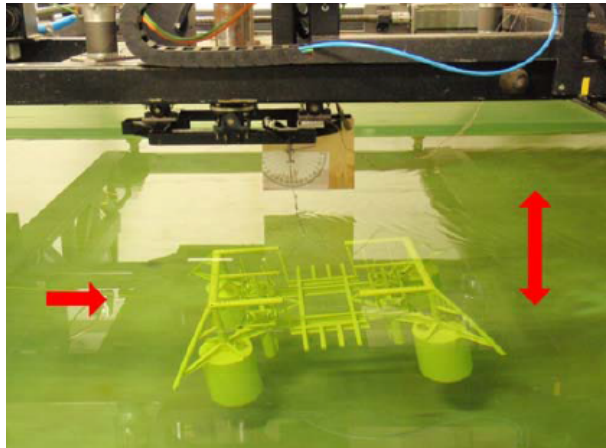
Figure 1.7: Experiment performed on subsea towing of template (Jacobsen and Leira, 2012)

The paper finds that the results are comparable for the towing force in the wire for all of the methods tested. An important observation, is that the experiment results will deviate somewhat from the results from SIMO, possibly because of the influence of limited water depth. They conclude that the analytical solutions should only be used for feasibility studies, since they may deviate from the correct values. In order to get even better results, the authors used a more extensive model in SIMO. In conclusion, the authors state that for models with several degrees of freedom, numerical time integration will give precise results for submerged

towing.

Installation of Subsea Structures Using Mid-Size Construction Vessels in Harsh Environments by Tore Jacobsen and Tor-Bjørn Næss, Subsea 7, 2014 (Jacobsen and Naess, 2014)

The purpose of this paper was to outline the two main methods for installing subsea structures, and the relevant criteria for equipment and operation. According to the authors, the traditional method for installing subsea structures is by transporting it on the deck of a barge or a crane vessel. This operation method has several potentially hazardous elements, including the lift-off from deck and the crossing of splash-zone. This method is highly dependent on the weather conditions in order to conduct the operation safely. As a consequence of this, some offshore operations will be restricted to the summer months.

On this basis, the authors recognize the need for an alternative method, which will increase the operation window. They propose a submerged tow of the structure through the moonpool of a suitable vessel. This method will exclude any lifting operations, and thus they claim that the operation window will be increased. The hydrodynamic forces acting on the different components will set the limitations of the operation with this set-up. According to the article, this method has been used successfully on several of Subsea7 installations between 2003 and 2007.

The authors highlight several challenges associated with the submerged towing method, and categorize them into geographic, template properties and operational. By the geographic challenges, the significant wave height is of importance, as well as fatigue related to the distance the structure is towed. Furthermore, the water depth in the area of installation must be considered, due to the possibility of vertical resonance. Regarding the template properties, the weight compared to the vessel is of concern, in addition to the possibly large hydrodynamic loads caused by the suction anchors. As for the challenges related to the operation, the authors consider the heavy rigging, challenging ROV operations, and finally that the system is not heave-compensated.

An experiment was conducted in association with the paper, where the focus was on the

tension in the main wire. The authors find that the largest response in the towing wire was caused by swell dominated sea. Furthermore it is discovered that for towing through the moonpool of a vessel, there will be a clashing frequency with the wire against the edges of the moonpool. This frequency is increased with increasing towing speed. An illustration of towing through the moonpool of a vessel is seen in figure 1.8.
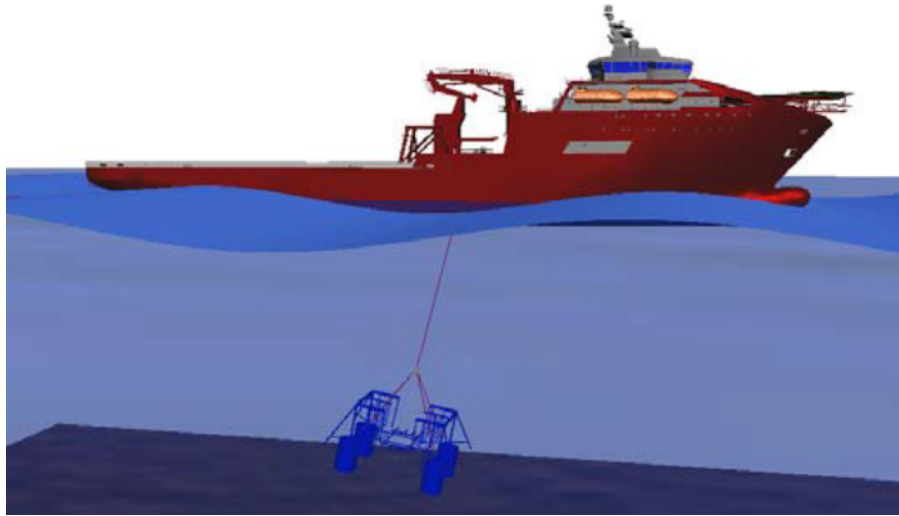
Figure 1.8: Towing through moonpool of a vessel (Jacobsen and Naess, 2014)

To conclude, the authors believe the submerged tow is suitable for installing the type of structures considered in this paper, and besides the method will increase the number of available vessels that can perform these tasks.

1.6.5 Similarities and Differences in Submerged Towing

The reason for developing this method is the same for all the studies. They see the challenges related to the conventional method for transporting structures to offshore sites, and the aim is to increase the operational window and make the transportation safer. Furthermore, the studies have similar challenges related to the submerged tow of a structure. These include the challenges with current, issues related to the main wire of the towing and possible collision between the wire and the edges of the ship. Additionally, effects in the towing wire due to environmental loading is regularly mentioned as a challenge. However, one of the studies stand out because it also includes the effect on the towed object due to the vessel induced motion.

Chapter 2

Description of Concept

2.1 Introduction to the Case

The proposed solution that is to be studied in this Master's Thesis, have been developed by Reinertsen in cooperation with DeepOcean, amongst other companies (Engineering Department, Deep Ocean, 2014). This chapter aims to give the relevant details that is utilized in order to develop and model the concepts of this study.

2.2 Details about the Bundles

From preliminary studies on the concept, several conclusions about the bundles have been made. First and foremost, the bundles will be produced at a location far away from the installation point. They will consist of three pipes that will be tied together at the production site. This method is preferred before towing single pipes and assemble them at the installation site. This will cause reduced complexity of the installation, and thus be beneficial with respect to time and costs (Engineering Department, Deep Ocean, 2014). The three pipes will be produced separately, but simultaneously at three different centers for welding at the production site. When the three pipes are assembled to a bundle, they are ready to be transported (Engineering Department, Deep Ocean, 2014). An illustration of the bundle is seen in 2.1
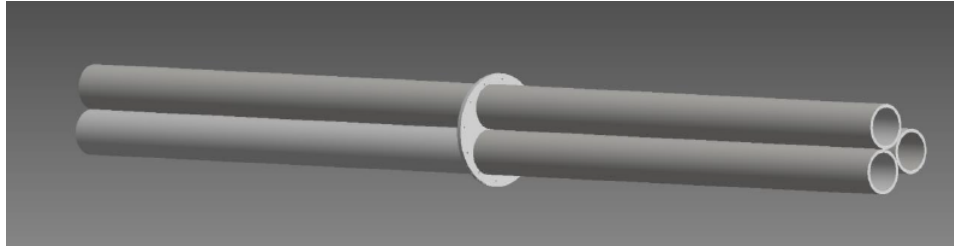
Figure 2.1: Illustration of the bundle, with connection between two sections (Engineering Department, Deep Ocean, 2014)

The length of the bundle will be 3700 m, to be used for a crossing of 3604 m (Reinertsen, 2014b). The external diameter of the internal pipes will be 0.9144 m, and the internal diameter will be 0.8534 m (Reinertsen, 2014c).

2.3   Transportation

The bundles will be close to 4 km in length, and will have to be transported from the production location in Scotland to Sognefjord (Engineering Department, Deep Ocean, 2014). The part of transporting the bundles over the North Sea is assumed feasible. However, the transportation through the Sognefjord needs to be studied closer since it is not conducted before. This requires navigation with the long bundles through limited areas, and will be studied in this Thesis. The method which will be utilized for the transportation of the bundles is CDTM. This method will avoid any direct wave loads, which will reduce the loading of the bundles during tow. In addition, the current will also decrease with increased depth, and thus also give lower loading. As a result, near surface or surface tows are excluded for towing the bundles, because these will cause larger wave loads and current forces than CDTM. Additionally, the depth of the fjord makes off-bottom tow ruled out.

For the practical implementation, it is important to control the stresses and the movement of the bundle during transportation and installation. Therefore strain gauges will be applied, and the motion will be monitored by acoustic positioning system (Engineering Department, Deep Ocean, 2014).

The bridge concept will connect Lavik and Opedal, as seen in figure 2.2. Furthermore, it is observed that the depth at the crossing site is very large, with 1250 m at the deepest according

to this map (Norgeskart).
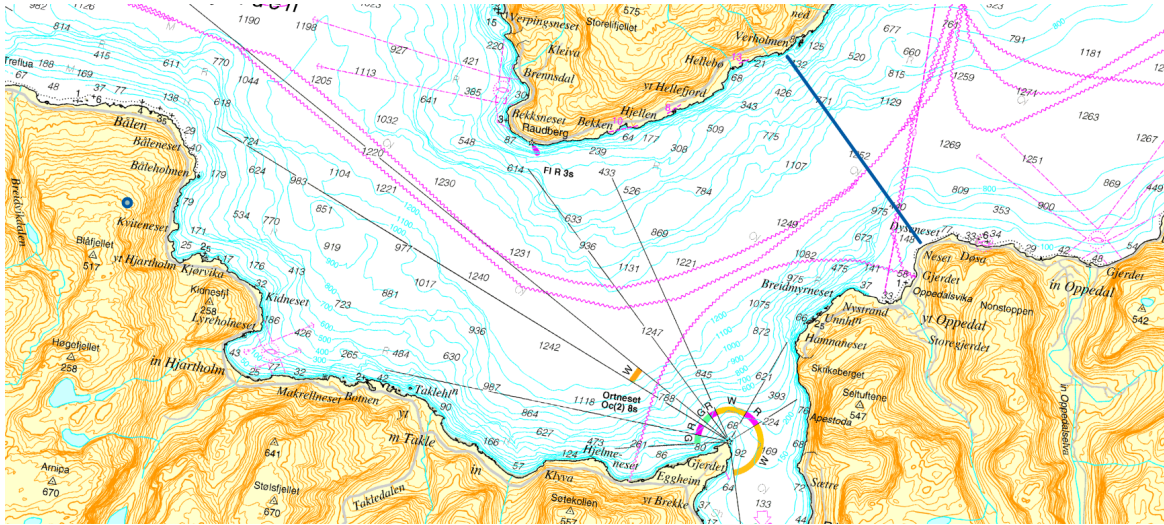
Figure 2.2: The bridge will connect Lavik and Opedal (Norgeskart)

Sognefjorden is one of the deepest fjords of Norway, with depths larger than 1000 m. However, near the mouth of the fjord, in Sognesjøen, the sea depth decreases. Figure 2.3 show the entry of the fjord, along with the depths. It is observed that these depths are still large for towing at -30 m. Additionally, due to the open area, the bundle can be kept straight.
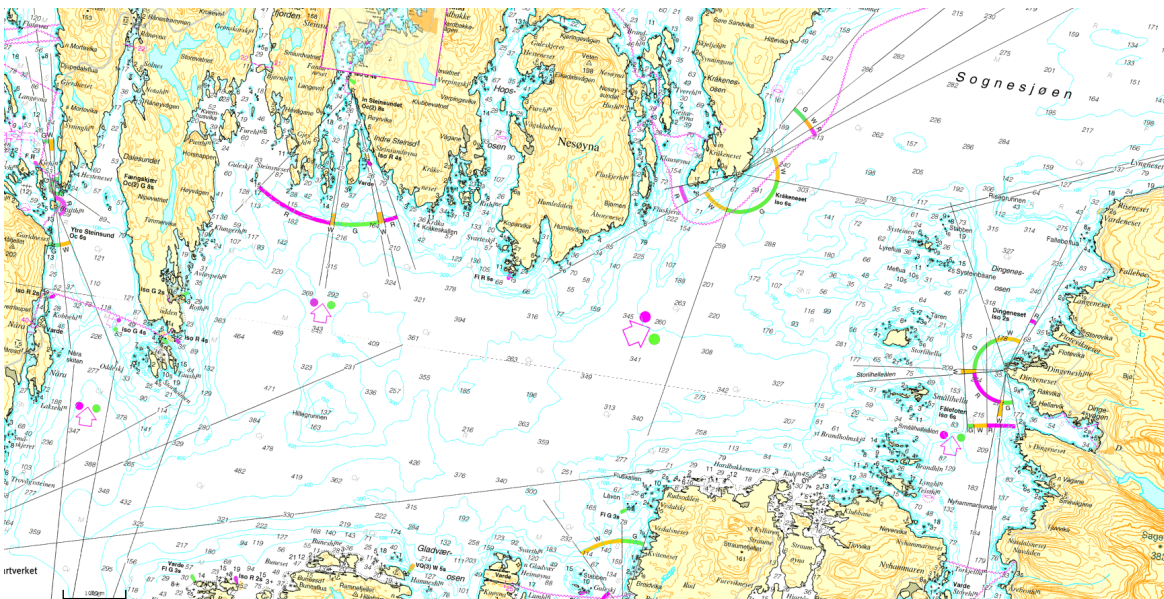
Figure 2.3: Entrance of the Sognefjord from the North Sea, Sognesjøen (Norgeskart)

Further in, the turns and twists of the fjord begin. The fjord is wide, but it still might be

necessary to bend or curve the bundle with the turns of the fjord. Figure 2.4 shows the first turn into Sognefjord, which is Rutletangen. It is a large open area at this place, with depths from 140 to 500 m.
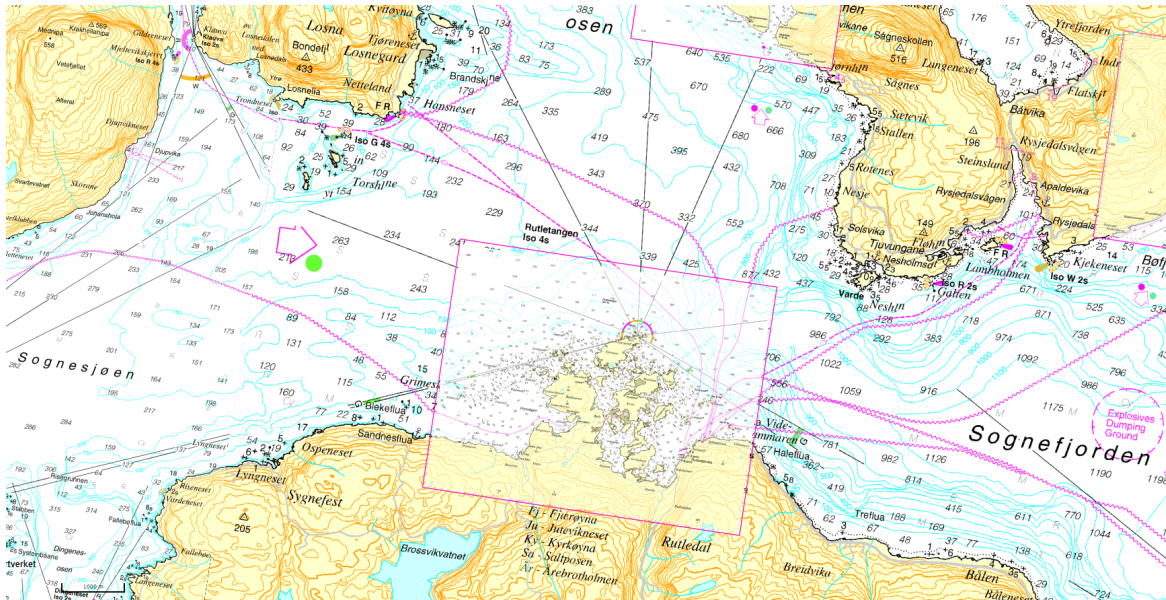
Figure 2.4: Rutletangen, in between Sognesjøen and the Sognefjord (Norgeskart)

Finally, the last stage of the transportation is inside the Sognefjord, see figure 2.5. The depths are now increasing rapidly, and in the middle of the fjord it is more than 1000 m deep. The last turn before entering the installation location is Raudberg.
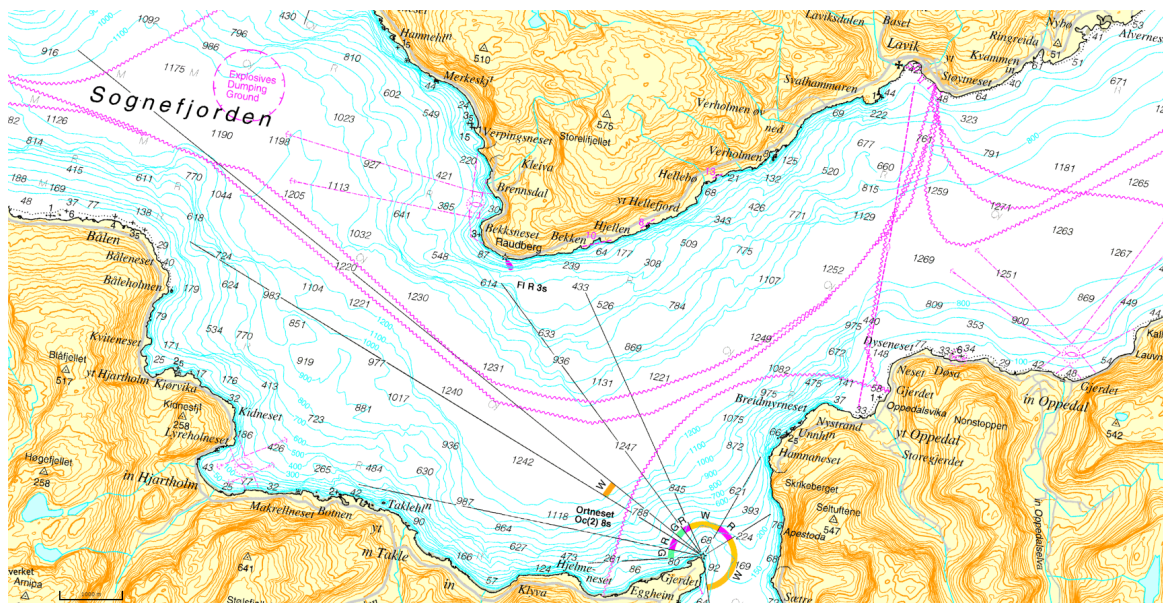
Figure 2.5: Inside Sognefjorden, Lavik and Opedal to the right of the picture (Norgeskart)

Aspects that must be considered during the transportation of the bundles include current, wind and waves, positioning through the fjord and depth throughout the operation. The environmental values utilized in the analyses will be based on measurements and calculations from the installation site.

2.4 Installation

The second part of this Master's Thesis is to study the installation phase of the bundles. When the bundles are installed in the correct configuration of the artificial sea bed, they will be in an arch shape, bent. Thus, they are longer than the width of the fjord. This will require the bundles to be bent in order to install them, and it is important not to impose the wires with too large forces.

As seen in the literature review, the normal approach when installing long slender marine structures is to conduct the operation in off-bottom mode. This will not be possible when installing the bundles in the Sognefjord, because of the large depth. Therefore the installation phase must be implemented with the bundles still floating in the water. This will be challenging due to the current in the fjord, and can cause risk of snapping.

There are several approaches that can be utilized in order to install the bundles without any damage. Due to the large depth of the Sognefjord, one could utilize this and lower parts of the bundle to avoid severe bending. Furthermore, it might be necessary to use several tugs to keep control of the movement of the bundle. This is the second part of the problem that will be studied in this Master's Thesis.

Chapter 3

Theory of Loads

3.1 Introduction to Loads

This chapter will cover the main theoretical aspects that are of importance for the bundles during transportation and installation. This include the environmental loading from waves and current, but will also cover submerged towing and the relevant loads and effect this will cause. Finally, some short theory about statistical responses and extreme value distribution will be covered.

3.2 Wave Loads

The following sections are adapted from the author's Project Thesis "Structural Response of Submerged Floating Tunnels Exposed to Current and Waves" (Kjelsaas, 2015). The sections include 3.2.1, 3.2.2, in addition to the text below.

The main environmental effects that will affect the bundle will come from waves and current. The incoming waves are defined by a given sea state. A sea state can be described statistically by measurements taken in the specific area. The JONSWAP spectrum (Joint North Sea Wave Project) is based on measurements taken in the North Sea in 1968-1969. The spectra has most of the energy focused around the top frequency, with less energy on larger or lower frequencies (Myrhaug and Lian, 2014). Sognefjord is connected to the North Sea, which can be described by the JONSWAP spectrum. The waves entering the fjord is thus based on this sea

state.

Waves that hit a structure will cause loads that can create motions of the structure. These loads can be categorized in linear and non-linear effects, which affects marine structures differently.

3.2.1 Linear Effects

The loads from wave-induced motions can be described by linear theory. One of the advantages of using this theory, is that irregular waves can be separated into regular waves, and the total result can be found by adding the contributions together (Faltinsen, 1990).

A system with dynamic behavior can be described by the equation of motions, here given by equation (3.1) (Larsen, 2014).

$$m\ddot{u} + c\dot{u} + ku = P(t) \tag{3.1}$$

In this equation, $m\ddot{u}$ represents the inertia force, $c\dot{u}$ the damping and ku the restoring force. $P(t)$ is the load that act on the structure, and is varying with time. This is the wave excitation loads, which is found from contributions from Froude-Kriloff and diffraction forces (Faltinsen, 1990). By superimposing all these terms, the total response of the structure can be found.

The equation given above, (3.1), is a second order differential equation. This has a solution that consists of two terms, one homogenous and one particular solution. This is shown in the equation below, equation (3.2) (Larsen, 2014).

$$u(t) = u_H(t) + u_P(t) \tag{3.2}$$

The homogenous solution of the system can be calculated by putting the right hand side equal to zero, $P(t) = 0$. The particular solution is found from the actual load P(t) in equation 3.1. The right hand side of this equation needs to be solved in order to find the hydrodynamic loads on the structure. The Morison equation can be used to find the force acting on a structure, (3.3) (Faltinsen (1990), p. 61). This equation is the sum of two contributions, where one is from inertia force and one is from drag force.

$$dF = \rho\pi\frac{D^2}{4}C_M a_1 + \frac{\rho}{2}C_D D|u|u \tag{3.3}$$

The equation gives the horizontal force on a structure per unit length.

3.2.2 Slow Drift Motions

A structure floating in water will have motions of several types; wave-frequency motion, high-frequency motion, slow-drift motion and mean drift motion. The wave-frequency motion is motion in the same frequency range as the significant wave energy in the sea spectrum. The remaining motions are usually caused because of non-linear effects such as resonance oscillations (Faltinsen, 1990). Resonance oscillations are motion caused by the wave being in the same frequency range as the natural frequency of the structure.

When a structure is hit by an irregular wave, it will generate slowly varying drift-forces on the structure. These will cause a motion of the structure that is slowly varying, and is a resonance oscillating motion (Faltinsen, 1990). In order to calculate the slowly varying response on the structure, one need to divide the irregular sea state into local regular parts. The slowly varying motions cannot be caused by only one incoming wave, thus it is necessary to divide the sea into pairs of two incoming waves with different frequencies. A mean-drift force is then calculated for the first pair of waves, and all the following pairs. The equation below gives the slow-drift excitation loads on a structure, (3.4) (Faltinsen (1990), p. 155).

$$F_i^{SV} = \sum_j \sum_k A_j A_k \left[T_{jk}^{ic} cos((\omega_k - \omega_j)t + (\epsilon_k - \epsilon_j)) + T_{jk}^{is} sin((\omega_k - \omega_j)t + (\epsilon_k - \epsilon_j)) \right] \tag{3.4}$$

For an irregular sea state, all the local incoming waves will have different frequencies, and thus the mean-drift force will vary for each section. From this the slowly-varying drift force is developed through time.

When calculating the slow-drift excitation loads, it is necessary to include the second-order effects for the mean wave loads (Faltinsen, 1990). The second order effects can for some cases be larger than the linear effects. This is because the second order effects occur at low

frequencies, where the linear effects are small (Faltinsen, 1990). The second-order effects are resonance oscillations that occur at low frequencies, and thus structures with low natural frequencies can be exposed to these effects.

It is necessary to have small damping in order to obtain large motions, which is exactly the problem for slowly-varying motions. Damping coefficients are strongly dependent on frequency, and when the frequency goes to zero, the linear wave-radiation damping will also go to zero (Faltinsen, 1990). Slowly-varying motions act at low frequencies, and at low frequencies the wave-radiation damping is thus small.

3.2.3 Wave Motion

For submerged towing it is relevant to study the motion of the waves, including the effect of waves down into the water depth. The motion of the water particles will depend on the incoming wave, but also on the water depth. For finite water depths, the water particles will move in ellipses for incoming waves. For deep water depths however, the particles will move in circles (Lundby, 2013). An illustration of this is shown in figure 3.1 for elliptical wave particle motion and figure 3.2 for circular wave particle motion. As a result of the motion in a closed path, the particles will not move in space.
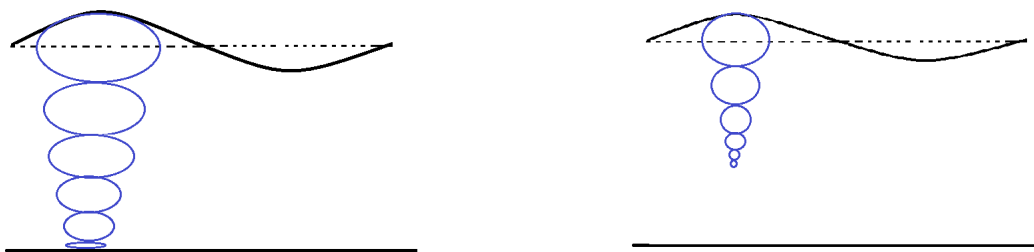
Figure 3.1: Elliptical motion for finite depth (Lundby (2013), p.48)

Figure 3.2: Circular motion for infinite depth (Lundby (2013), p. 49)

The circle the water particle will move in for deep water will never be perfectly circular. This is because the wave top will always have a larger amplitude than the wave trough (Lundby, 2013). Consequently, there will be a small forward motion in the same direction as the waves. Due to the motion of the top circle, the water particles below this circle will also start to move

in circles. However, the motion of these particles will be less affected by the wave, and accordingly will the circle diameter decrease with increased water depth (Lundby, 2013). This effect is illustrated in figure 3.3, as seen below.
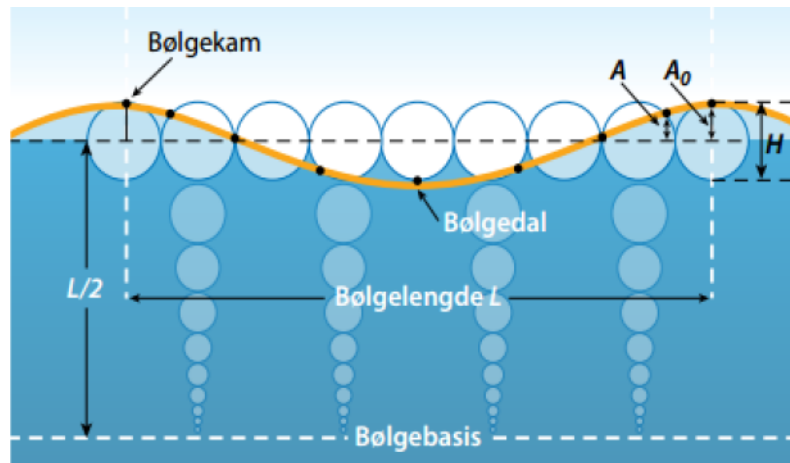
Figure 3.3: Motion of water particles relative to water depth (Lundby (2013), p. 48)

In figure 3.3 it is seen that the wave motion subsides with the water depth. The effect of the wave is gone for depths larger than half of the wave length, in other words for depths larger than L/2.

3.3 Current Loads

The chapter about current is also adapted from the author's Project Work (Kjelsaas, 2015), and include section 3.3.1 in addition to the text below.

The current in the Sognefjord is important to take into account. For slender structures, there are several aspects in connection to current that are of importance. VIV is one of the most essential effects that originates from a current affecting the object.

3.3.1 Vortex Induced Vibrations (VIV)

A slender marine structure in a current may be subjected to VIV. This effect will make the structure vibrate when it is exposed to a flow perpendicular to the cylinder axis. The effect can give vibrations orthogonal to the incoming current, called cross-flow, or vibrations in the same

direction as the flow, in-line (Larsen, 2015). The vibration of the structure is caused by the vortex shedding behind the structure. For the bundle it will be important to consider VIV for the installation procedure.

It is important to be able to control VIV if the structure may be affected by it. When the structure vibrates, it can suffer from fatigue damage due to dynamic bending stresses. In addition, the "effective" diameter of the structure will increase when vibrating. This will cause the drag force to increase, which will give larger static forces (Larsen (2015), p. 4).

VIV can be calculated using Computational Fluid Dynamics (CFD) or empirical models (Larsen, 2015). It is the Reynolds number and the Strouhal number that will define the vortex pattern and vortex shedding frequency respectively. Experiments have shown that the Strouhal number, shown in equation (3.5), are largely dependent on the surface roughness (Larsen, 2015). It is thus important to know the roughness of the structure studied.

$$St = \frac{f_v D}{U} \tag{3.5}$$

In this equation f_v is the vortex shedding frequency, D is the diameter of the cylinder and U is the velocity of the current. The vortex shedding frequency is therefore also important, because if increased, it will lead to increased fatigue (Larsen, 2015). The vortex shedding frequency of the system can be calculated by solving the equation above with respect to f_v. The Strouhal number can be found by figures. Figure 6.26 in "Sea Loads on Ships and Offshore Structures" by O.M. Faltinsen (Faltinsen (1990), p. 207) shows the Strouhal number for different Reynolds numbers. The figure is for a fixed circular cylinder in steady flow.

3.3.2   Added Mass and Drag Coefficients

A structure can be categorized in areas dominated by drag responses, mass responses or diffraction responses (Faltinsen, 1990). Current can represent a large part of the loading on a structure that is drag dominated. For cases where the natural period of a drag-dominated structure move towards the energetic wave frequency band, the non-linearized drag term of the Morison equation can shift frequency (Haver, 2011). This means that although the natural frequency of the structure is far away from the frequency of the waves, ω, it can still give large

responses for 2ω, 3ω, and so on. Therefore it is important to consider the multiplication of the eigenfrequency for these types of structures, that is, the dynamic amplification of the response (Haver, 2011). If the structure is dominated by mass forces, the non-linear drag term of the Morison equation can be linearized, and the problem can be modeled as linear (Haver, 2011).

In order to find the added mass and drag coefficients of a structure, it is necessary to know the cross section geometry. The geometry of the bundle studied in this Master's Thesis is as a combination of a circle and a triangle, a shape which is not easy to find the coefficients for. As a result of this, both the coefficients for circles and triangles will be described in this section.

For a circular bundle, DNV-RP-H103 Appendix A can be used to find the values for the added mass coefficients. The equation for added mass per unit length is given as shown below, equation 3.6 (DNV GL, 2011c).

$$A_{ij} = \rho C_A A_R \tag{3.6}$$

In this equation C_A is the added mass coefficient, and A_R is the reference area. For a circular bundle, the properties given in table 3.1 will apply (DNV GL, 2011c). These are valid for two-dimensional bodies. For a circular cylinder with its axis parallel to the incoming flow, the drag coefficient can be put to 0.99 (DNV GL, 2011c).

Table 3.1: Properties for added mass for a circular bundle (DNV GL, 2011c)

Parameter	Value
C_A $[-]$	1.0
A_R $[m^2]$	πa^2
Added mass moment of inertia $[(kg/m) \cdot m^2]$	0

In order to find the drag coefficients, it is necessary to know the Reynolds number and the surface roughness of the structure. The Reynolds number can be calculated as shown in equation 3.7 below (DNV GL, 2011c).

$$Rn = \frac{UD}{\nu} \tag{3.7}$$

In this equation, U is the current speed, D is the length of the side of the structure which the current is crossing, and v is the kinematic viscosity. Furthermore to find the drag coefficients, the surface roughness must be calculated. The surface roughness can be calculated by equation 3.8 given below (Faltinsen (1990) p. 177).

$$Roughness = \frac{k}{D} \tag{3.8}$$

In this equation, k is the height of the surface roughness and D is the diameter of the structure.

For a calculated Reynolds number and the roughness of the structure, the drag coefficient C_D can be found from experimental values on circular cylinders. Figure 6.3 is found from "Sea Loads on Ships and Offshore Structures" by Faltingsen (Faltinsen (1990)), and shows values of C_D for different Reynolds numbers and surface roughness, and will be used for finding the values for C_D on the circular bundle.

For an equilateral triangular rod with Reynolds number larger than 10^4, the drag coefficient will vary from 1.5 to 2.0 dependent on the direction of the triangle (Cengel and Cimbala, 2010). The figure below, figure 3.4, the two different orientations are seen. With a current flow coming in from the left and to the right, orientation 1 will give the drag coefficient of 1.5, and orientation 2 will give the drag coefficient of 2.0.
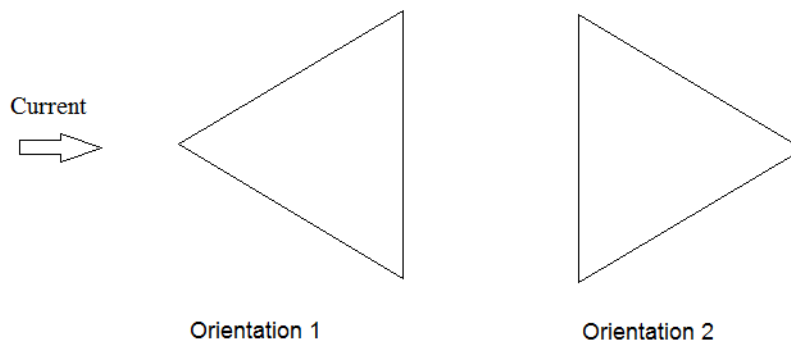
Figure 3.4: Orientation of triangles in relation to drag coefficient (Cengel and Cimbala (2010), p. 595)

In order to find the added mass of the triangular bundle, some simplifications were done. Due to lack of information about a triangular shape and its added mass, a tilted square shape was used instead. The coefficients of this shape was found in DNV-RP-H103 (DNV GL, 2011c).

3.4 Submerged Towing

Towing is in general used to transport different objects that can float by themselves. These objects are transported using one or several tugs or barges, depending on the type of structure that needs to be transported. Submerged towing is mainly used for long slender structures or subsea modules (Larsen, 2016).

There are differences in towing objects inshore and offshore. Offshore there will not be any restrictions to the towing range to the sides. This makes it possible to have a relatively high speed and long towing lines (Larsen, 2016). The towing configuration offshore can be as shown in figure 3.5, which shows the offshore towing of Heidrun TLP (Larsen, 2016).
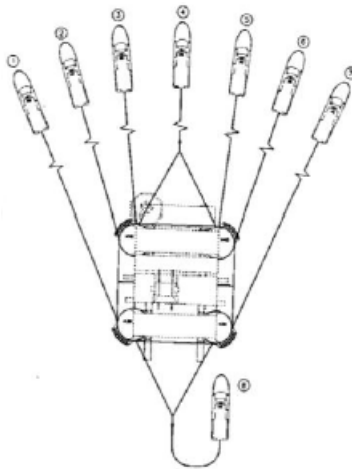
Figure 3.5: Offshore Towing of Heidrun TLP (Larsen, 2016)

For inshore tow, the sideways displacement of the object is of more importance, due to the restricted area. For this type of towing, the speed must be lower than for offshore as well as shorter towing lines (Larsen, 2016). In figure 3.6 given below, the inshore towing configuration of Heidrun TLP can be seen.
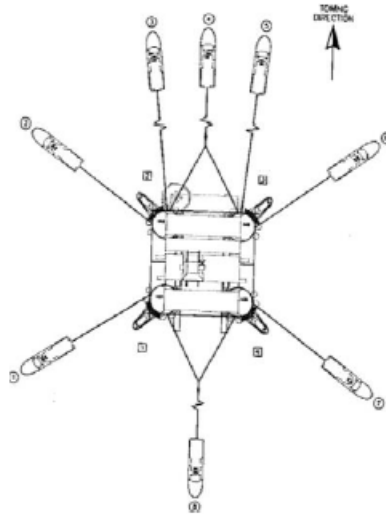
Figure 3.6: Inshore Towing of Heidrun TLP (Larsen, 2016)

The objects involved in the towing operation will be exposed to several loads. The most important loads that act during towing are loads from waves, wind and current (Larsen, 2016). Especially the effect of VIV is important to take into account.

As seen in the literature review, submerged towing can be separated into several phases, depending on the depth at the current location. These phases differ in which depth the object is towed at in the water. In shallow water, the object can be towed either in surface tow or near surface tow. In these configurations it is often required that there are additional buoyancy given to the object (da Cruz and Davidson, 2006). This extra bouyancy must be removed before the next stage of the submerged tow. For slender structures towed in this configuration, it is important to consider wave loads (Larsen, 2016). This is because the structure is so close to the surface that the forces from the waves can be large.

Another configuration is the off bottom mode, usually used for the first stage of an offshore tow (da Cruz and Davidson, 2006). At this stage, the usual practice is to attach ballast chains at regular intervals to overcome the excess buoyancy. An illustration of this configuration is shown in figure 3.7 (da Cruz and Davidson, 2006).
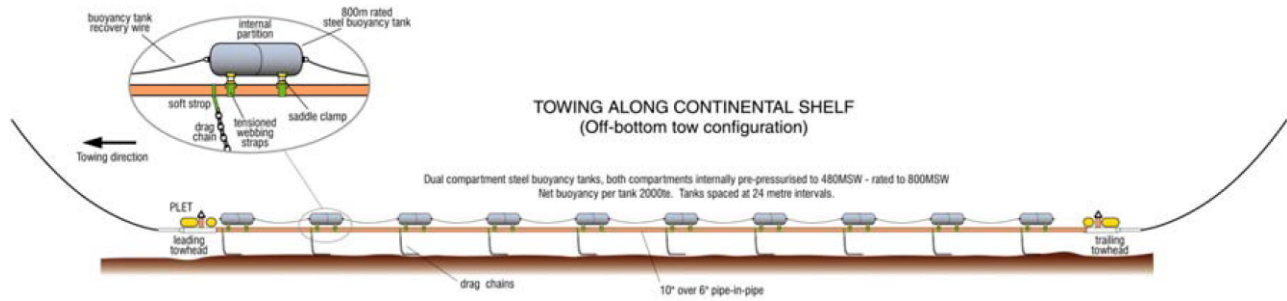
Figure 3.7: Submerged towing in off bottom mode (da Cruz and Davidson, 2006)

The next stage is the CDTM, where the object is lifted of off the sea bed. Usually the object will be neutral in the water, and not subjected to any wave motion (da Cruz and Davidson, 2006). For structures towed in this configuration, it is important to take lift effects into account (Larsen, 2016). Figure 3.8 shows the different configurations used in submerged towing (Larsen, 2016). The first two show the configuration when towing close to the sea surface, the third shows CDTM, and the last configuration is the off bottom tow.
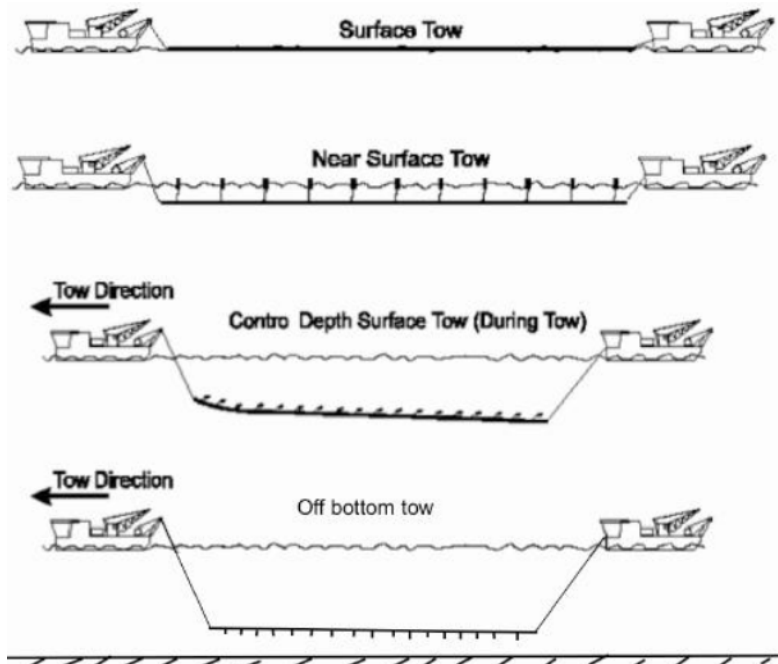
Figure 3.8: Different submerged towing configurations (Larsen, 2016)

3.5 Statistical Response - Extreme Value Distribution

In order to find the statistical response of a given sample of responses, it can be useful to plot the results as an extreme value distribution in a probability paper. The principle behind plotting results in a probability paper, is to introduce the relevant transformation of the axes so that the plotted distribution is linear (Leira, 2015). The Gumbel distribution is often used for this purpose. The cumulative distribution function for the Gumbel distribution is given in equation 3.9 (Haver, 2011).

$$F_{Y_m}(y) = exp\left[-exp\left[-\frac{y-\alpha}{\beta}\right]\right] \tag{3.9}$$

The parameters used in the cumulative distribution function for the Gumbel distribution should be estimated by the principle of moments. By using the principle of moments, the parameters can be estimated as given in equation 3.10 and 3.11 (Haver, 2011).

$$\hat{\beta} = 0.7797s \tag{3.10}$$

$$\hat{\alpha} = \bar{y} - 0.57722\hat{\beta} \tag{3.11}$$

It is seen from these equations that the parameters are linear functions of the mean and the standard deviation of the sample. In order to plot the distribution as a Gumbel distribution, the cumulative distribution function is linearized as shown in equation (3.12) below.

$$-ln\left[-ln\left[F_{Y_m}(y)\right]\right] = \frac{y-\alpha}{\beta} \tag{3.12}$$

The next step is to sort the sample of maximum responses, Y_m, in increasing order. Then the probability of each response, $F_{Y_m}(y)$ is given as the order number of the response, i, divided by the total number of responses in the sample, n, as seen in equation (3.13) (Leira, 2015).

$$F_{Y_m}(y) = \frac{i}{n} \tag{3.13}$$

The value of this is put into the linearized equation of the Gumbel cumulative distribution

function, which is plotted as a line. Then each of the sample values are plotted in to the graph. By using the calculated values for α and β, the sample values are linearized by the right hand side of equation (3.12). It can then be seen how good the distribution fits the given sample points, which will reveal whether the choice of distribution might be correct or not (Leira, 2015).

3.6   Loads During Transportation and Installation

Altogether it is found that the wave loads and the current will cause the most significant responses on the bundle. From the wave loads, slow drift motions can affect the bundle during both transportation and installation. Additionally, it is found that the wave motion will move downwards into the depth, such that submerged towed object can still be affected by wave loads. However, the wave motion will be totally extinguished for a certain depth, such that submerged towing can potentially avoid all wave loads.

For the submerged towing the theory highlights that the loads coming from the waves, wind and current are the most significant. There are direct wave loads for towing close to the sea surface, and in addition the motion of the towing vessels may impact the towed object. Finally, effects of VIV from the current is important to consider in connection to fatigue.

Chapter 4

Theory and Calculations based on Rules

4.1 Introduction

For the different parts of the project related to the Artificial Seabed, a GAP analysis has been conducted on the rules and regulations that apply (Engineering Department, Deep Ocean, 2015).   For the transport and the installation of the bundles, the GAP-analysis has recommended five relevant standards that will be studied in this section:

1. DNV-OS-H101 Marine Operations, General.

2. DNV-RP-H103 Modelling and Analysis of Marine Operations

3. DNV-OS-C301 Stability and Watertight Integrity

4. DNV-RP-C205 Environmental Conditions and Environmental Loads

5. DNV-OS-H202 Sea Transports

The "DNV-RP-H103 Modelling and Analysis of Marine Operations" and "DNV-RP-C205 Environmental Conditions and Environmental Loads" are of direct relevancy to this study, and will be covered in detail. The other regulations will be covered shortly here.

The "DNV-OS-H101 Marine Operations, General" applies for the planning of, the preparation of and the performance of marine operations (DNV GL, 2011b). The standard contains five main aspects, including planning, environmental conditions, operational

requirements, stability requirements and systems, equipment and vessels. The Offshore Standard from DNV GL, DNV-OS-C301 *Stability and Watertight Integrity* (DNV GL, 2011a), covers equations and rules related to stability of mobile offshore units and floating offshore installations. This standard is very specific for the stability terms, should be studied closer in relation to the optimization of the bundle geometry and shape.

The Offshore Standard DNV-OS-H202 (DNV GL, 2015) is about sea transportation and gives information about both the preparations before an operation, as well as the requirements for the towed objects and the tugs. It states that for submerged towing the standard DNV-RP-H103 will complement this standard. Section 4 in this standard is about towing. In connection to clearances it is stated that for the towing vessel and the object it should be 5 meters for inshore tow and 10 meters for offshore tow (DNV GL, 2015). In relation to the width of the towing area, this should at a minimum be three times the width of the object being towed. In addition there should be enough space for tow yaw.

4.2 Marine Operations: DNV-RP-H103

The Recommended Practice from DNV GL called "Modelling and Analysis of Marine operations" (DNV GL, 2011c) includes relevant rules for transportation and installation of the bundles for this project. Chapter 7 is about Towing operations, and includes the relevant practices for the transportation of the bundles.

4.2.1 Wave Loads

First, the recommended practice covers wave loads on different structures. For a structure that is situated offshore, it is usually stated as either a large volume or a small volume structure (DNV GL, 2011c). This is important because the size of the structure relative to the wave conditions will affect which load components that are dominating. The diffraction forces are important for large volume structures, and drag- and inertia forces are relevant for small volume structures. Figure 4.1 below shows an illustration of the different force regimes, and can be utilized to find which regime a specific structure is in.
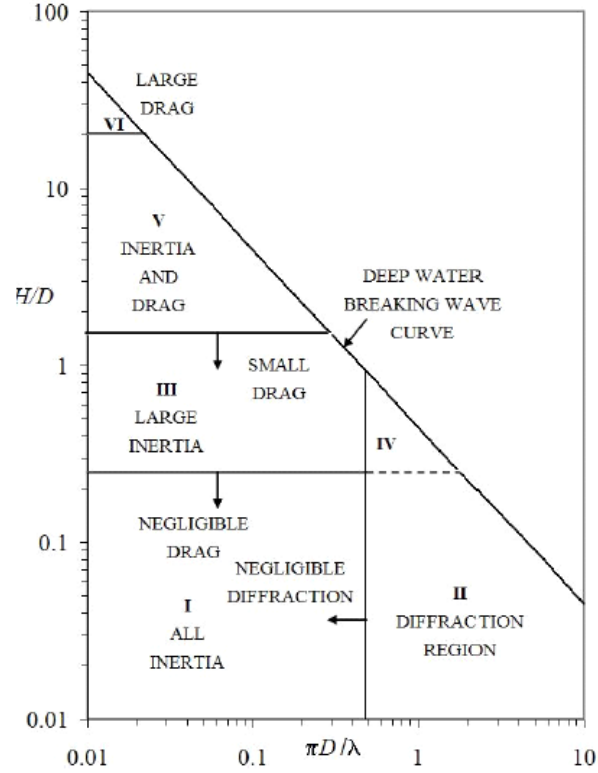
Figure 4.1: Illustration of the different force regimes from waves (DNV GL, 2011c)

Furthermore, the important force coefficients are stated. Equation 4.1 below gives the drag coefficient, C_D (DNV GL, 2011c). This expression is a non-dimensional expression.

$$C_D = \frac{f_{drag}}{\frac{1}{2}\rho D v^2} \tag{4.1}$$

In this equation f_{drag} is the drag force per meter, ρ is the density of the water, D is the diameter of the structure, while v is the current velocity. Another important force coefficient is the added mass coefficient, C_A. This is shown in equation 4.2 below, which also is non-dimensional (DNV GL, 2011c).

$$C_A = \frac{m_a}{\rho A} \tag{4.2}$$

From the terms given here, m_a is the added mass given per meter and A is the area of the structure's cross section. Additionally, the mass coefficient is found by using the added mass coefficient, as shown in equation 4.3 below (DNV GL, 2011c).

$$C_M = 1 + C_A \tag{4.3}$$

Finally, the lift coefficient is defined as given in equation 4.4 below (DNV GL, 2011c). As can be seen from the equation, it is comparable with the equation for the drag coefficient. In this equation f_{lift} is the lift force given per meter length.

$$C_L = \frac{f_{lift}}{\frac{1}{2}\rho D v^2} \tag{4.4}$$

The next chapter that will be studied in this regulation is chapter 7, which covers relevant aspects in connection to towing operations.

4.2.2   Towing Operations - General

The first requirements in a towing operation is connected to the environment, giving either weather restricted operations or unrestricted operations (DNV GL, 2011c). According to the recommended practice, an operational window less than 72 hours is classified as restricted. In order to calculate the operation reference period, the planned operation time and the estimated contingency time should be included, as given in equation 4.5 (DNV GL, 2011c).

$$T_R = T_{POP} + T_C \tag{4.5}$$

In this equation T_R is the operation reference period, T_{POP} is the planned operation period and T_C is the estimated contingency time (DNV GL, 2011c). Although operations over 72 hours usually are called unrestricted, these operations can be restricted if certain requirements are fulfilled. These requirements include continuous observations of weather and forecast, safe spots on the route, as well as the system must satisfy the requirements for accidental limit state (ALS) for unrestricted weather conditions (DNV GL (2011c), p. 104). Furthermore, it is stated that the operations lasting more than 72 hours that are classified as unrestricted must use the extreme value statistics as basis for calculating the environmental criteria.

4.2.3 Dynamic Effects of Towing Lines

In order to analyze the dynamic responses of the towing line, it is necessary to know the behavior of both the tug and the object being towed. Both objects must be analyzed in the same sea state to find the correct response of the towing line in the chosen sea state (DNV GL, 2011c). In order to find the dynamics, the problem can be solved in the frequency domain or in the time domain. Both methods will have advantages and disadvantages. For calculations in the frequency domain it is necessary to linearize the model. This will make it quick to calculate, but leave the nonlinear effects out. For calculations in the time domain, nonlinearities are included (DNV GL, 2011c).

According to the recommended practice will a frequency domain analysis give sufficient results for the relative motion between the tug and the object (DNV GL, 2011c). This is because linear equations can describe the system reasonably well, due to small influence from the towing line regarding first order wave induced response.

If modeling the system in a non-linear finite element method (FEM) analysis program, the analysis conducted will be a nonlinear time domain analysis (DNV GL, 2011c). This will thus include the non-linear effects.

4.2.4 Submerged Towing

Chapter 7.3 in DNV-RP-H103 (DNV GL, 2011c) covers submerged towing, and the focus of the section will be on the towing phase to the offshore site. As given in the chapter, the critical parameters of this stage include vessel motion characteristics, wire properties, towing speed, route, stability of towed object, forces in towing wire and corresponding elements, clearance between object and vessel, VIV, lift effects and wave loads (DNV GL (2011c), p. 116). Consequently, a time domain analysis is required in order to cover all the effects.

The section of most interest is section 7.3.5, "Tow of long slender elements" (DNV GL, 2011c). The Recommended Practice supports three methods for submerged towing, which are off bottom tow, CDTM and methods for surface tow. The given parameters that influence the tow configuration are submerged weight in water, temporary buoyancy or weight, tow speed and length of towing line, back tension caused by trailing tug and drag loads (DNV GL (2011c),

p. 118). In order to retain control of the towed object, it is important to monitor the lift effects and the stability of the object. By towing the object deep enough in the water to avoid direct wave loads, fatigue loading might be avoided.

In order to model and analyze the system, it is recommended to calculate the transfer function and hydrodynamic coefficient corresponding to six degrees of freedom (DNV GL, 2011c). As for the towed object, it is important to model it correctly to catch the dynamic effects. Therefore the object should be modeled using Morison elements. The important issue for long slender structures is effect of VIV, and this should be analyzed by finding the global behavior under dynamic loading (DNV GL (2011c), p. 119).

If it is found that VIV might be a problem and should be considered, the eigenmodes of the object should be found using a FEM program (DNV GL, 2011c). If the results from this analysis show that there are eigenmodes close to the vortex shedding frequency, more thorough studies should be conducted. For calculating the first natural frequency, equation 4.6 given below (DNV GL, 2011c), for a simply supported beam can be used.

$$f_1 = 1.57 \sqrt{\frac{EI}{m'L^4} \left[1 + 0.8 \left(\frac{\delta}{D} \right)^2 \right]}$$ (4.6)

Here EI represent the bending stiffness, m' the total mass per unit length, L the span length and D is the characteristic cross-sectional diameter. The static deflection is given by δ, and can be calculated as given in equation 4.7 (DNV GL, 2011c).

$$\delta = \frac{5}{384} \frac{qL^4}{EI}$$ (4.7)

In DNV-RP-H103 it is stated that only 10 % of the allowable fatigue damage can be used during installation (DNV GL, 2011c). It must be documented if the structure is affected by VIV, or the properties should be altered to avoid it. To find the important effects acting on the structure, a three hour time domain analysis should be conducted (DNV GL (2011c), p. 119-120). The results should be verified for criteria in connection with the critical parameters mentioned previously.

The towed object can be put down to the sea bed, if the weather conditions become bad during transportation (DNV GL, 2011c). The usual practice for this is to attach anchors at the

end of the structure and ballast chains that will cause friction forces against the sea bed. This will keep the structure stable even when exposed to current. Figure 4.2 below shows a bundle being towed and in off bottom mode.
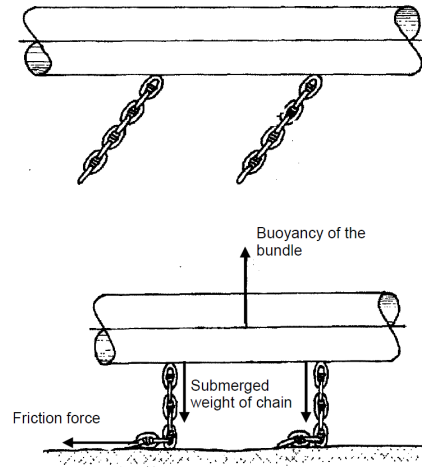
Figure 4.2: Bundle being towed and in off bottom mode (DNV GL, 2011c)

4.3   Environmental Loads: DNV-RP-C205

The recommended practice from DNV GL, DNV-RP-C205 *Environmental Conditions and Environmental Loads*, is created in order to give guidelines in connection to predictions of the environmental conditions, as well as assist when calculating the loads from the environments.

4.3.1   Wave Conditions

Chapter 3 in this recommended practice covers Wave Conditions. As given in this chapter, if a structure has quasi-static response, it will be adequate to use deterministic regular waves (DNV GL, 2007). Furthermore, it is stated that the characteristic values to be used to define the wave for the quasi-static analysis, can be found from statistical methods. However, structures that are dominated by dynamic response must be analyzed with waves based on stochastic modeling (DNV GL, 2007).

According to C205, the characteristics of the wave will decide which wave theory that needs to be used for the specific problem (DNV GL, 2007).   Figure 4.3 below shows different requirements for the various wave theories that can be utilized.
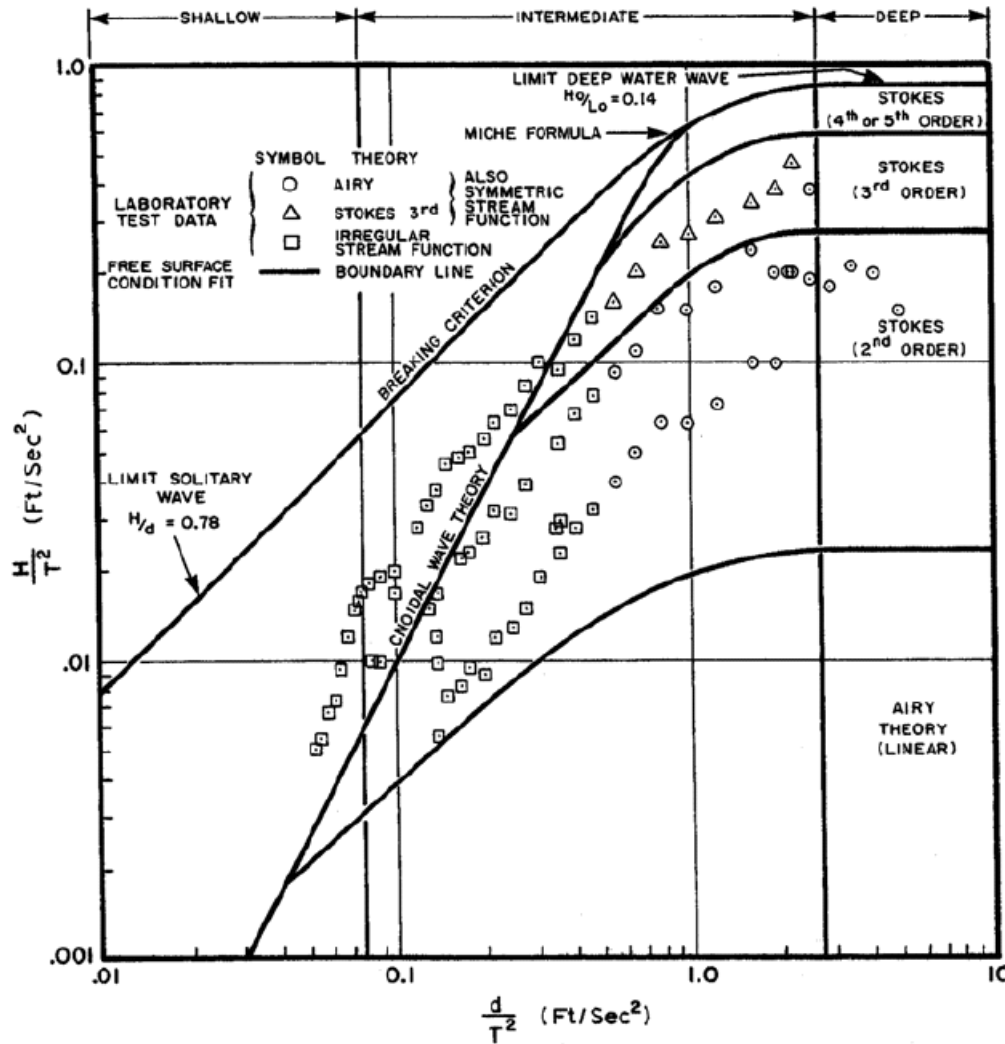
Figure 4.3: Limitations and requirements for different wave theories (DNV GL (2007))

The different wave theories in this figure cover Airy Theory (linear theory), Stokes 2nd order, Stokes 3rd order and Stokes 4th or 5th order. Airy Theory is the most basic wave theory, and assumes that, compared to the wave length and the water depth, the wave height is small (DNV GL, 2007). The Stoke wave theory cover the wave theory from 2nd order and up to 5th theory. According to the recommended practice, the Stoke Wave theory is an expansion of the waves, as the surface elevation raised to the linear wave height. For that reason, a Stoke first order wave is equal an Airy Wave.

4.3.2 Current

In Chapter 4 in DNV-RP-C205 (DNV GL, 2007), the recommended practice when it comes to current and tide is explained. It is stated in the chapter that the main aspects that current can influence on a long slender and submerged structure are drag- and lift forces and VIV.

Chapter 6, *Wave and Current Induced Loads on Slender Members*, is important for structures such as the bundle in this study. It is stated that the Morison's load formula can be used on structures with diameter sufficiently smaller than the wave length, see equation 4.8 (DNV GL, 2007).

$$\lambda > 5D \tag{4.8}$$

Furthermore, it is stated that for long slender structures with length that largely exceeds the transverse dimensions, it is not necessary to take the end-effects into account (DNV GL, 2007).

Chapter 5

Theory of Sima Riflex

The computer program Sima Riflex was also utilized for the author's Project Work, "Structural Response of Submerged Floating Tunnels Exposed to Current and Waves", and this chapter is adapted from this report (Kjelsaas, 2015). However, section 5.4 is added specifically for this report.

Sima Riflex is a computer program for analyzing slender marine structures. A marine structure that is defined as slender can have big deflections as well as small bending stiffness (Marintek, 2015). Riflex is a subprogram of the main program SIMA. SIMA consists of three subprograms, which are Simo, Riflex and Simla (Moxnes, 2011). These subprograms can interact with each other, making this program suitable for all stages of an analysis. Riflex is used for modeling and analyzing the bundle in this study.

For the structural analysis, Riflex uses the finite element method (Marintek, 2015). The finite element method solves the equations by a numerical approach, resulting in an approximate solution. The equations represents the physical problem that needs to be solved, and is only valid on a small element (Ottosen and Petersson, 1992).

The three different analyses that will be run with Riflex are a static finite element analysis, a dynamic time domain analysis and an eigenvalue analysis. The theory behind each of these analyses will be described in this chapter.

5.1 Static Finite Element Analysis

A static finite element analysis is necessary to conduct in order to find all the nodal displacements, such that the system is in static equilibrium (Marintek, 2015). This is found when the internal and the external forces are equal to each other, equation (5.1).

$$R_{ext} = R_{int} \tag{5.1}$$

In the Riflex Theory Manual (Marintek, 2015), it says that Riflex uses the Incremental-Iterative procedure with Euler-Cauchy incrementation in order to find the static equilibrium of the problem. The Euler-Cauchy method is an incremental method that stepwise apply the external loading. For each of these load steps, the displacement increment is calculated (Moan, 2003). The incremental stiffness matrix is calculated from the previous load step, and kept constant over the new increment. In equation (5.2) the incremental equation of equilibrium is given, with dR as stepwise external loading, dr as displacement increment, and $K_I(r)$ as incremental stiffness (Moan, 2003).

$$K_I(r)dr = dR \tag{5.2}$$

The method uses the information on the previous load step in order to find the static configuration at the next step. The starting point is then the stressfree configuration, and the loads will be put on the structure incrementally. This will introduce an error in the solution, because the incremental stiffness matrix calculated from step k is staken as the incremental stiffness for step k+1. This can be seen in figure 5.1, found from *TMR4190 Finite Element Modelling and Analysis of Marine Structures* by Torgeir Moan (Moan (2003), p. 12.49). In this illustration the error is seen as the difference between the true graph and the graph from the Euler-Cauchy method. So the method does not fulfill the static equilibrium equation, and thus not fulfill total equilibrium (Moan, 2003).
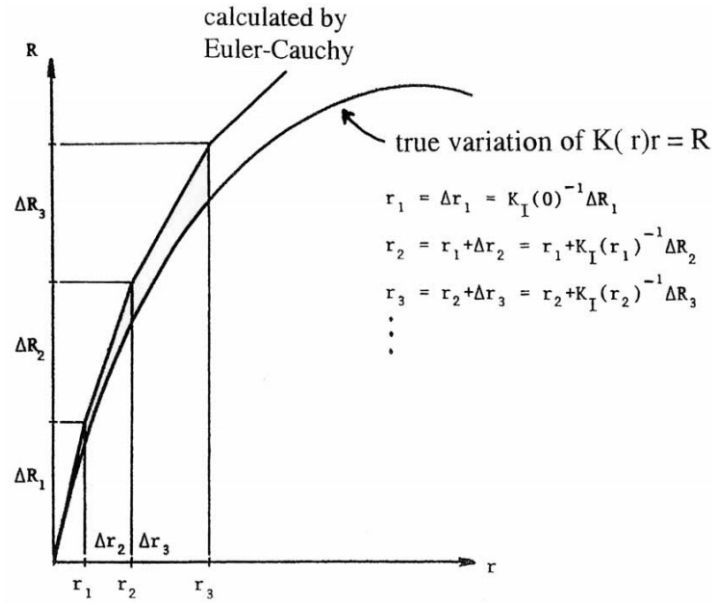
Figure 5.1: Representation of the Euler-Cauchy method (Moan (2003), p. 12.49)

In order to correct this difference and move closer to the real solution, Sima Riflex introduces a force imbalance vector, as given in equation (5.3) (Marintek, 2015).

$$R_k(r) = R_k^S(r) - R_k^E(r) \tag{5.3}$$

An iterative procedure is introduced in order to improve the result. Sima Riflex uses the Newton-Raphson method, because it has a quadratic convergency rate (Marintek, 2015). The Newton-Raphson algorithm is given by equation (5.4) (Marintek, 2015).

$$x_{n+1} = x_n - \frac{f(x_n)}{f'(x_n)} \tag{5.4}$$

We have the configuration at load step k, that $R_{Int}^k = R_{Ext}^k$, but we want the same balance for the unknown configuration at load step k+1. This method goes forth by estimating the internal reaction forces at load step k+1 based on the information at load step k. This will give an unbalanced force, and it is necessary to do iterations in order to find this balance. The iterative procedure is continued until balance is achieved, and we have $R_{Int}^{k+1} = R_{Ext}^{k+1}$ (Sævik, 2015). Equation (5.5) and (5.6) gives the iteration steps for this method, given as the displacement vector for the load step j (Marintek, 2015).

$$\Delta r_k{}^j = \left[\frac{\partial R_{k-1}}{\partial r} \right]^{-1} R_k{}^{j-1} \tag{5.5}$$

$$r_k{}^j = r_k{}^{j-1} - \Delta r_k{}^j \tag{5.6}$$

To get a satisfactory result will the solution for each load step be compared with a predefined tolerance criterion. The iteration process will stop when the criterion or the maximum number of iterations is reached(Marintek, 2015).

5.2   Dynamic Analysis

The dynamic analysis will find the responses of the structure when it is exposed to a predefined sea state. This analysis allows the dynamic equilibrium equations to be solved step by step, which will include the important nonlinear features (Marintek, 2015). For this type of analysis the equation of equilibrium now consists of an inertia force, a damping force, an internal structural reaction force, and the external force. All these forces are dependent on the displacement, velocity and acceleration of the system, see equation (5.7) (Marintek, 2015).

$$R^I(r, \ddot{r}, t) + R^D(r, \dot{r}, t) + R^S(r, t) = R^E(r, \dot{r}, t) \tag{5.7}$$

Due to the inertia force and the damping force being dependent on the displacement, this system of equations will be nonlinear. In addition, the external force is also dependent on the displacement and the velocity. In equation (5.7), the inertia force is found from equation (5.8) (Marintek, 2015). As seen will this expression be dependent on the structural mass, M^S, the mass matrix that accounts for the internal fluids, M^F, and the mass matrix taking the hydrodynamic mass into account, M^H.

$$R^I(r, \ddot{r}, t) = \left[M^S + M^F(r) + M^H(r) \right] \ddot{r} \tag{5.8}$$

The damping force in equation (5.7) is expressed as shown in equation (5.9) below (Marintek, 2015). This expression is dependent of the internal structural damping, C^S, the

damping from hydrodynamics, C^H and also the damping matrix for physical dampers on the structure, dashpot dampers, C^D.

$$R^D(r, \ddot{r}) = \left[C^S(r) + C^H(r) + C^D(r) \right] \dot{r} \tag{5.9}$$

According to Riflex Theory Manual (Marintek, 2015), there are certain nonlinear effects that are especially important to take into account for this type of analyses. The geometric stiffness is important for nonlinear deformation, because it accounts for the additional stiffness that occur. When a material is deformed this way, the nonlinear material properties are also of significance.

Sima Riflex has three different approaches for solving nonlinear systems, which are nonlinear time domain analysis, linearized time domain analysis and frequency domain analysis. These are explained shortly in the following.

Nonlinear Time Domain Analysis

This approach uses a step by step numerical time integration in order to solve the problem. It starts by dividing the total required time interval into sub-intervals of equal length. The method is based on that the start values at the beginning of the interval is known. Then a certain development over the interval can be assumed for these values. On this way we will get an approximate solution at the given points that represent the time sub-intervals (Langen and Sigbjörnsson, 2007).

Sima Riflex uses the Newmark β-family as the method for numerical time integration. This method has two integral equations, called the Newmark's general integral equations, and are given in (5.10) and (5.11) (Langen and Sigbjörnsson, 2007).

$$\dot{u}_{k+1} = \dot{u}_k + (1 - \lambda) h \ddot{u}_k + \lambda h \ddot{u}_{k+1} \tag{5.10}$$

$$u_{k+1} = u_k + h \ddot{u}_k + \left(\frac{1}{2} - \beta \right) h^2 \ddot{u}_k + \beta h^2 \ddot{u}_{k+1} \tag{5.11}$$

Where h represents the load step, λ and β the weighting terms that are determined from requirements of accuracy and stability. The Newmark β-family method is unconditionally stable for

$$\lambda \geqslant \frac{1}{2} \tag{5.12}$$

$$\beta \geqslant \frac{1}{4}\left(\lambda + \frac{1}{2}\right)^2 \tag{5.13}$$

(Langen and Sigbjörnsson, 2007).

Linearized Time Domain Analysis

This approach also uses a step by step numerical integration, but by linearizing the mass, damping and stiffness matrices at the point of static equilibrium (Marintek, 2015). Thus will these matrices be kept constant during the analysis, and this will give a large reduction in computation time compared with the unlinearized approach. The external loads can however be kept nonlinear. Normally the required accuracy is obtained for the coupling between external loads and structural velocity by using the information of previous steps (Marintek, 2015)

Frequency Domain Analysis

The equation of motion is usually given as a function of time. The excitations in these systems are harmonic, and they can therefore be expressed as a sum of harmonic components that are functions of the frequency, ω. The Fourier-transformation is usually used for this purpose. The same is done for the response of the system, in order to get this as a function of frequency as well (Langen and Sigbjörnsson, 2007). When the system is written as a function of frequency, it can be written on complex form, where only the real part is considered. Then the properties of the complex function can be taken advantage of in order to solve the system.

5.3 Eigenvalue Analysis

In order to find the natural frequencies of a structure, an eigenvalue analysis should be conducted. This will also give the corresponding mode shapes, which will show how the structure will behave when exposed to dynamic loading (Gracewski, 2009). The eigenfrequency

of a beam is given by equation (5.14) (Larsen, 2014). In this equation m represents the mass and k represents the stiffness of the beam.

$$\omega_0 = \sqrt{\frac{k}{m}} \tag{5.14}$$

5.4   Ship Motion Characteristics

The towing tug motion will depend on the sea state and the corresponding responses of the tugs. This must be considered for the towing of the bundle. In order to describe and measure the motion of the vessels, a transfer function will be used. The transfer function represents the response amplitude of the structure per unit wave amplitude (Faltinsen, 1990). The transfer function will be dependent on the frequency of oscillation. There are six transfer functions, one for each degree of freedom for a vessel. These degrees of freedom are surge, sway, heave, roll, pitch, and yaw (Marintek, 2015). Usually it is necessary to calculate the transfer functions for coupled motions, which must then include the phase angle. The phase angle represents the phase shift between the incoming wave and the motion of the structure. According to the Riflex Theory Manual, it is necessary with the relation between the harmonic waves and the linear response of the structure in order to find the transfer function (Marintek, 2015). Equation (5.15) gives the physical relationship between the incoming waves and the response (Marintek, 2015).

$$X(t) = R_X \zeta_a sin(\omega t + \phi_X) \tag{5.15}$$

Then the transfer function will be the response amplitude of the structure per unit wave amplitude, as given in equation (5.16).

$$R_X = X_a / \zeta_a \tag{5.16}$$

A Response Amplitude Operator (RAO) must be entered into Sima Riflex for the vessels. This file will include the information about the transfer functions for all the degrees of freedom for the given vessel.

Chapter 6

Modeling

This chapter contains the information about the analysis conducted in Sima Riflex in connection with the Master's Thesis. The background for the decisions regarding the parameters and input data are presented, as well as the modeling approach in Sima Riflex.

6.1   Background of the Analysis

The towing will start at the production site in Scotland, and will not end until the bundles arrive at the installation point in the Sognefjord. From start until the end of the towing, it will go more than 72 hours. As mentioned in chapter 4.2.2, this is a towing operation that should be characterized as unrestricted, as it will last for more than 72 hours. As a consequence of this, the environmental criteria for this operation should be based on the extreme value statistics. For this study the environmental data from SINTEF will be used.

Furthermore, a static calculation will be conducted in Sima Riflex for both the transportation and the installation phase. This will be the basis for further calculations of the dynamic response. A time domain analysis in irregular sea will be conducted in order to give sufficient results for dynamics.

As found in chapter 4, the model should be analyzed using FEM and Morison elements. The Morison equation is utilized by Sima Riflex in order to calculate the hydrodynamic forces (Marintek, 2015). In the analysis one can chose both quadratic and linear drag force coefficients. An eigenvalue analysis will be conducted in order to find the eigenvalues of the structure. If

it is found that these are close to the frequency of the vortex shedding, the structure must be analyzed further for possible VIV during tow, as seen in 4.3.2.

6.2   The Model in Sima Riflex

The computer program Sima Riflex is chosen for this analysis, due to its ability to analyze slender marine structures. Additionally, it is a user friendly computer program that allows the user to see the changes on the model as they are conducted. Furthermore, it is easy to run both static and dynamic analyses in Sima Riflex, and see the results at once.

The model in Sima Riflex consists of the bundle, two towing vessels and towing lines. The bundle is created by two nodal points with a line in between. The line properties will be as for a beam, and is separated into elements of 1 m. At both the end points of the bundle it is a connection to another line, the towing line, which again is connected to the tugs. The information about the RAO for the tugs can be found in Appendix A.3. The towing line should have cross section properties as a bar, since it can only take axial loading. However in order to make the model stable, a bar-beam connection should not be used in Sima Riflex. Thus is the towing line modeled as a beam as well, with its axial stiffness being the dominant stiffness parameter.

6.3   Characteristics of the Model

This section contains the input values used in Sima Riflex to describe the environmental conditions, the properties of the bundle, and the towing lines. The decisions behind the values will be explained and important calculations will be shown in this section. For the more detailed calculations, see Appendix A.

6.3.1   Environmental Values

The Sognefjord is connected with the North Sea, but also to several rivers coming from the high mountains surrounding the fjord (Askheim and Thorsnæs, 2015). This will affect the salinity and the water density in the fjord. Table 6.1 below shows the different densities for the water in

Sognefjorden (Reinertsen, 2014a). The calculations in Sima Riflex will be based on a water density of 1005 $[kg/m^3]$. The choice of this number is based on test runs in Sima Riflex, with water densities of 1005 and 1025 $[kg/m^3]$. The results revealed that the test run with water density of 1005 $[kg/m^3]$ gives the largest values for the forces and moments in the bundle. Although the results did not show any significant differences, a water density of 1005 $[kg/m^3]$ is chosen for this study in order to stay on the conservative side.

Table 6.1: Density of water in Sognefjord (Reinertsen, 2014a)

	Density $[kg/m^3]$
Minimum	1005
Mean	1015
Maximum	1025

The kinematic viscosity v, is chosen from tables for a temperature of 5 degrees and fresh water, and is taken as 1.52E-06 $[m^2/s]$ (DNV GL, 2011c). This is to correspond to the minimum water temperature at 25 meters depth, which is given as 4 degrees Celsius (Reinertsen, 2014a). The kinematic viscosity for fresh water is chosen to be as close to the water density of 1005 $[kg/m^3]$ as possible. In the North Sea, the surface roughness can be estimated as 10 cm due to marine growth, all the way down to 40 m depth (Faltinsen (1990) p. 177).

The values given for the sea state in Sognefjorden is taken from the calculations by SINTEF. For waves induced by wind, table 6.2 shows the specific values (Lothe and Brørs, 2011). The calculations and measurements were conducted for three different locations, point A being north in the fjord, point B in the middle of the fjord and point C to the south of the fjord. The worst sea state is chosen for the modeling in Sima Riflex to keep the results conservative. Consequently the significant wave height of 2.34 m and corresponding peak period of 4.8 s is chosen.

Table 6.2: Wind induced waves in Sognefjorden (Lothe and Brørs, 2011)

	Point A	Point B	Point C
Significant wave height [m]	2.22	2.34	2.13
Peak period [s]	4.6	4.8	4.8

As for current, these data are also based on information given from SINTEF, and can be seen in table 6.3 (Reinertsen, 2014a). It is stated that these data include tide and wind in their calculations. The current move in two directions, in and out of the fjord along with the tide. A safety margin of +0.50 m/s has been added to the current in the top layer, and safety margin of +0.25 m/s has been added to the other results (Lothe and Brørs, 2011). The current values chosen for this study are based on test runs with the the U_{out} values and the U_{in} values. The results from the two runs gave no significant difference in response values. However, due to slightly larger responses with the U_{in} values, these will be used in the study to give the most conservative results.

Table 6.3: Current in the Sognefjord (Reinertsen, 2014a)

Depth [m]	$U_{out}[m/s]$	$U_{mean}[m/s]$	$U_{in}[m/s]$
0-10	-1.06	-0.533	1.27
30	-0.55	0.258	0.48
75	-0.44	0.257	0.39

6.3.2   Area of Bundle

The bundles are made up from three pipes that are tied together, as seen in figure 6.1 below (Reinertsen, 2014c). In this figure it is seen that the cross section resembles a combination of a triangle and a circle. Furthermore, in this illustration the three pipes are not in contact with each other, but is separated by a thin layer of an unspecified material.

Figure 6.1: Cross section of bundle (Reinertsen, 2014c)

In order to create this bundle in Sima Riflex, some simplifications had to be done. The bundle could only be modeled as a circle. In order to get results as comparable to the real situation as possible, it was desired that the properties of the real bundle was transferred to the modeled circular bundle.

As a start, the properties of the real bundle were calculated. This would create the basis in order to transfer them to the circular bundle. Table 6.4 shows the given internal and external diameter of the pipes (Reinertsen, 2014c) and the density of the steel (Reinertsen, 2014b). The bundle should lie neutral in the water with D/t = 30 (Reinertsen, 2014c).

Table 6.4: Properties of bundle (Reinertsen, 2014c) (Reinertsen, 2014b)

Parameter	Value
External diameter of pipe [m]	0.8534
Internal diameter of pipe [m]	0.9144
Density Steel [kg/m^3]	7850

In order to find the correct area of the bundle, some assumptions were made. If the circular bundle would be created out of the area of the real bundle, the height and width would have been smaller than for the real bundle. This would affect the drag and the added mass of the structure, giving smaller values than for the real bundle. Consequently, the conclusion was to model a circular bundle with edges going outside of the real bundle. Furthermore, to simplify the geometry of the problem, it was assumed that the internal pipes would be in contact with each other. This assumption will give a smaller area of the bundle. However, by assuming that the bundle have the area of an external circle outside of the real bundle, the area will be exaggerated. As a result of these assumptions, the geometry given in figure 6.2 is the geometry that is to be calculated for the bundle (Grevstad, 2015).
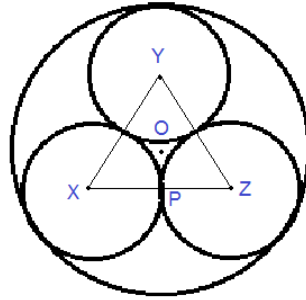
Figure 6.2: Geometry for calculations on the bundle (Grevstad, 2015)

From figure 6.2 it can be seen that the triangle YZP can be used to calculate the length YP. The triangle is shown in the figure 6.3 below.
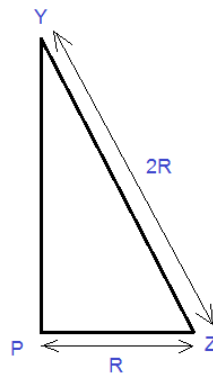
Figure 6.3: Triangle from the bundle geometry

From this figure it is seen that Pythagoras theorem can be used to find YP, as shown in equation 6.1 below. The result is shown in equation 6.2.

$$YP = \sqrt{YZ^2 - PZ^2} \tag{6.1}$$

$$YP = \sqrt{4R^2 - R^2} = \sqrt{3R^2} \tag{6.2}$$

Furthermore, it is necessary to use the triangles XOP and YZP to find the distance OP. Due to the fact that these two triangles share the same angles, this can be taken advantage of. It is seen that the angle $\angle$ PXO and $\angle$ PYZ is the same, due to the fact that the original triangle XYZ is equilateral. Then the relation given in equation 6.3 below is valid, and the distance OP can be expressed as in equation 6.4.

$$\frac{OP}{XP} = \frac{ZP}{YP} \tag{6.3}$$

$$OP = \frac{ZP}{YP}XP = \frac{R}{\sqrt{3R^2}}R = \frac{R}{\sqrt{3}} \tag{6.4}$$

Next the distance XO can be calculated for the triangle XOP by using Pythagoras theorem once again. Equation 6.5 and 6.6 below show the method and the result for calculating XO.

$$XO = \sqrt{OP^2 + XP^2} \tag{6.5}$$

$$XO = \sqrt{\left(\frac{R}{\sqrt{3}}\right)^2 + R^2} \tag{6.6}$$

Finally the radius of the circle containing the three pipes can be calculated as given in equation 6.7 below, which also show the final result.

$$R_{circle} = R + XO = R + \sqrt{\left(\frac{R}{\sqrt{3}}\right)^2 + R^2} = 0.9851m \tag{6.7}$$

The properties of the bundle are seen in table 6.5 below. With a radius of 0.9851 m, the area of the circle becomes 3.05 m^2. The details of the calculation can be found in Appendix A.1.1.

Table 6.5: Properties of modeled circular bundle

Parameter	Value
Radius [m]	0.9851
Area [m^2]	3.05

With a diameter of 1.97 m, a Reynolds number of 7.15E+05, and a current at -30 m depth of 0.48 m/s, the vortex shedding frequency can be calculated as explained in chapter 3.3.1. The vortex shedding period of the bundle then becomes 19.5 s.

6.3.3   Weight and Buoyancy

The bundle is assumed to lie neutral in the water during both tow and installation (Engineering Department, Deep Ocean, 2014). Additional buoyancy can be added with floating pontoons attached to the bundle, and additional weight can be added by applying chains to the bundle. In this study the bundle is basically considered neutral, but with a slightly larger weight than buoyancy. The buoyancy given per meter of the structure were calculated first, with equation 6.8 shown below.

$$B = \rho A \tag{6.8}$$

This was used as the basis for finding the mass per meter of the structure that would result in an almost neutral position of the bundle. The calculated buoyancy and the mass are given in table 6.6 below, please see Appendix A.1.2 for more details. This resulted in a bundle with slightly larger weight than buoyancy.

Table 6.6: Calculated buoyancy and mass of the structure for a neutral position

Parameter	Value
Buoyancy $[kg/m]$	3064.09
Mass $[kg/m]$	3065.26

6.3.4   Strength Calculations

Some of the strength parameters used for the bundles are given in the preliminary work on the project. The values are mostly guidance numbers, but are taken as the basis for the calculations in this Thesis. The material yield stress, elastic modulus and Poisson's ratio are given in table 6.7.

Table 6.7: Material properties of bundles (Reinertsen, 2014a)

Parameter	Value
Yield stress [MPa]	480
Elastic modulus, E [MPa]	207 000
Poisson's Ratio, v [$-$]	0.3

From these values the shear modulus of the structure can be calculated. According to equation 6.9 (Irgens, 2010), the shear modulus is found by using the properties of the elastic modulus and Poisson's ratio.

$$G = \frac{E}{2(1 + v)} \tag{6.9}$$

Furthermore, the stiffness properties are calculated for the bundles. The axial stiffness, bending stiffness and shear stiffness are calculated as shown in equation 6.10, 6.11 and 6.12, respectively (Supratik, 2014).

$$K_{Axial} = EA \tag{6.10}$$

$$K_{Bending} = EI \tag{6.11}$$

$$K_{Shear} = GA \tag{6.12}$$

In these equations, E is the elastic modulus, A is the area, I is the moment of inertia and G is the shear modulus. The moment of inertia for the structure can be calculated according to equation 6.13 below (Irgens, 2010). This equation gives the area moment of inertia for a circular ring. The moment of inertia is calculated for the original shape and applied to the simplified model in Sima Riflex.

$$I = \frac{\pi}{4}(r_{outer}^4 - r_{inner}^4) \tag{6.13}$$

The result from this equation will give the moment of inertia for one of the pipes. In order to take all three pipes into account, it is necessary to use the parallel axis theorem, as shown in the equation 6.14 below (Kelley, B. S., 2009).

$$I_{tot} = \sum (I_{pipe} + Ad^2) \tag{6.14}$$

In this equation I_{pipe} is one pipe's own moment of inertia, and d is the distance from the pipe central point to the central point of the whole object. A corresponds to the area of the pipe. The moment of inertia for one pipe and the bundle are shown in table 6.8 below.

Table 6.8: Moment of inertia

Parameter	Value
Moment of Inertia for one pipe $[m^4]$	0.0083
Moment of inertia for bundle $[m^4]$	0.57

The torsional stiffness was calculated using equation 6.15 shown below (Bai and Bai, 2005). The equation is for composite risers, but is utilized in this study for the circular cross section of the bundle. In this equation, G is the shear modulus and J is the polar moment of inertia. If the structure is given a twisting motion equal to one radian per length, the torque it will experience will be the same as the torsional stiffness (Orcina Ltd., 2015).

$$GJ_{model} = GJ_{casings} + GJ_{tubing} + GJ_{otherlines} \tag{6.15}$$

The polar moment of inertia needs to be calculated for the structure. For a circular hollow cylinder, as in this study, equation 6.16 is utilized (Irgens, 2010).

$$J_z = \frac{\pi}{2} (r_{outer}^4 - r_{inner}^4) \tag{6.16}$$

In table 6.9, the values for the calculated shear modulus and stiffness properties can be seen. These properties are the ones that are used for the modeling in Sima Riflex. For detailed calculations of the stiffness properties, see the Appendix A.1.4.

Table 6.9: Shear modulus and stiffness properties for modeling in Sima Riflex

Parameter	Value
Shear Modulus [MPa]	7.96E+10
Axial Stiffness [N]	6.31E+11
Bending Stiffness [Nm^2]	1.19E+11
Shear Stiffness [N]	2.43E+11
Torsion Stiffness [Nm^2/rad]	4.77E+10

6.3.5 Radius of Gyration

The radius of gyration must be calculated for the bundle. The calculations are based on the moment of inertia and the area of the cross section, and explains how the mass is distributed around the central axis of the object (eFunda, 2016). The equation is given below as equation 6.17.

$$k_z = \sqrt{\frac{I_z}{A}} \tag{6.17}$$

For the bundle consisting of three pipes, table 6.10 shows the values used for calculating the radius of gyration.

Table 6.10: Values for calculating the radius of gyration for the bundle

Parameter	Value
Moment of inertia [m^4]	0.57
Area [m^2]	3.05
Radius of gyration [m]	0.43

6.3.6 Added Mass and Drag Force

According to the illustration of the different force regimes from waves, seen in Section 4.2.1, it is seen that for the given sea state the structure is in the area of inertia dominated responses

and small drag. However, the result is just on the line for inertia and drag dominated responses, so drag can be of importance for the structure. As a result, the non-linear drag terms will be included in the analysis in Sima Riflex.

The added mass and drag forces for the bundle is desired to be as close to the real bundle as possible. Three different alternatives were considered for finding the most suitable values for the added mass and the drag forces:

1. Using the added mass and drag coefficient for a circular bundle.

2. Using the added mass and drag coefficient for a triangular bundle.

3. Using results from model experiments on the real bundle geometry.

The added mass of a circular and triangular bundle are calculated as explained in section 3.3.2. This required information about the Reynold number and surface roughness, which can be found in table 6.11 below. The current velocity is chosen as the velocity of -30 m depth, where the bundle is situated.

**Table 6.11:** Properties for added mass for a circular bundle

Parameter	Value
Kinematic viscosity	1.52E-06
Current velocity $[m/s]$	0.48
Reynolds number	6.22E+05
Surface Roughness $[m]$	0.001

Based on the calculated Reynolds number and surface roughness, the drag coefficients could be found. The results for the added mass and drag coefficient for the circular and triangular bundles are given in table 6.12 below.

Table 6.12: Drag and added mass coefficients for circular and triangular bundle

Parameter	Circular	Triangular
C_D [$-$]	0.85	2.0
C_A [$-$]	1.0	0.67
A_R [m^2]	3.05	3.05
Added mass, A_{ij} [kg/m]	3064.10	2052.94

The last approach is to use the added mass and drag coefficients from model experiments on the real bundle geometry. According to the Master's Thesis by Grevstad, "Vortex Induced Vibrations on an "Artificial Seabed" for Support of a Floating Bridge" (Grevstad, 2015) the orientation of the bundle that will give the longest fatigue life, is the orientation as shown in figure 6.4 below. This orientation gave the longest fatigue life both attached to the bridge structure and detached from the structure, and is thus least affected by VIV. As a consequence of this result, the same orientation will be the basis for the calculations of this study.
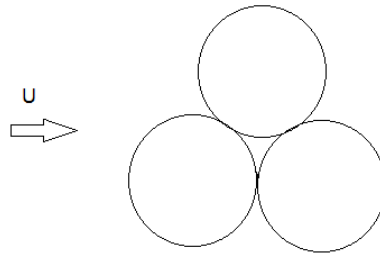
Figure 6.4: Orientation of the bundle during towing and installation (Grevstad, 2015)

The results from Grevstad's model tests are for pure cross flow from the current. From the stationary model test with the given orientation, the results gave a drag coefficient of 0.5, and an added mass coefficient of 0.7 (Grevstad, 2015). The final properties can be seen in table 6.13 below.

Table 6.13: Added mass and drag coefficient from model experiments

Parameter	Value
C_D	0.5
C_A $[-]$	0.7
A_R $[m^2]$	3.05
Added mass, A_{ij} $[kg/m]$	2144.87

When comparing the results for added mass and drag coefficients for the different alternatives, it is seen that the results for the added mass are varying. The largest added mass result is from the circular bundle. In order to be on the most conservative side, the circular bundle results should be utilized in this study. However, these results are based on a cross sectional area that is larger than for the other two geometries, thus overestimating the added mass coefficient. In order to get results as close to the real bundle as possible, the results from the model experiments will thus be utilized in the analysis in Sima Riflex. For more details, see Appendix A.1.5.

6.3.7   Towing Depth

The wave length, λ, corresponding to the given significant wave height of 2.34 m and period of 4.8 s can be calculated according to equation 6.18 (Faltinsen (1990) p. 16).

$$\lambda = \frac{g}{2\pi} T^2 \tag{6.18}$$

By utilizing this equation, the wave length becomes 36 m. According to the wave theory given previously, the wave motion will be extinguished for a depth larger than L/2, which here equal 18 m. Consequently, for these wave properties will direct wave loads be avoided at -30 m. However, the effect of current will still be important, although it will be considerably reduced at this depth.

With a λ equal to 36, this is larger than 5 timed the diameter of the structure, thus making Morison's load formula possible to use on the calculations (see Section 4.3.2). Additionally, due

to the fact that the length of the structure largely exceeds the transverse dimensions, the end-effects of the structure can be neglected.

6.3.8 Towing Line

The properties of the towing lines must also be entered into Sima Riflex. As found in chapter 4, towlines for offshore towing should be made out of steel. Since the bundles are first transported offshore, the towing ropes that will also be used inshore are steel wire ropes. The properties of the steel wire ropes can be seen in table 6.14 (Lankhorst Ropes, Offshore Division, 2013). To find more details about the calculations, see appendix A.2.

Table 6.14: Properties of steel wire rope for towing

Parameter	Value
Diameter [mm]	102
External area [m^2]	0.00817
Weight [kg/m]	43
Axial stiffness [N]	7.259E+06
Radius of gyration [m]	0.0255
Drag coefficient [$-$]	1.8

The value for the drag coefficient of the towing line is based on information found in DNV-RP-H103, Appendix B (DNV GL, 2011c). The Reynolds number of the wire is calculated to be 8.30E+04, based on the given kinematic viscosity and the largest current of 1.27 m/s. According to the recommended practice, the largest drag coefficient for the wire is 1.8, chosen to be on the conservative side (DNV GL, 2011c).

According to the rules, section 3.4, the length of the towing line will affect the analysis. With the bundle being submerged to -30 m, it was assumed that the bundle would be situated 30 m behind the first vessel and 30 m in front of the rear vessel. This gives a towing line of length 42.43 m. This corresponds to the information about clearances explained in chapter 4.1, which stated a minimum of 5 m clearance between the towed object and the vessel.

The towing line segment is connected with the bundle by a supernode. In order to have a stable analysis in Sima Riflex, the towing line is modeled as a beam section. Therefore, the remaining stiffness properties of the towing wire are put to small default values of 1000.

6.3.9 Static Analysis

For the static calculation, the load types are calculated in a specific order. In this study it was necessary to add a boundary change for the supernodes in the static calculation load types. These supernodes were defined as fixed in the initial configuration, and then changed to free as a step in the static calculation. However, the rotational degree of freedom about the X-axis was kept fixed, in order to keep the configuration more stable. The order the load types were calculated in the static calculation were first volume forces, then boundary change, specified displacements and finally current forces. For the analyses containing specified forces, these were added in between the specified displacements and the current forces. The number of load steps for the different load types were 20. The maximum number of iterations were put to 20, and the accuracy kept at 1.0E-06.

As for the different types of wave theories, it is seen from figure 4.3 in Section 4.3.1 that Stokes 2nd order theory is the theory that should be used for this analysis based on the given sea state. However, in Sima Riflex, Airy Theory is utilized. This is because the two options are Airy Theory and Stoke 5th order. The practical consequence of using Airy theory is that the wave induced velocity and acceleration will not be consistently described, this can only be described properly by the Stoke 5th order wave (Marintek, 2015). However, both wave theories will give equal wave height and wave length (Marintek, 2015)

6.3.10 Eigenvalue Analysis

The eigenvalue analysis was conducted for a number of eigenvalues and eigenvectors of 10. However, for the analyses necessary, more eigenvectors can be found. In the eigenvalue calculations, the maximum acceptable relative error was put to zero. Furthermore, the maximum number of iterations were put to 5. The result of the eigenvalue calculation were printed out for 10 of the bundle's eigenvectors.

6.3.11 Dynamic Analysis

According to the chapter of rules and regulations, Section 4.2.4, it was stated that a 3 hour simulation in irregular waves should be conducted in order to give a representative result for the dynamics of the problem. Due to the amount of simulations that are run in this study, the length of the dynamic analysis was not put to 3 hour. The length was 100 s for the regular analyses, and for finding the results for the statistical responses, 30 min simulations were run. The time step at which the responses should be calculated at was put to 0.1 s. The wave seed starting parameter for generating random numbers were 29852. This number is the starting parameter for the production of the irregular sea.

6.4 Transportation of Bundles

The limit of the maximum allowed stress in the bundle during towing and installation is set to 192 MPa (Engineering Department, Deep Ocean, 2014). This will thus be used as the limit of the stresses appearing in the bundle during the two phases.

In order to analyze the transportation phase of the bundles, three different scenarios were developed. The scenarios include different water depths and environmental conditions that represent different stages of the towing through the fjord. In order to maneuver the bundle properly through the turns of the fjord, it might be necessary to bend it. Therefore, two of the scenarios include a parameter study of the degree of bending of the bundle for the given sea states. The requirements in conjunction with clearances, see Section 4.1, have been taken into consideration when developing the different scenarios. The width of the towing area should be at least three times the width of the object being towed. For the transportation phase of the study, the towing configuration starting point was based on the typical towing configuration seen on the figure 6.5 below.

Figure 6.5: Towing configuration of the bundle (Engineering Department, Deep Ocean, 2014)

During the towing through the Sognefjord, the worst scenario of current and waves are modeled. The vessels are towing the bundle in to the fjord, and the waves and current will also move in to the fjord. Since the two vessels are towing the bundle in the negative X-direction in Sima Riflex, the waves and the current will be added to the analysis in that direction as well.

6.4.1   Scenario 1: Sognesjøen

The first scenario was developed to represent the mouth of the Sognefjord, Sognesjøen. As seen in the explanation to the case in Chapter 2.3, the depth at this stage is -140 m at the shallower areas that need to be passed. This depth is used in the analysis. Figure 6.6 below shows Scenario 1 illustrated. As seen from the figure, the tugs are positioned in a row.
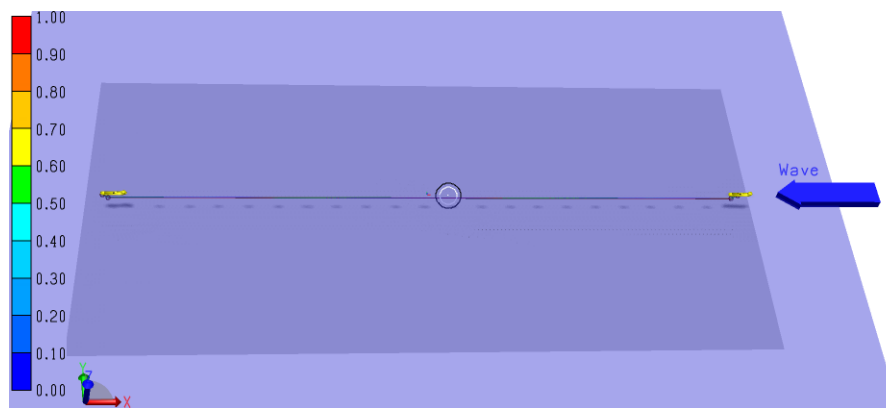
Figure 6.6: Illustration of Scenario 1, taken from Sima Riflex

The environmental impacts for this stage will represent the environmental condition this close to the North Sea, and the values will be calculated based on data from SINTEF. According to SINTEF, the wave with a 100 year return period in the North Sea outside of Sognesjøen is 10.6

m and 9.6 m respectively in directions 210 and 240 degrees, with peak period of 13-14 s (Lothe and Brørs, 2011). Furthermore, it is stated that at the location of Sognesjøen, the wave height will be reduced to 69 % of the waves in the North Sea. Therefore, the wave height used for this Scenario will be 6.97 m, calculated as the 69 % of the mean of the given wave heights. Table 6.15 shows the characteristic values used for modeling this stage of the tow in Sima Riflex.

Table 6.15: Characteristic values for Scenario 1

Parameter	Value
Towing depth [m]	-30
Water depth [m]	-140
Position, tug nr. 1 (X, Y)	(-1930,0)
Position, tug nr. 2 (X, Y)	(1930,0)
Significant Wave Height [m]	6.97
Peak Period [s]	13.5

When trying to run the dynamic analysis with the peak period of 13.5 s, the analysis is aborted. This is because the large peak period gives wave motion down to 285 m depth, and apparently this wave motion is too large for the bundle situated at -30 m. The change of peak period with reduced wave height is not known. Due to lack of information about this, the analysis is run for the largest peak period possible with this wave height, which is 6 s. In order to get a broader view of the bundle and its behavior in large sea, several peak periods were tested in this scenario.

6.4.2 Scenario 2: Transition from Sognesjøen to Sognefjorden

The second scenario will illustrate the transition from Sognesjøen to Sognefjorden. The turn about Rutletangen will be modeled with a depth of 140 m. The challenge will be to pass this turn in the fjord without applying too large forces on the bundle, or without crashing the end points into the shore. However, there is a large open space outside of Rutletangen, which might enable passing without curving the bundle.

According to information given from SINTEF (Lothe and Brørs, 2011), the wave height at this point will be 0.15 % of the waves in open sea. This gives a wave height of 1.52 m. Table 6.16 shows the characteristic values used for modeling Scenario 2 in Sima Riflex.

Table 6.16: Characteristic values for Scenario 2

Parameter	Value
Towing depth [m]	-30
Water depth [m]	-140
Position, tug nr. 1 (X, Y)	(-1850,-500)
Position, tug nr. 2 (X, Y)	(1750,0)
Significant Wave Height [m]	1.52
Peak Period [s]	13.5

The analysis of this scenario was possible to run for a peak period of 13.5 s. This is because the reduced wave height causes less motion with increased depth. Scenario 2 is illustrated in figure 6.7. For this scenario the challenge will be the bending of the bundle in combination with limited space, as well as the environmental impacts.
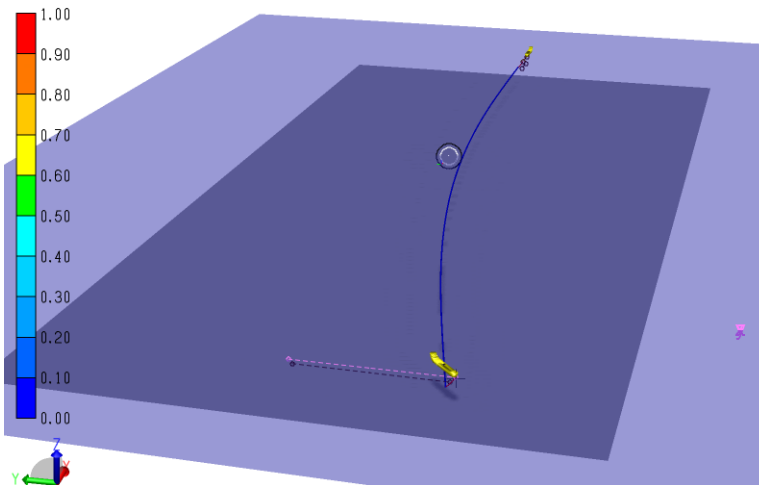
Figure 6.7: Illustration of Scenario 2, taken from Sima Riflex

Three tugs, simulated as horizontal forces, attached with equal distances along the bundle will be used for the purpose of bending the bundle to the correct position. The direction and magnitude of the forces from the tugs are shown in table 6.17 below.

Table 6.17: Magnitude of pulling forces for the towing tugs

Tug	Magnitude [N]	
	X-direction	Y-direction
Tug 1	-7 000	7 000
Tug 2	0	7 000
Tug 3	0	7 000

When the bundle is bent, the end points move slightly upwards. To avoid this effect, additional weight corresponding to -800 kg were added on each endpoint of the structure, to keep the tension in the towing wires.

The parameter study of the bending of the bundle were conducted for the given sea state. The results will give a picture of how the bundle will behave when forced to bend, and can be useful information when considering if this method is usable for other installations.

6.4.3 Scenario 3: Sognefjord

The last scenario will represent the towing phase inside of the Sognefjord. For this scenario, there will be large depths, but limited space to each side. The turn about Raudberg will be modeled, the last turn of the fjord before entering the installation location. The characteristic values used for modeling Scenario 3 are shown in table 6.18. Here the wave height and period correspond to the maximum wind generated wave heights in the fjord (Lothe and Brørs, 2011).

Table 6.18: Characteristic values for Scenario 3

Parameter	Value
Towing depth [m]	-30
Water depth [m]	-1200
Position, tug nr. 1 (X, Y)	(-1850,-500)
Position, tug nr. 2 (X, Y)	(1750,0)
Significant Wave Height [m]	2.34
Peak Period [s]	4.8

Figure 6.8 shows an illustration of Scenario 3. The large depth in this analysis can be seen on this illustration.
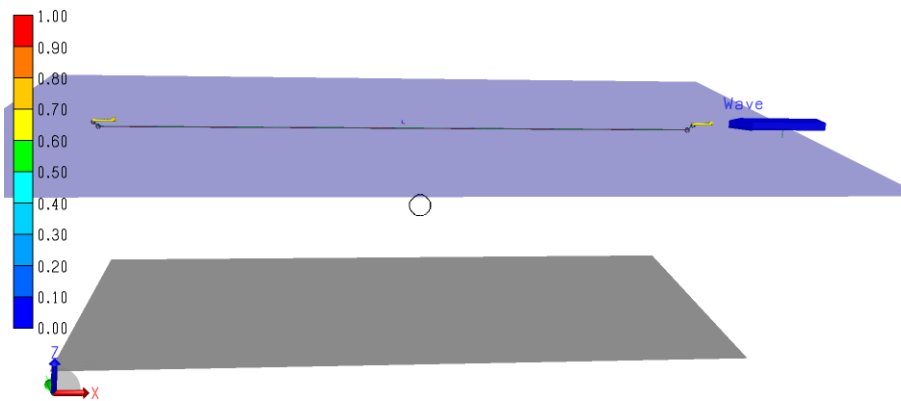
Figure 6.8: Illustration of Scenario 3, taken from Sima Riflex

Also for this scenario will several configurations of bending of the bundle be tested. This scenario has smaller peak period than the previous scenario, so less wave motion is likely to interact with the bundle. This will give a representative illustration of how the bundle will act when bent, but without large wave forces hitting the structure. Figure 6.9 below show the analysis viewed from the YZ-plane, in the final static configuration of the bent version of the bundle.
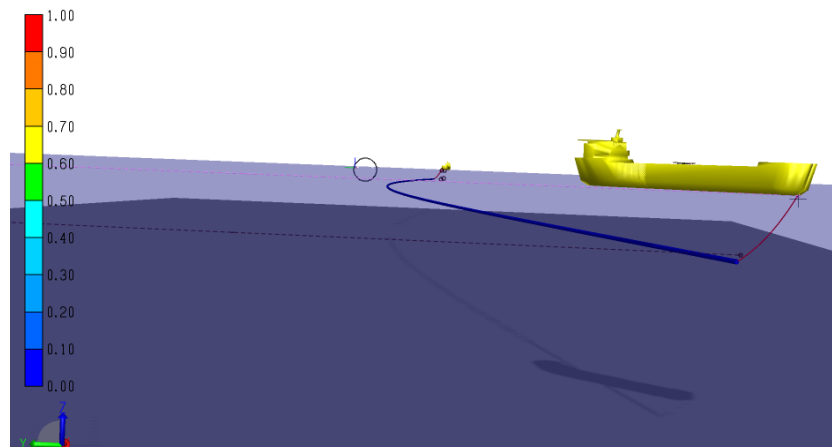
Figure 6.9: Illustration of Scenario 3, seen from the YZ-plane

6.5 Installation of Bundles

There is limited information about the installation of the bundles, which makes it important to study carefully. During installation, the bundle will be positioned almost completely sideways in the fjord, resulting in the current and wave forces affecting the bundle sideways. Figure 6.10 illustrates a step of a possible way for installing the bundle in the fjord (Engineering Department, Deep Ocean, 2014).
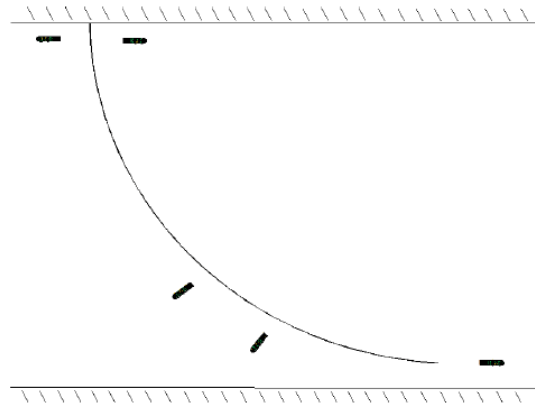
Figure 6.10: Example of installation of the bundle (Engineering Department, Deep Ocean, 2014)

In order to analyze the bundle configurations for the installation phases, "stress-free configurations" were first attempted in Sima Riflex. When using this configuration, a text file containing the coordinates for every node is read into Sima Riflex. The text file was created using Matlab. However, as the name of the method suggests, this configuration will give a bundle in the correct shape, but without any stresses related to the shape. This method was thus abandoned in favor of a method using nodal displacements with additional tugs for creating the correct configurations.

In order to find a suitable method for installing the bundles, three different scenarios are developed. The first scenario utilizes the horizontal plane to bend and position the bundle correctly. Scenario 2 utilizes the vertical plane instead, and finally the last scenario utilizes both planes for the installation. By first analyzing both planes separately, the knowledge and understanding of scenario 3 may increase. Additionally, the isolation of the scenarios might contribute in the understanding of the results.

6.5.1   Scenario 1: Bending in the Horizontal Plane

This scenario will keep the bundle in one plane, as seen in figure 6.11 below.
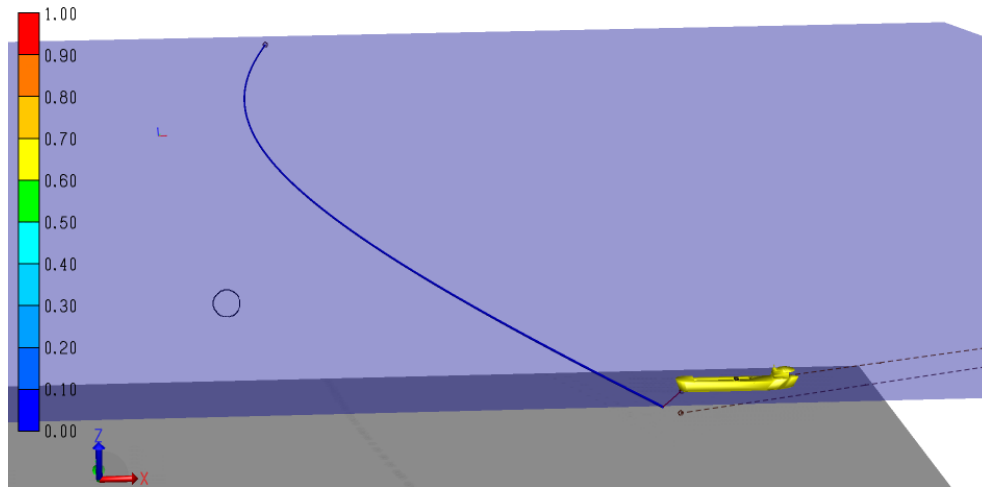
Figure 6.11: Static configuration of Scenario 1 for installation

For this scenario it was necessary with additional towing tugs, situated in the middle of the bundle. The force it had to pull with is given in table 6.19 below.

Table 6.19: Magnitude of pulling forces for the towing tugs

Tug	**Magnitude** [N]	
	X-direction	Y-direction
Tug 1	-25 000	-3 300
Tug 2	-25 000	-3 300
Tug 3	-25 000	-3 300

One of the end points of the bundle is supposed to simulate the end point that is fixed to the rock wall. This end was set to fixed for all translations and rotations, except for the rotation about the Z-axis. The other end point was connected to a towing line attached to a towing vessel, and set to free. Furthermore, the node at the tug was given free rotations to simulate a winch.

Additional weights corresponding to -9600 kg was separated over 100 m close to the end attached to the vessel. This was to reduce the upwards movement of the end points when the bundle was being bent.

6.5.2 Scenario 2: Bending in the Vertical Plane

The scenario wish to utilize the ocean space into the depths of the Sognefjord. The figure below, 6.12, show the final static configuration for this scenario.
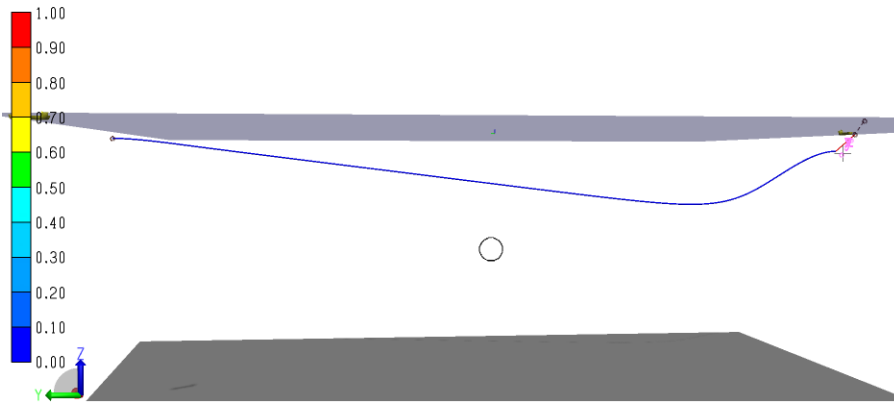
Figure 6.12: Illustration of Scenario 2, seen from YZ-direction

The idea behind this is to exploit that the current forces are reduced with depth, and so the responses of the bundle might be reduced by lowering it. By lowering one end point of the bundle vertically downwards, the bundle will "shorten". This will leave enough space for the installation to be conducted by fixing the other end point to the rock wall. Then the free end point can be gradually raised to installation level and attached to the wall. This scenario is modeled with one end point fixed to the rock wall, while the other end point is submerged. The analysis do not simulate the entire operation, but aims to see an excerpt of the most important responses during this installation.

In order to lower one end of the bundle without applying too large forces on that point, it is necessary to add weights and buoyancy sections along the bundle. The additional weight and buoyancy are added as Nodal Bodies in Sima Riflex, but represent chains and pontoons in a real marine operation.

The end point that is lowered downwards is supposed to be attached to a towing line connected to a towing vessel. In the real marine operation, the towing wire will be gradually released from the vessel. However, due to difficulties with modeling a gradually increasing line in Sima Riflex, another approach was used. The full towing line length is modeled from the beginning, as can be seen in figure 6.13. This towing line is then assumed fixed to an imaginary

point 80 meters above the vessel, but will at the final static configuration be as illustrated in the figure 6.14 below.
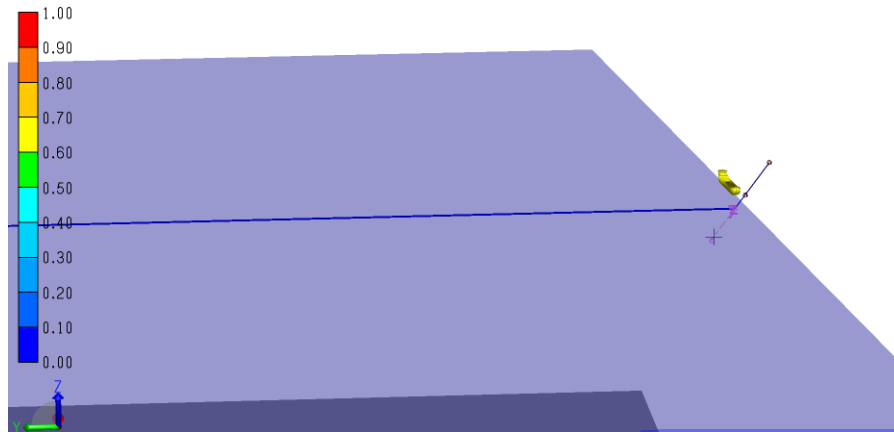
Figure 6.13: Initial configuration of the towing line
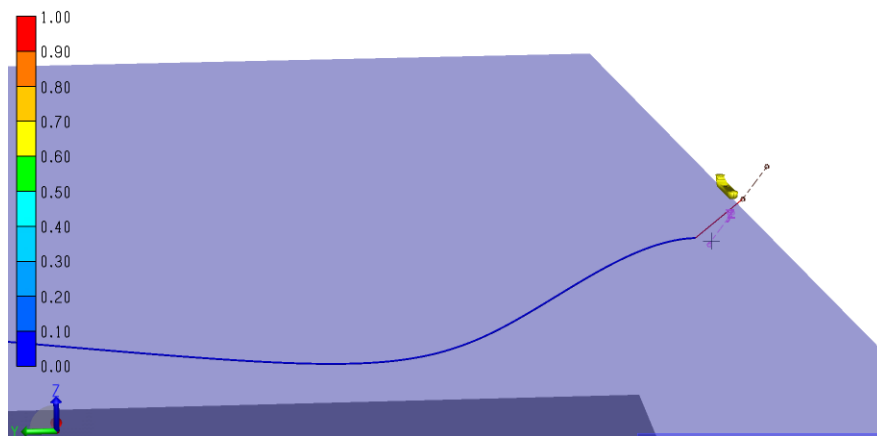
Figure 6.14: Final static configuration of towing line

This scenario turned out to be more challenging than Scenario 1. This is due to the fact that the bundle will experience large forces when being lowered in one end point as in this scenario. The bundle would, without any additional weight, take a shape consisting of several half circles. Due to the added weight, the bundle is forced downwards into the fjord instead. The additional weights that force the bundle downwards, will in addition create irregular forces and moments along the bundle. When the bundle is being pulled down and held down by additional weights, the end attached to the towing vessel tends to pull up. This will create compressive loads on the towing line. The towing line is modeled as a beam segment, as explained earlier, and will be unstable when exposed to large compressive forces (Marintek, 2015). With an unstable towing

line, it is not possible for Sima Riflex to find the eigenvalues for either of the two lines. Based on this, it was necessary to add even more loads on the bundle close to the end point attached to the towing vessel. In total additional weights corresponding to -400 000 kg separated on 720 m was added to the free end, with most of the weight close to the end point. Additionally, -30 000 kg separated on 760 m was added at the end close to the fixed end point. It was also found that this scenario is very sensitive to minor changes in the model, which made the analysis crash.

Furthermore, it should be noted that although the bundle is inside of the fjord limits, the vessel is situated outside of the fjord borders in this analysis. It would be possible to put the vessel inside of the fjord, but this would cause even larger forces acting on the structure. On this basis, the vessel is kept outside of the fjord borders in this analysis. It should also be taken notice of that it was necessary to increase the axial stiffness of the towing wires to be able to run this analysis. The stiffness used for this analysis is 7.259E+07. The combination of these issues underlines the fact that this scenario alone is not the most suitable scenario for this operation.

6.5.3   Scenario 3: Bending in both the Vertical and the Horizontal Plane

This scenario wish to exploit the space in both the vertical and the horizontal plane, which might cause the bending of the bundle to be less critical than for Scenario 1 and 2. In order to take advantage of the ocean space in several planes, both additional tugs and additional weights are necessary.

In order to achieve the required bundle shape in the computer program Sima Riflex, a combination of the methods used for Scenario 1 and 2 were used. The node connected to a towing vessel were given displacements in both the horizontal plane and the vertical plane. In order to analyze the full installation procedure, it was necessary to divide the analysis into two parts. The whole installation phase is thus not done in one single analysis, due to limitations in the computer program. The limitations of this simplification will be discussed in Chapter 8. For both parts, a parameter analysis is conducted to find the most suitable installation configuration.

Since the same installation phase is analyzed in separate analyses, the additional weights are chosen to be equal for both parts. This means that the weights are not necessarily optimized for each single analysis, but for both the analyses as a whole. This decision is made because

it is desired to make the operation as simple as possible, and therefore not change the weights during the installation. Three additional weights are added to the analysis at three different line segments. Each of the weights have a negative buoyancy of -5799 kg. The weights are distributed in such a way that -5799 kg are separated on the 50 m close to the end that is first attached to the rock wall. These weights are only necessary under part 1 of the installation, but kept on for part 2 as well. The remaining -11598 kg are separated on 100 m at the other end.

Part 1

Part 1 is created to simulate the beginning of the installation, where the bundle is assumed to be towed directly into the initial position. Thus are both end points connected to towing wires and tugs. The transition from the initial straight configuration to the final curved configuration is aided by three additional towing tugs. Both configurations are shown in figure 6.15 below. In order to find the most suitable installation procedure, different depths are tested for this part of the analysis, from -30 m to -200 m.
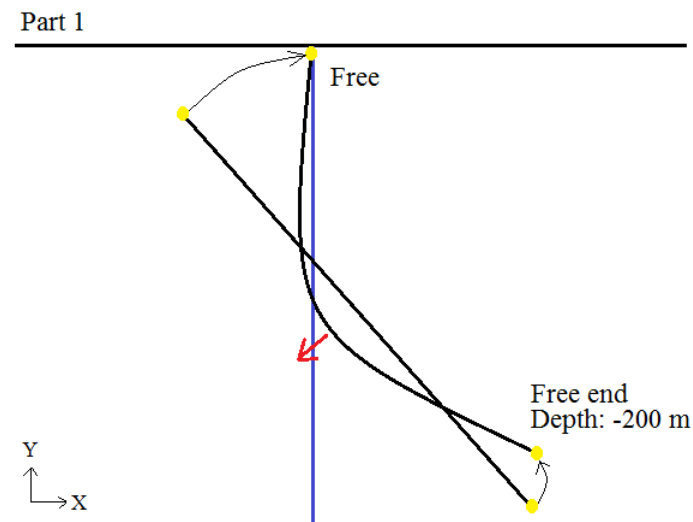
Figure 6.15: Illustration of the modeling of Part 1 for installation

The three additional towing tugs are situated with equal distances along the bundle. The direction of the tugs are illustrated in figure 6.15 with a red arrow. The tugs are pulling in the negative X- and Y-direction. The magnitude of the tow pull is given in table 6.20 below.

Table 6.20: Magnitude of pulling forces for the towing tugs, Part 1

Tug	Magnitude [N]	
	X-direction	Y-direction
Tug 1	-10 000	-3 300
Tug 2	-10 000	-3 300
Tug 3	-10 000	-3 300

It should be noted that for the configuration with a shape going against the current, it is necessary with additional pull from the towing tugs. Otherwise will the installation procedure be equal, only mirrored. However, due to the fact that it is not possible to turn the bundles inside of the fjord, different end points will be connected to the sides of the fjord. This is illustrated in figure 6.16 below.
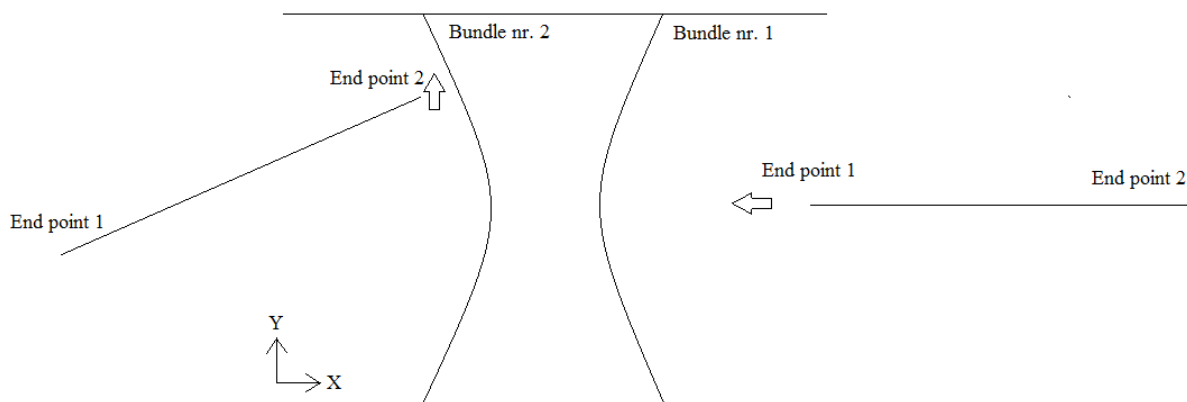
Figure 6.16: Direction of bundle during installation, shown for bundle 1 and 2

Part 2

This part aims to continue from Part 1, and thus the initial configuration of Part 2 is as close to the final static configuration of Part 1 as possible. The aim of this part of the installation is to fix the other end to the rock wall.

It should be noted that, in order to obtain the bending forces appearing in the bundle when it is bent, the initial configuration for each part will always be a straight bundle. This will of course cause some errors in the analysis, but compared to the option of using a bent stress-free configuration, this decision is conservative.

Figure 6.17 shows the modeling for part 2 of the installation scenario. The initial configuration is shown as the straight line, while the bent configuration is the final static configuration. This part is quite similar to Part 1, however now the upper end point is put to fixed, except for a free rotation about the Z-axis.
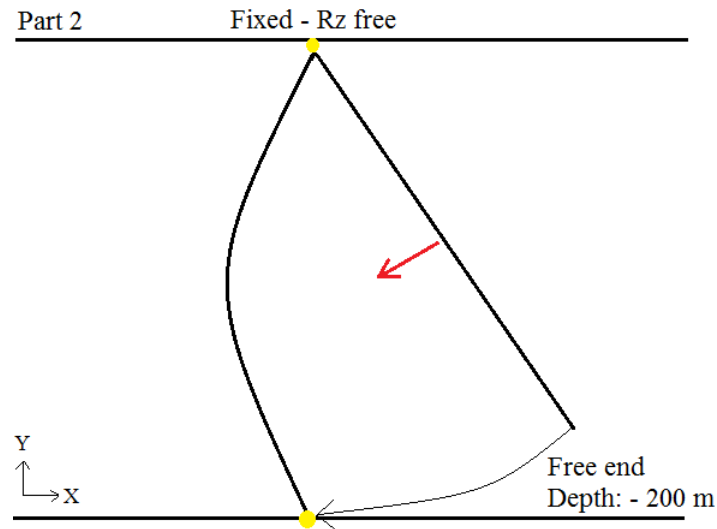
Figure 6.17: Illustration of the modeling of Part 2 for installation

Also for this part, three additional tugs with equal distances are used to obtain the given shape. One tug is indicated by a red arrow in the figure above, and the magnitude of the pulling forces are given in table 6.21. It is observed that the bending of the bundle will for this scenario require larger forces from the tugs than in part 1.

Table 6.21: Magnitude of force from tug for bundle 1, Part 2

Tug	Magnitude [N]	
	X-direction	Y-direction
Tug 1	-25 000	-3 300
Tug 2	-25 000	-3 300
Tug 3	-25 000	-3 300

Chapter 7

Results from Analysis

In the following sections, the results for all the different scenarios are presented, starting with the transportation phase and then the installation phase. Within each phase, the three scenarios are presented separately. The results are commented upon and extreme values are highlighted, but the discussion and further studies of the results will be in Chapter 8. For detailed results regarding the parameter studies, see Appendix B.

7.1 Transportation of Bundle

7.1.1 Scenario 1: Sognesjøen

In this scenario the most severe environmental loading will apply. Due to the increased wave height, the bundle is being exposed to large loading. The results are seen in the sections below.

Parameter Study of Peak Period

The figures below shows a graph of the bundle response due to increased wave period with a constant wave height of 6.97 m. The figures 7.1 and 7.2 show respectively the bending moment and the dynamic displacement and their relationship to the peak period. It is observed that all the responses increase for the results for larger peak periods. However, a significant increase is observed for peak periods larger than 5.75 s.
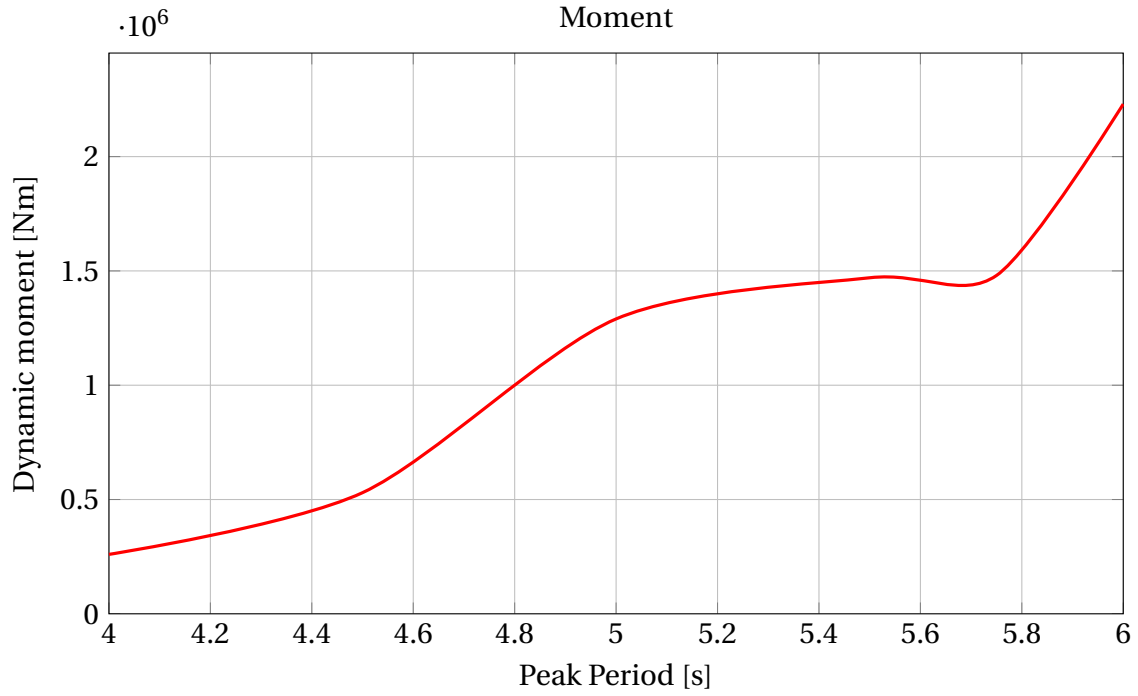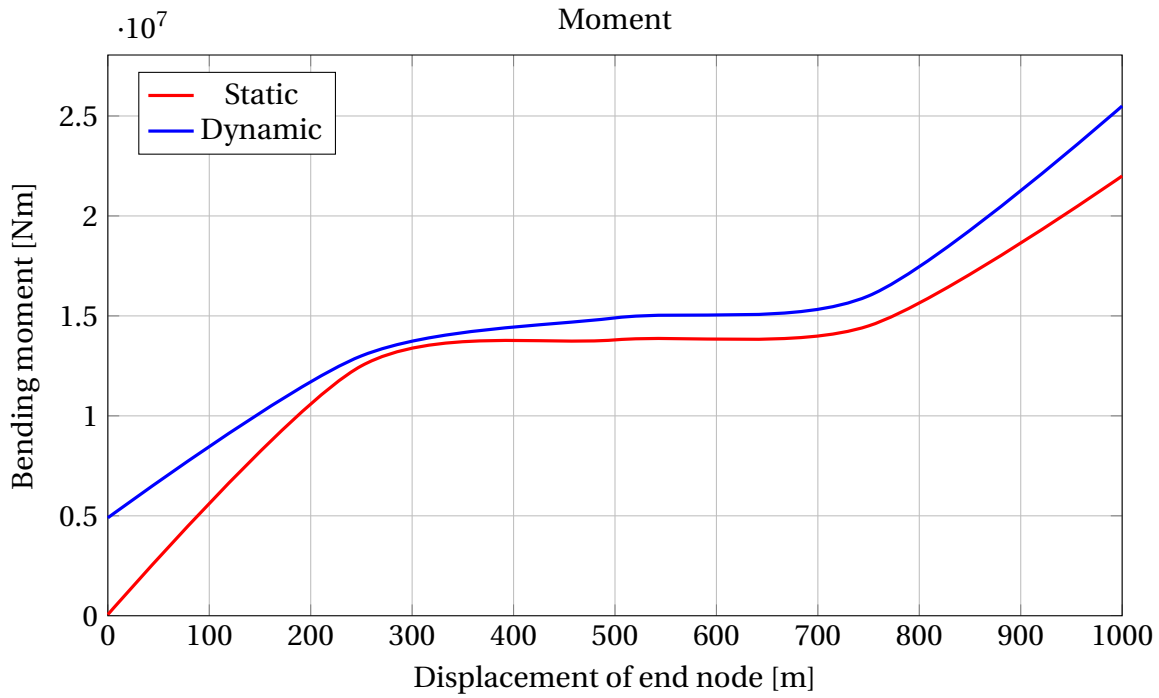
Figure 7.1: Parameter study for Scenario 1, Moment
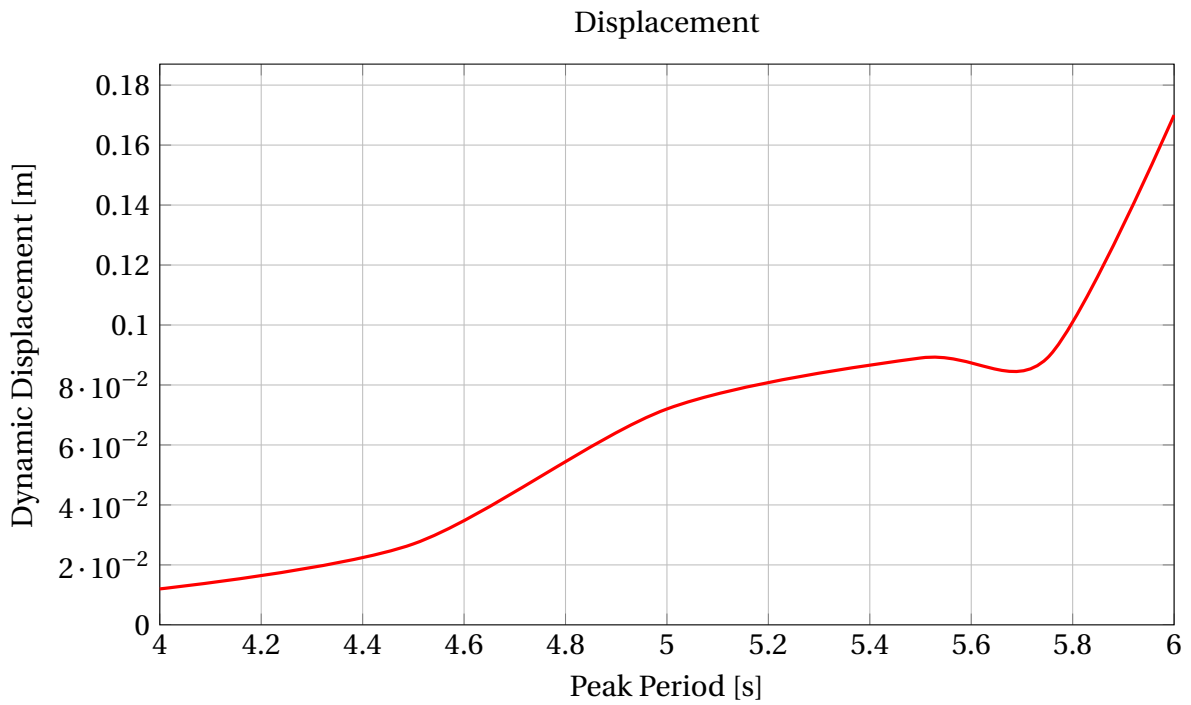
Figure 7.2: Parameter study for Scenario 1, Displacement

Detailed Results

The static results are equal for all the peak periods, since the static configuration is equal. Figure 7.3 show the static bending moment of the bundle. It is observed that is has an even shape, with maximum point of 6.25E+04 on the middle. The static torsional moment can be seen in Appendix C.1.1, and develops as a straight line over the length of the bundle. With a magnitude of 10^{-6}, the static torsional moment can be considered as negligible.
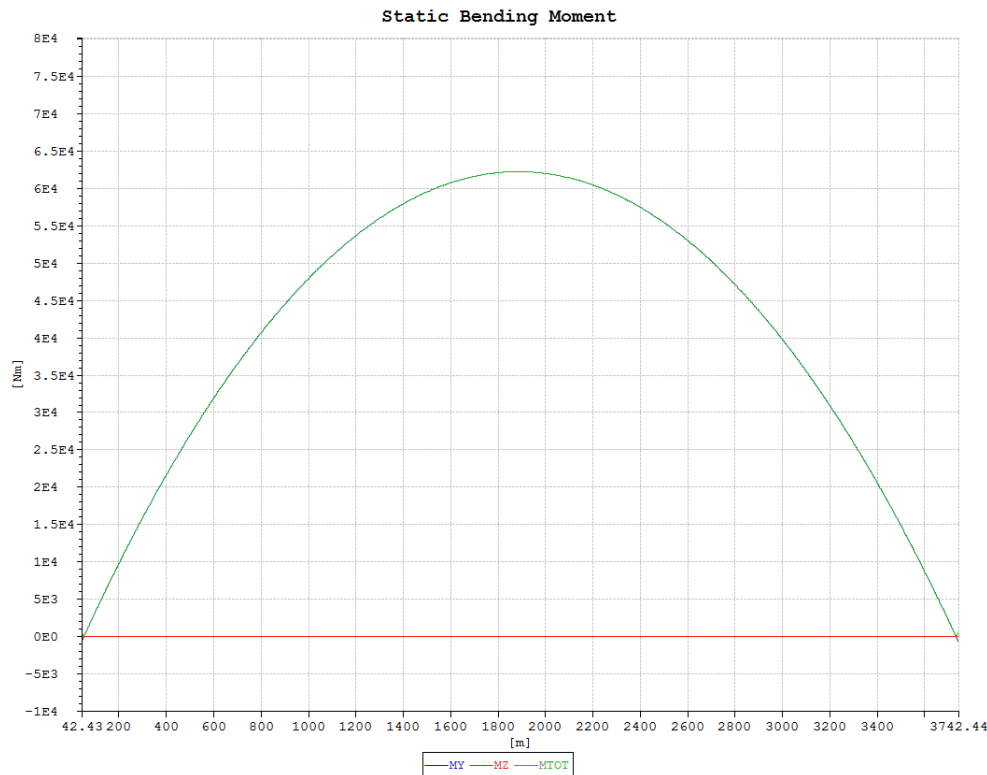
Figure 7.3: Static bending moment, Transportation, Scenario 1

The dynamic moment and displacement can be seen in figures 7.4 and 7.5 below for a peak period of 4 s. The dynamic displacement show rapid changes over the length. The magnitude of the displacement is not large, with 0.012 m as the largest displacement. In comparison, the largest dynamic displacement for a peak period of 6 s is 0.17 m, as seen in the parameter study above. The dynamic moment is also observed to have rapid variations. The largest moment occur at the rear end point, and reach a value of 2.6E+05 Nm. As a comparison, the largest moment for a peak period of 6 s is found to be approximately 2.2E+06, which is significantly larger than for 4 s.
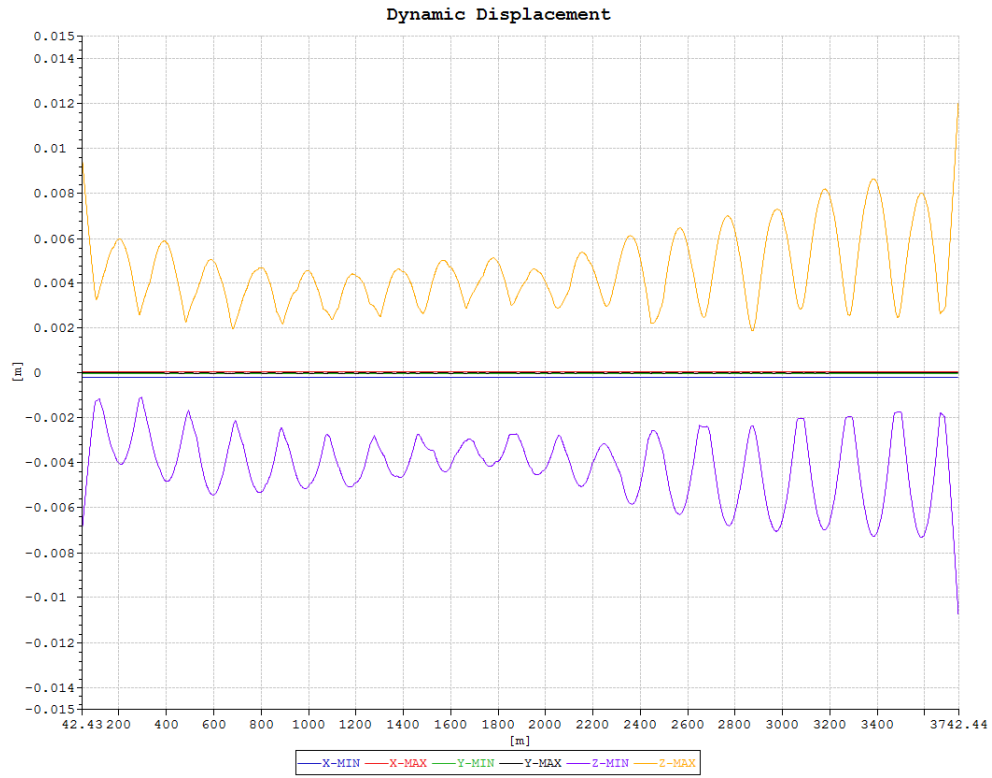
Figure 7.4: Dynamic displacement, $T_P = 4$ s
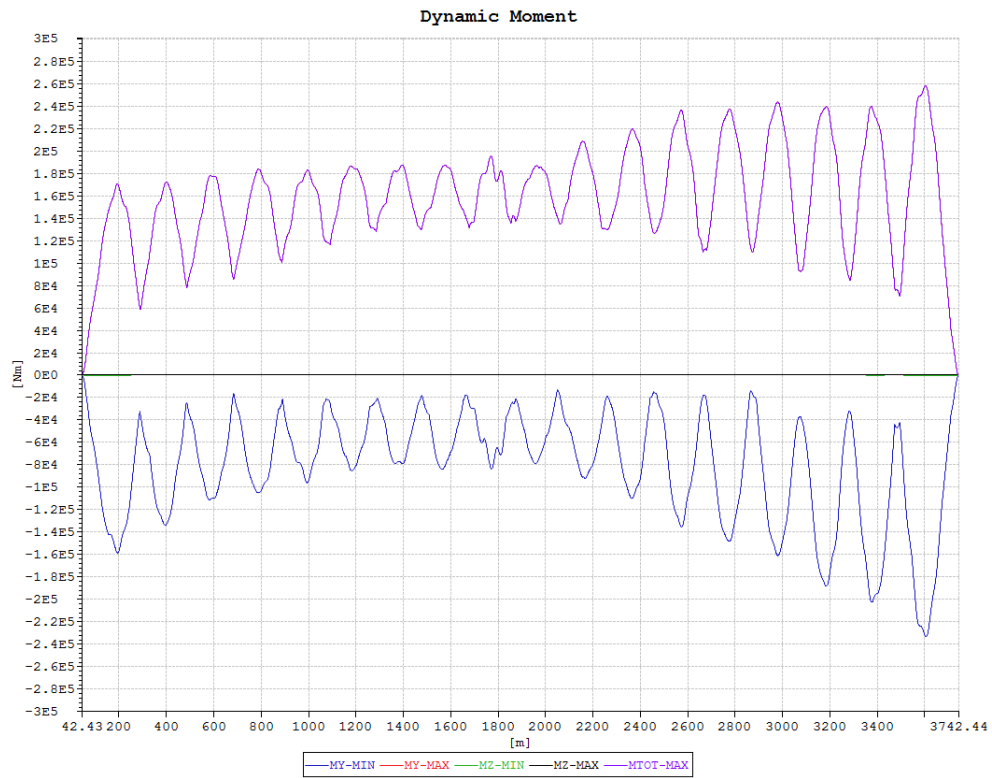
Figure 7.5: Dynamic moment, $T_P = 4$ s

The torsional moment for 4 s peak period can be found in Appendix C.1.1, and develops almost as a straight line. The largest response is found to be 2.7E-06, which make this response negligible.

7.1.2   Scenario 2: Transition from Sognesjøen to Sognefjorden

Parameter Study of Degree of Bending

This section contains the parameter study of the bundle response to being bent to different degrees. In the following graphical representations will the X-axis show how many meters the first end is being displaced in the Y-direction. This is illustrated in figure 7.6 below, where the dashed line represents number of meters of displacement from the initial configuration of a straight line.
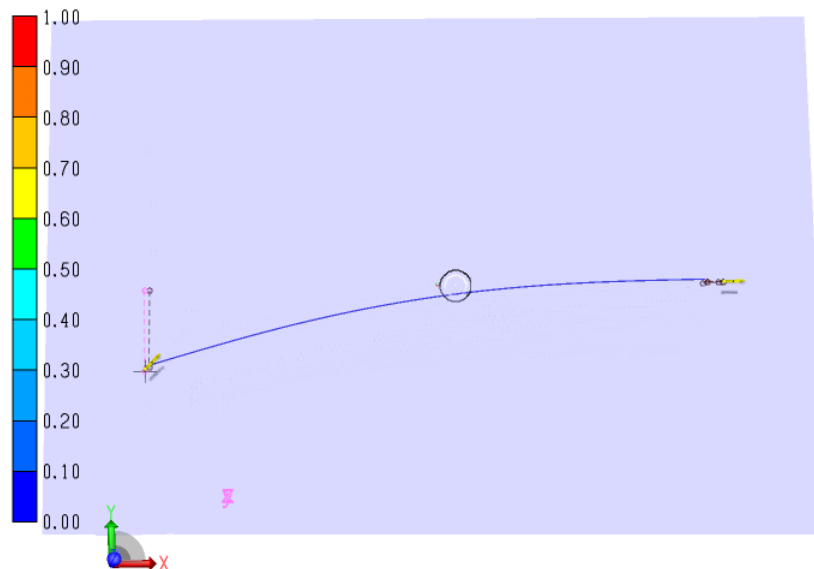
Figure 7.6: Illustration of Scenario 2, taken from Sima Riflex

The tables below contain the static and dynamic moment in figure 7.7, and the dynamic displacement in figure 7.8 plotted against the increased bending. It is seen in the results for the static and dynamic moment that the X-values between 200 and 800 m do not vary significantly. Rather it seems to reach a plateau, with close to constant moment. The limit is seen to be approximately 750 m, where the moment increase rapidly. Similar results apply for the dynamic displacement. The displacement increase evenly until reaching a plateau between

X-values of 500 and 750 m. Then it increases for the results for X-values larger than 750 m.

Figure 7.7: Parameter study for Scenario 2, Moment
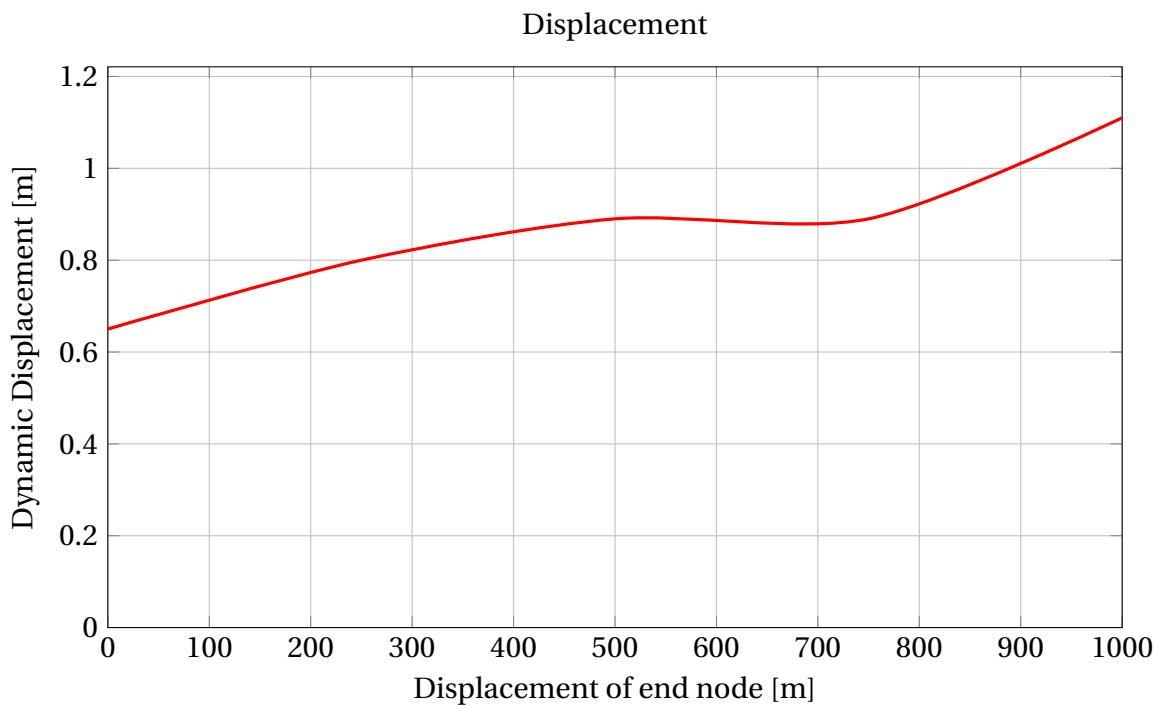
Figure 7.8: Parameter study for Scenario 2, Displacement

Detailed Results

The results of the most bent bundle will be presented here. The static moment for a bundle bent 1000 m is seen in figure 7.9. The largest moment is 2.2E+07 Nm, and the locations of the three tugs are easily observed. The static torsional moment, Appendix C.1.2, varies over the length of the bundle, and reaches the largest negative moment at the end point of the bundle. The maximum magnitude of the torsional moment is found to be -2800 Nm.
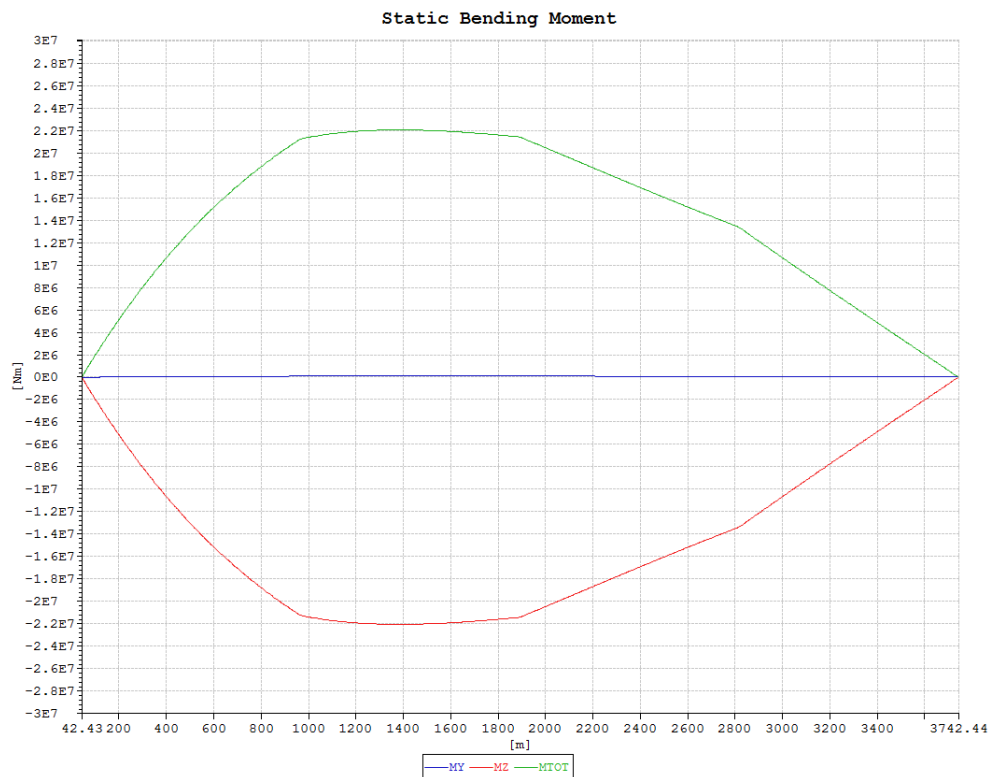
Figure 7.9: Static bending moment for Scenario 2, X=1000

The eigenmodes and values for the straight and the most bent bundle are compared. In table 7.1 the eigenvalues for the two bundles are shown for both period and frequency. For the straight bundle, X=0, the eigenvalues are the same as for the straight bundle in scenario 1, 2 and 3 of the transportation. It is observed that the first ten eigenfrequencies are small for both cases.

Table 7.1: Eigenvalues for the bundle, Scenario 2 of transportation

	X=0		X=1000	
Mode	**Frequency** $[1/s]$	**Period** $[s]$	**Frequency** $[1/s]$	**Period** $[s]$
1	0.0005	2000	0.0014	714.29
2	0.0005	2000	0.0017	588.24
3	0.0014	714.29	0.0027	370.37
4	0.0016	625.00	0.0046	217.39
5	0.0025	400.00	0.0072	138.89
6	0.0026	384.62	0.0078	128.21
7	0.0042	238.10	0.0105	95.24
8	0.0047	212.77	0.0123	81.3
9	0.0071	140.85	0.0153	65.36
10	0.0084	119.05	0.0178	56.18

The plot of the first ten eigenmodes can be found in the appendix, C.1.2. It is observed that there are large differences between the modes of the straight and the bent bundle, with the bent bundle appearing with a larger number of half circles than the straight.

The dynamic displacement for the most bent bundle is seen in figure 7.11 below. It is observed that the largest displacement occur in the Y- and Z-directions, with the largest value of 1.1 m for Z-displacement. In comparison is the largest displacement for a straight bundle 0.65 m, almost half that of the bent.

The dynamic moment, figure 7.11, show more variations than for the static moment. The largest value of 2.55E+07 Nm is significantly larger than 4.8E+06 Nm for the straight bundle.
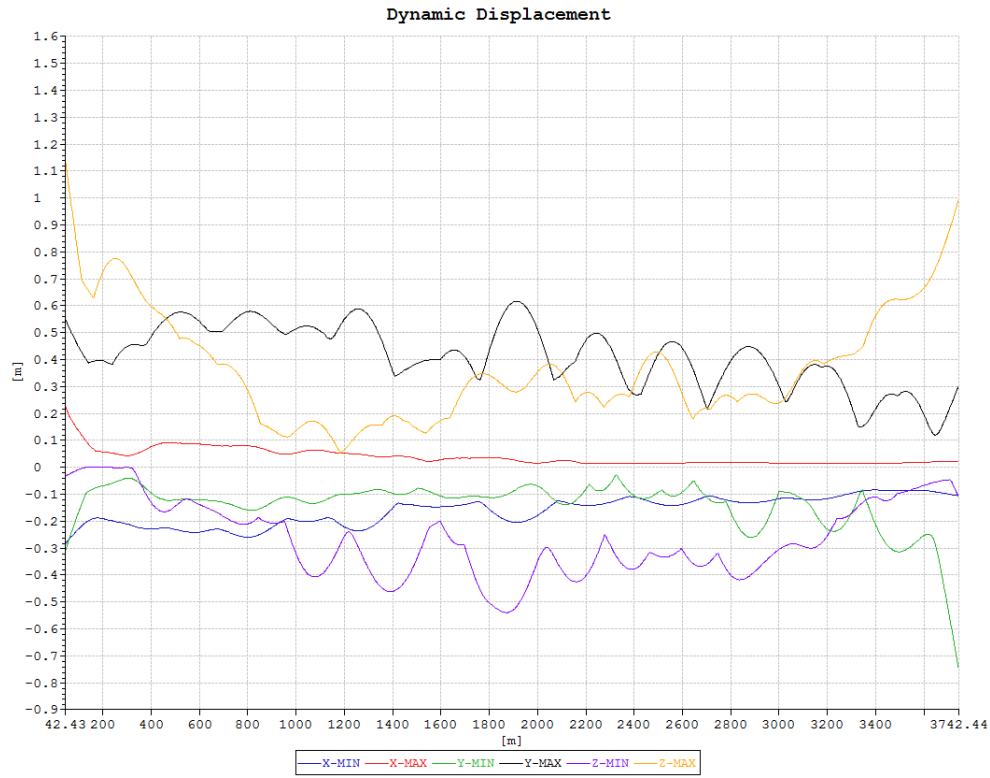
Figure 7.10: Dynamic displacement, X=1000
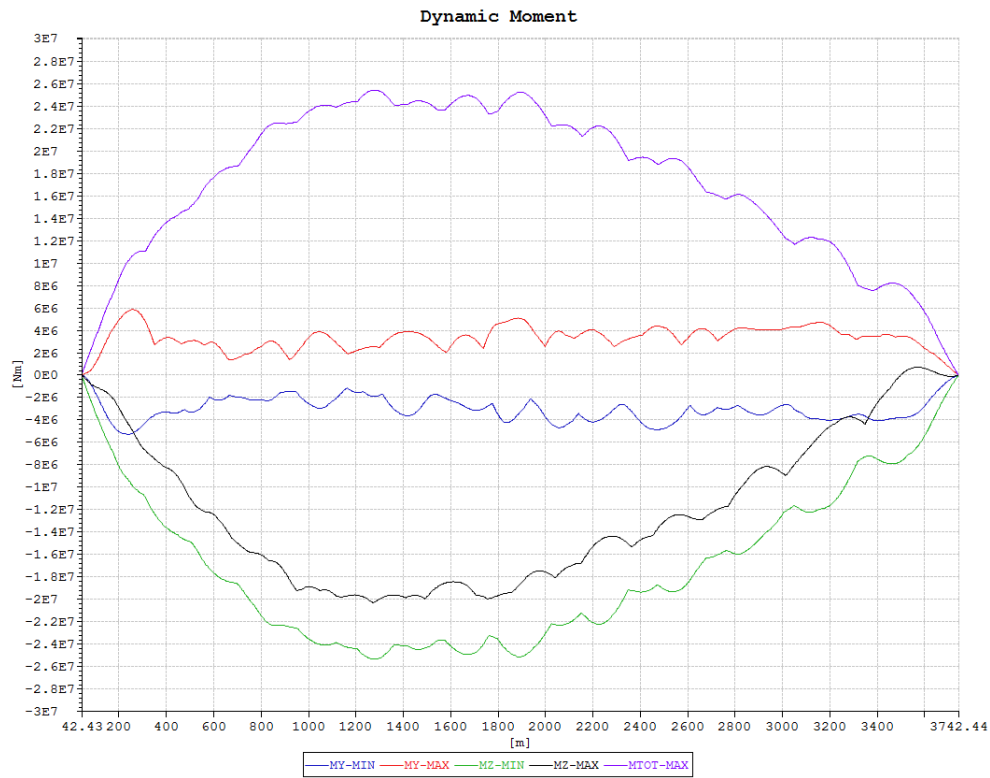
Figure 7.11: Dynamic moment, X=1000

The torsional moments can be found in Appendix C.1.2, and is seen to develop as a constant line, only with some small deviations. The bent bundle has a torsional moment of size 10^4, compared with negligible size for the straight bundle.

7.1.3 Scenario 3: Sognefjord

The final scenario of the transportation phase is through the Sognefjord. The results are given in the sections below.

Parameter Study of Degree of Bending

In the following tables, the X-axis represents the meters the first end of the bundle is being bent in the Y-direction, just as the previous scenario. From figure 7.12, the static and dynamic bending moments are seen plotted against the degree of bending. Similar to the results in scenario 2, a plateau is reached for X-values between 250 and 750 m. After this point the moment increases again.
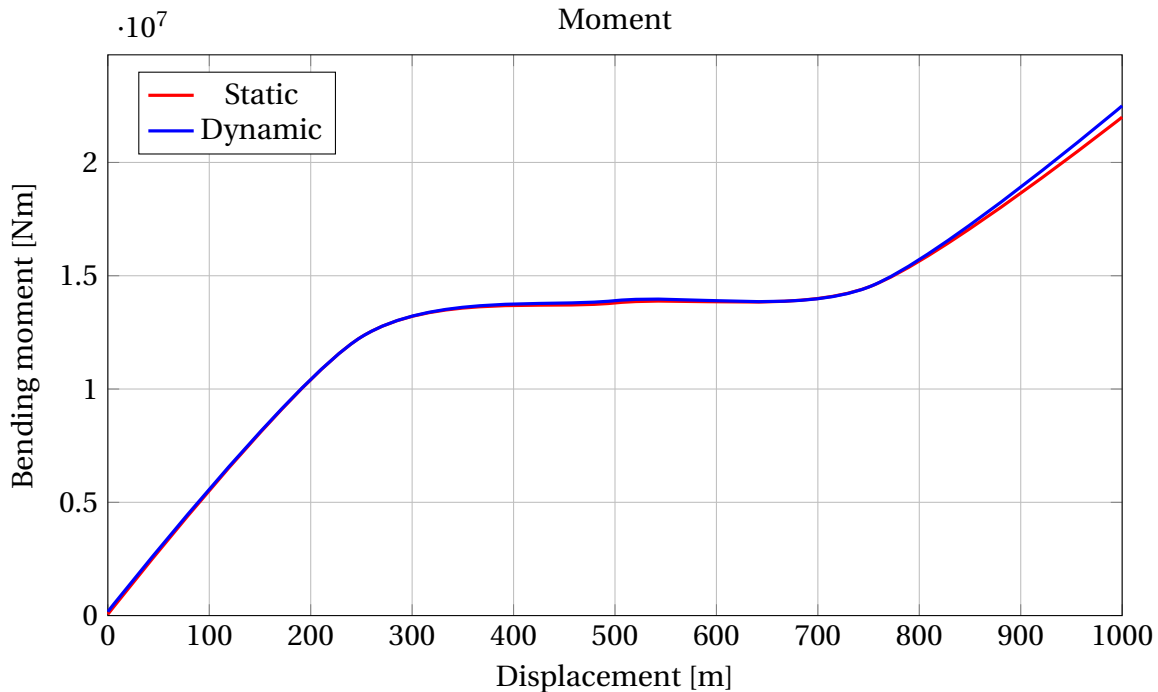
Figure 7.12: Parameter study for Scenario 3, Moment

The dynamic displacement is shown in figure 7.13 plotted against the degree of bending.

Similar as for the other results, the response is not significant for the X-values between 0 and 750, but show large dynamic displacement for a X-value of 1000.
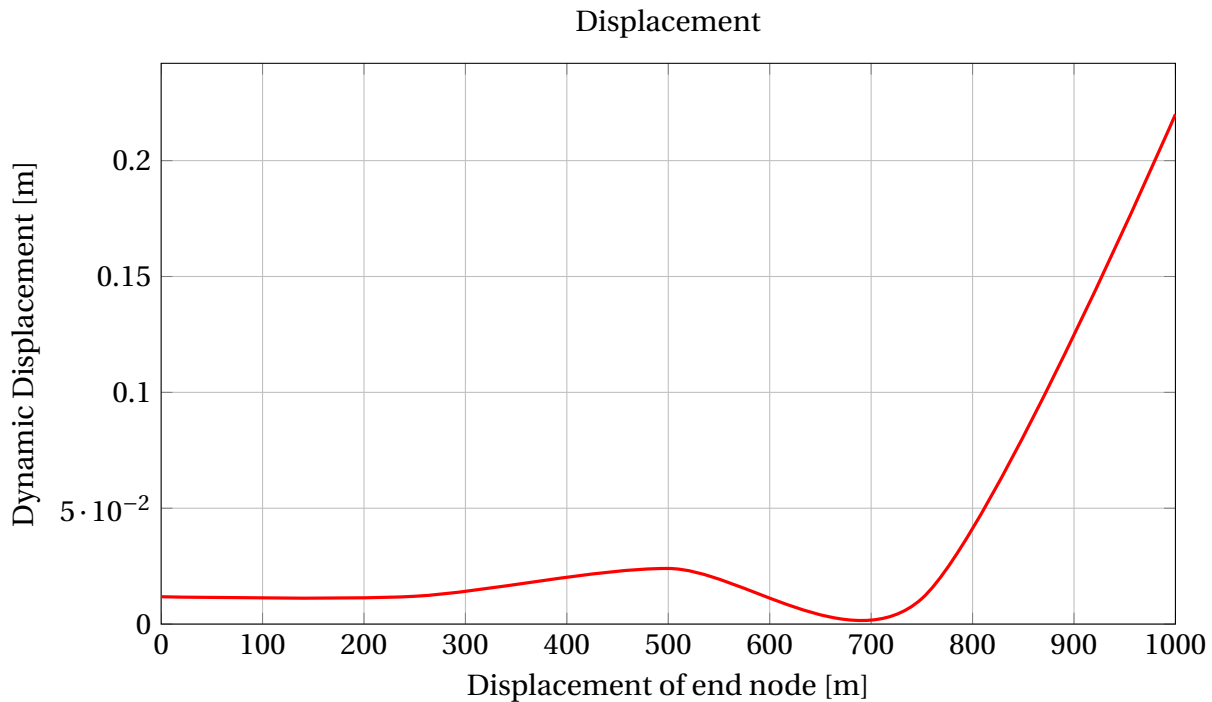
Figure 7.13: Parameter study for Scenario 3, Displacement

Detailed Results

The static responses of this scenario are the exact same as for the previous scenario, because the static configurations are equal for both scenarios. Thus will they not be shown here, but can be found in Appendix C.1.3.

Also the eigenmodes are similar as the previous scenario, and will not be presented here. However, in order to describe the dynamic behavior of the bundle properly, it turned out to be necessary with more eigenvectors than 10. As a result the important eigenvectors are plotted and shown for X- and Z-displacement. The Y-displacements are so small that they are negligible. Figure 7.14 show eigenvector number 29 for X-displacement. The frequency of this vector is 0.0863 $1/s$, which corresponds to 11.59 s. Eigenvector number 56 for displacement in Z-direction is shown in figure 7.15 below. This vector has frequency of 0.3564 s, which corresponds to 2.8 s.
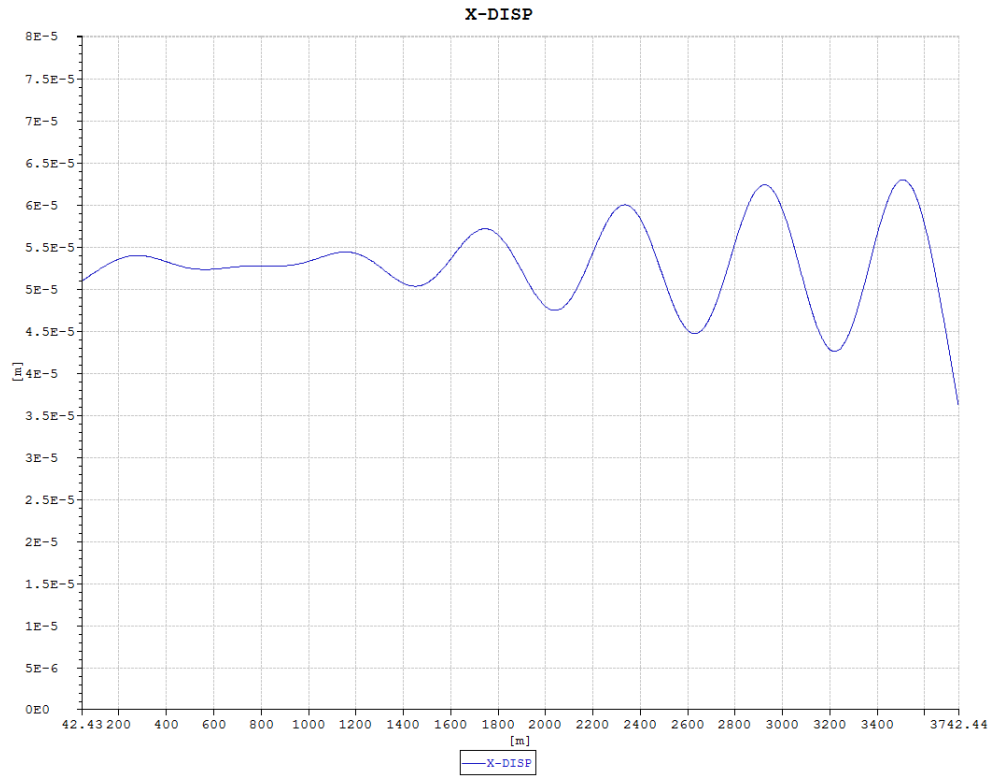
Figure 7.14: Eigenvector no. 29 for X-displacement
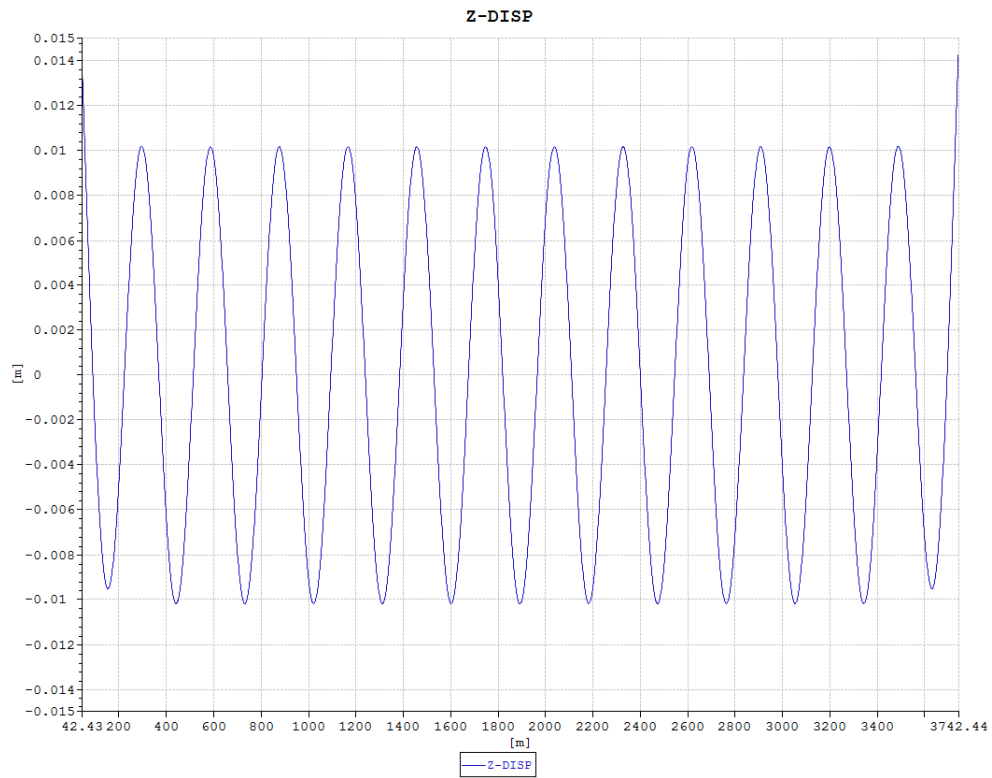
Figure 7.15: Eigenvector no. 56 for Z-displacement

The dynamic displacement for the most bent bundle is seen in figure 7.16, and show that very large displacements occur in the Z-direction. The other responses are much smaller in comparison. The largest displacement is found to be 0.22 m, which is significant compared with 0.012 m for the straight bundle.
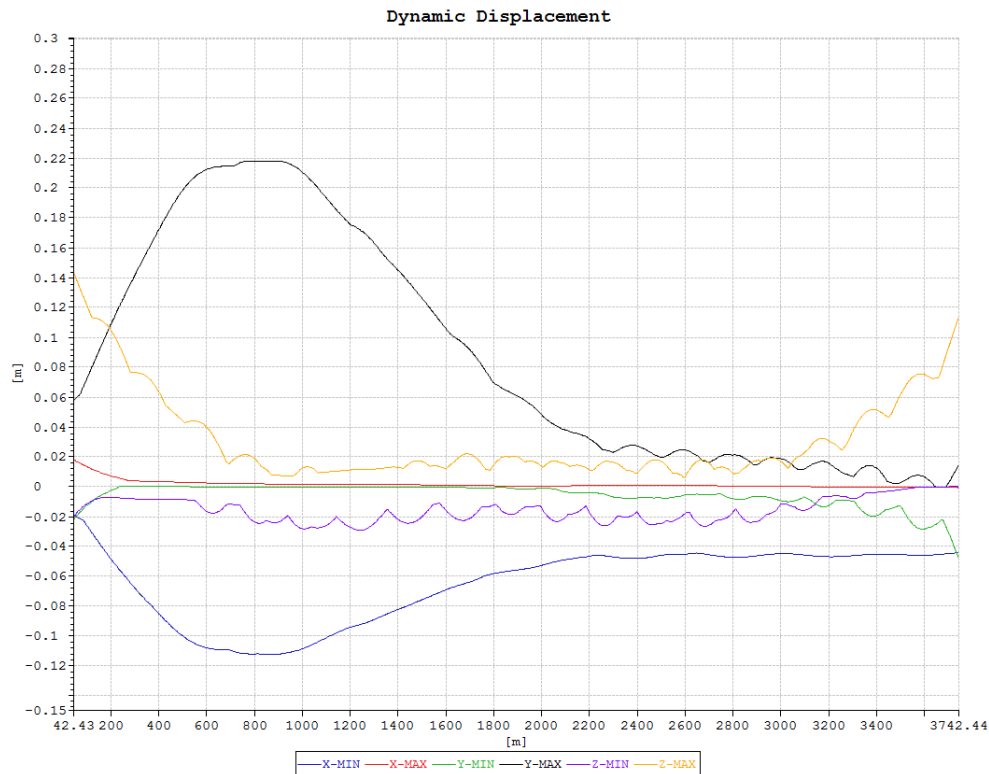
Figure 7.16: Dynamic displacement, X=1000

The dynamic moment, figure 7.17, show large moments about the Z-axis. The maximum value is approximately 2.3E+07 Nm, compared with 1.75E+05 Nm for the straight bundle.
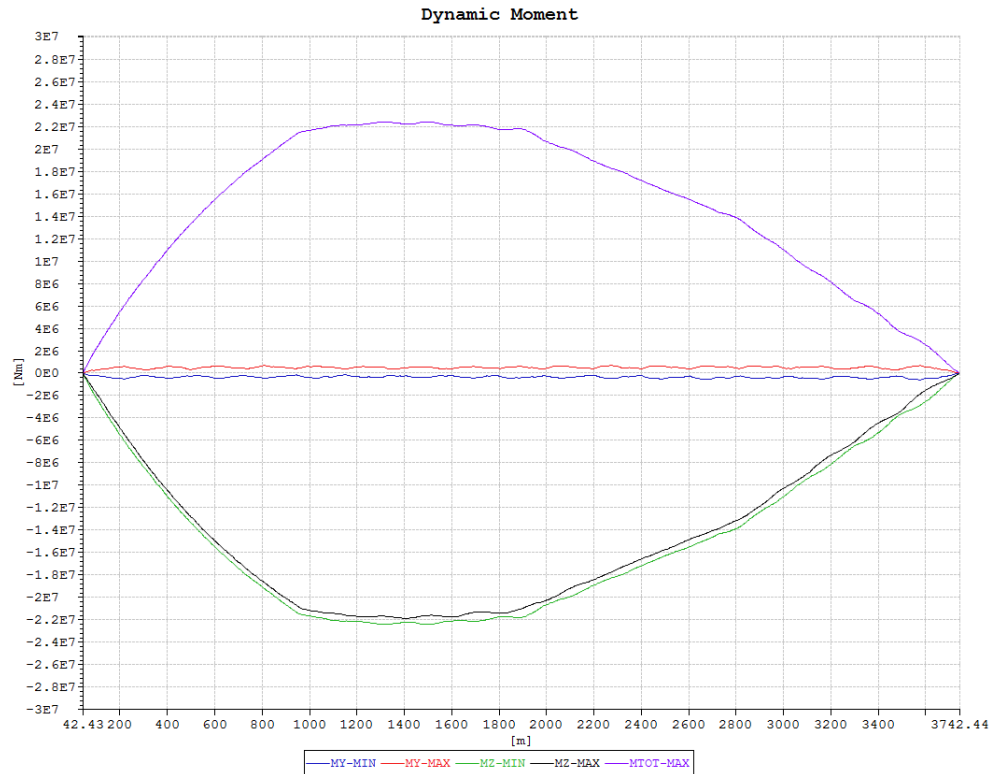
Figure 7.17: Dynamic moment, X=1000

The behavior of the bundle during transportation is difficult to interpret based on these results alone. For the straight bundle it is seen that both the moment and the displacement are varying over the length of the bundle. It is thus relevant to find out which modes are active during the analysis, as it will reveal more about the behavior of the bundle. Based on this, snapshots of the bundle displacements were taken out at two different time instants of the 100 s long dynamic analysis. The results below show the displacement in X- and Z-direction for time instant 50 s (blue) and 70 s (red).

The snapshot of the X-displacement is seen in figure 7.18. Both the graphs have approximately 11 half circles, counting both the positive and negative peaks. This corresponds with eigenvector number 29 shown above. Furthermore, it is likely that other modes are interacting as well, making the displacement differ somewhat from mode number 29.
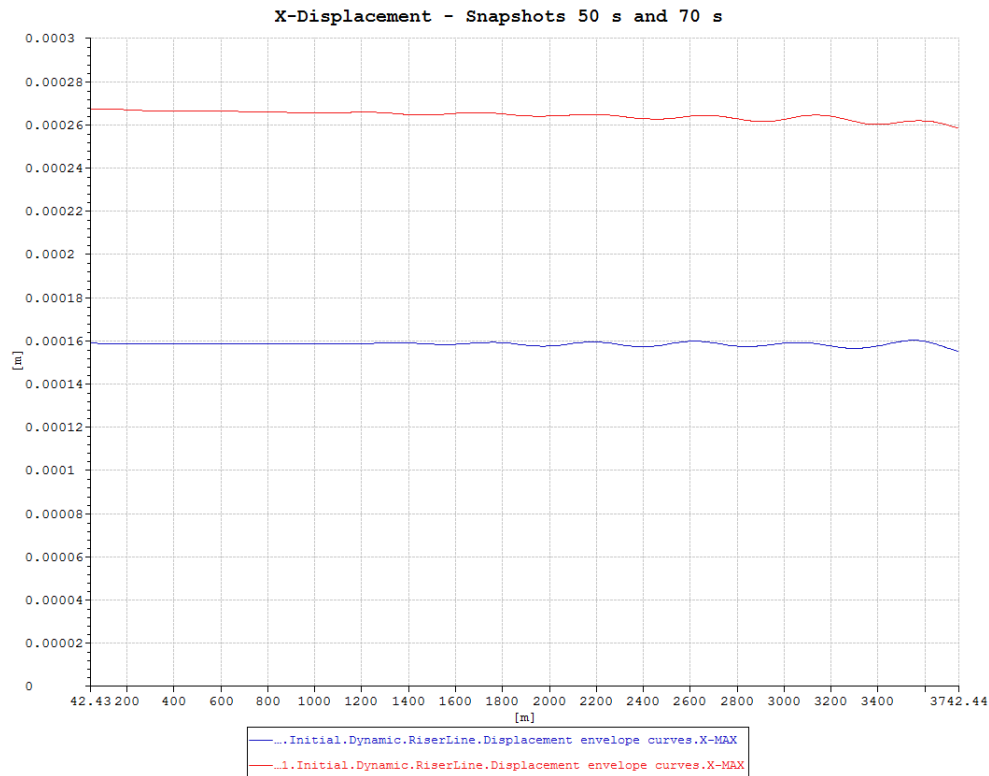
Figure 7.18: Snapshot of X-displacement

The snapshot of the Z-displacement is shown in figure 7.19 below. It is observed that the displacement show approximately 12 positive peaks, when studying the red line. This behavior corresponds to eigenvector number 56 shown above. Additionally, it is seen that the end points of mode 56 follow the same development as for the displacement below. This mode is thus causing the main behavior of displacement in Z-direction in the bundle during tow. However, there are observed additional "double-peaks" in the displacement, which suggests that more modes than one interact in the behavior of the bundle. The blue line show more peaks than 12, which may indicate that an even higher mode is activated, or that several modes interact on this behavior as well.
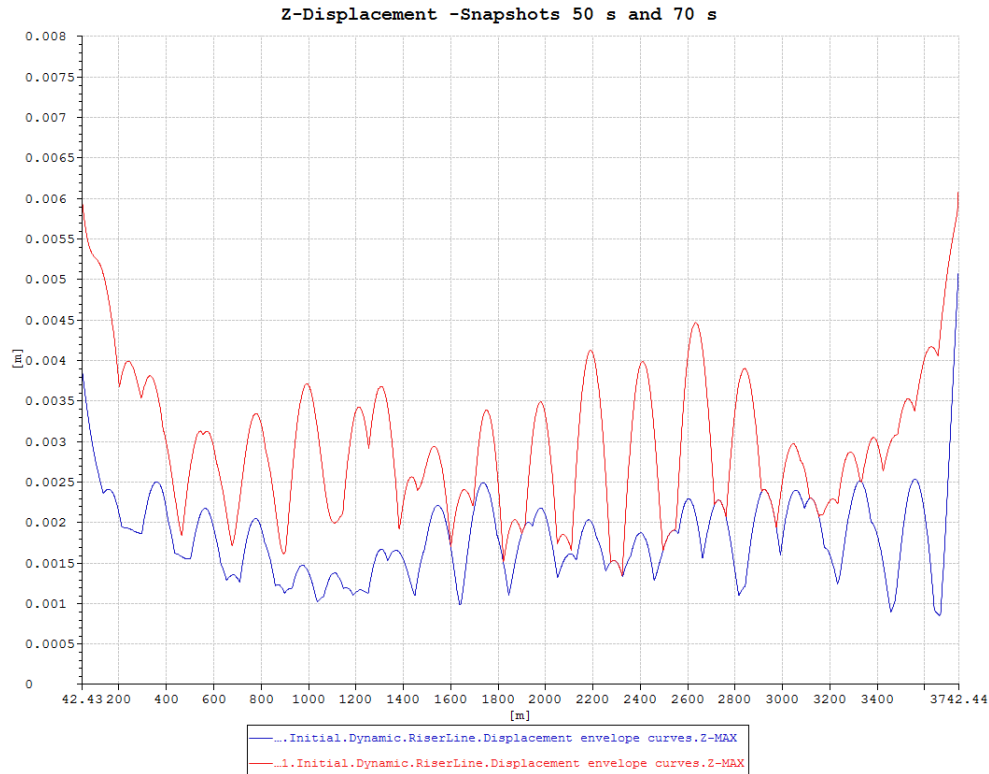
Figure 7.19: Snapshot of Z-displacement

The dynamic torsional moment, which can be found in Appendix C.1.3, show values that are quickly shifting. The uneven response show the largest values for the moment about the Y-axis.

7.1.4   Assessment of Scenario 1, 2 and 3

This section aims to compare the results from the different scenarios, to find which of the three scenarios that are likely to be most critical. The maximum bending moments from scenario 2 and 3 are one exponent larger than in scenario 1. Of the two scenarios 2 and 3, it is scenario 2 that has the largest bending moments and dynamic displacements. The absolute largest torsional moment however, appear for scenario 3. This value only apply for the last bent configuration, and for all the other configurations the torsional moment is very small. For scenario 2 the torsional moments for the different configurations are of significant size, and the consequence of this is that scenario 2 has the largest responses for torsional moments as well.

7.2   Installation of Bundle

7.2.1   Scenario 1: Horizontal Plane

In this scenario only the horizontal plane is utilized for installing the bundle. The static and dynamic results for this scenario is showed in the following sections.

Detailed Results

The illustrations of the static displacements can be found in Appendix C.2.1. The displacement in the XY-plane show how many meters the middle point of the bundle is displaced due to towing tugs and current acting on it. The middle point is displaced approximately 420 m. For the displacement in the XZ-direction, the towed end point is observed to be positioned at -29 m, instead of -30 m. Thus should this end have added even more weight to be lowered the additional meter. However, it is seen that the middle part of the bundle is lowered additional 8 to 14 m. This could indicate that too much additional weight is added to the bundle, and that the weight should have been applied more densely to the ends instead. This tendency is also indicated in the figure illustrating the YZ-displacement.

The static bending moment for this scenario is shown in figure 7.20 below. The peaks are due to the towing tugs, and the largest moment is approximately 3.75E+07. It is the moment about the Z-axis that gives the largest responses, but the moment about the Y-axis is of significant size close to the end points. The static torsional moment develops as a straight line of magnitude 7.3E+05, and can be found in appendix C.2.1.
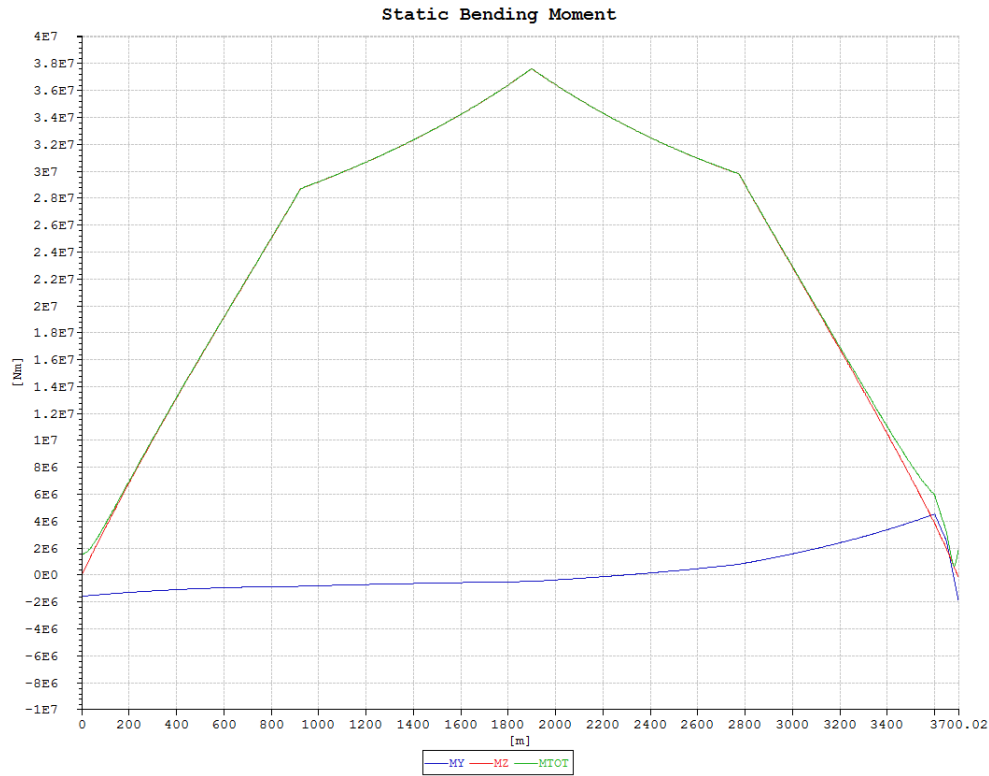
Figure 7.20: Static bending moment

The ten first eigenvalues of the bundle is given in table 7.2 below. The values are given for both frequency and period. The eigenvalues for the displacement in X-, Y- and Z-direction can be found in the appendix C.2.1. It is observed that the mode shapes for this configuration appear as regular mode shapes with an increasing number of half circles for larger mode numbers.

Table 7.2: Eigenvalues for the bundle, Scenario 1 of installation

Mode	Frequency [$1/s$]	Period [s]
1	0.0010	1000
2	0.0022	454.55
3	0.0024	416.67
4	0.0031	322.58
5	0.0049	204.08
6	0.0061	163.93
7	0.0079	126.58
8	0.0101	99.01
9	0.0116	86.21
10	0.0151	66.23

The dynamic displacement is seen in figure 7.21 below. It shows small values for all displacements, with a peak for displacement in Z-direction equal to 0.05 m. It is also observed that the displacement in X-direction give the second largest responses.
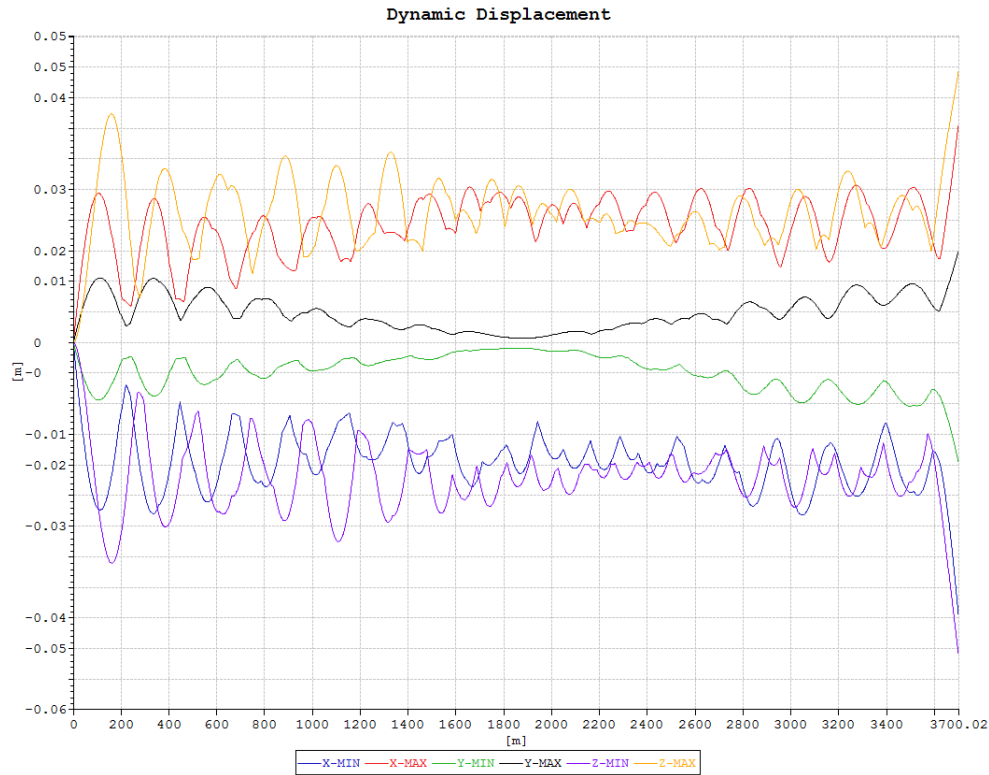
Figure 7.21: Dynamic displacement

The dynamic moment can be seen in the figure 7.22 below. The dynamic moment gives large responses, and once again the positions of the towing tugs are clearly indicated by the peaks. The dynamic torsional moment can be found in appendix C.2.1. From the graphs it is observed that the torsional moment will behave as constant over the length of the bundle. However, it is noted that there are some varying peaks along the bundle, although these variations are small. The size of the torsional moment is of an exponent 10^5, thus giving moments of significant size.
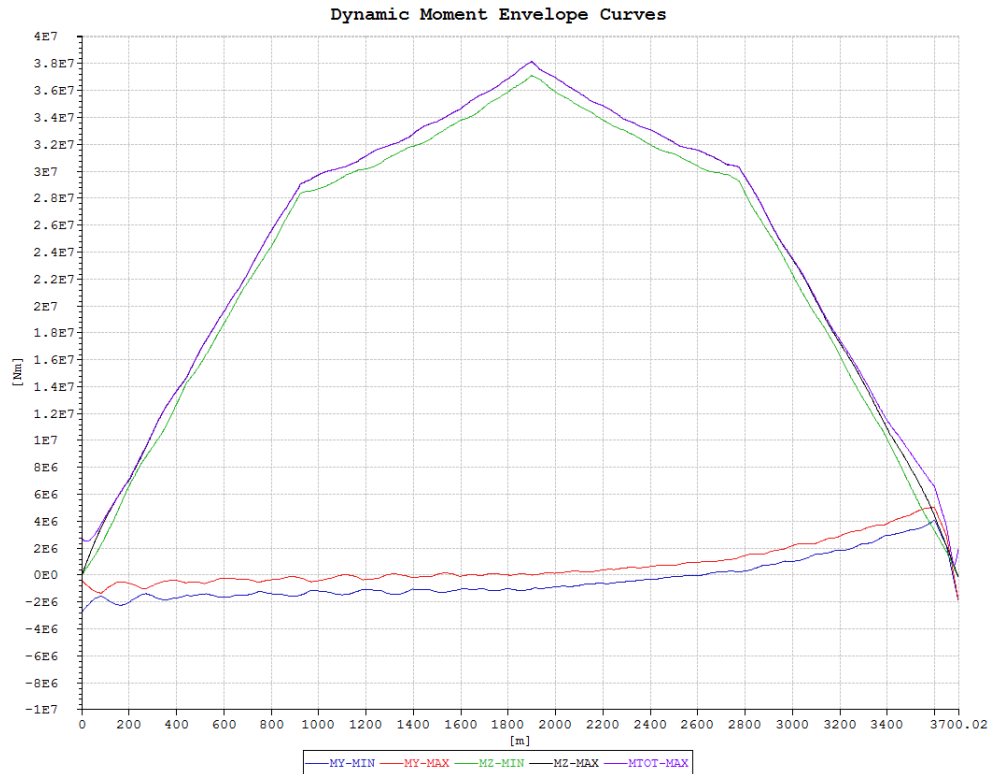
Figure 7.22: Dynamic moment

7.2.2 Scenario 2: Vertical plane

Detailed Results

The static displacements can be found in the Appendix, C.2.2. It observed that there are 6 m displacement of the middle point of the bundle in the horizontal direction. This is due to the current pushing the bundle sideways. Furthermore it is seen that the distance between the two end points of the bundle is 3600 m, as it should be. The XZ-displacement show that the horizontal displacement of the bundle is not the same over the length of the bundle. The figure showing the static YZ-displacement emphasizes why the bundle is exposed to large forces in this configuration. The bundle is subjected to large differences in depth over a very short distance of the bundle.

The static bending moment in this configuration is shown in figure 7.23. It is seen that the bending moment is unevenly distributed over the length of the bundle, with a peak at the fixed and point. The moment about the Y-axis is largest. The static torsional moment develops almost

as a constant line, with maximum of 2.58E+06 Nm.
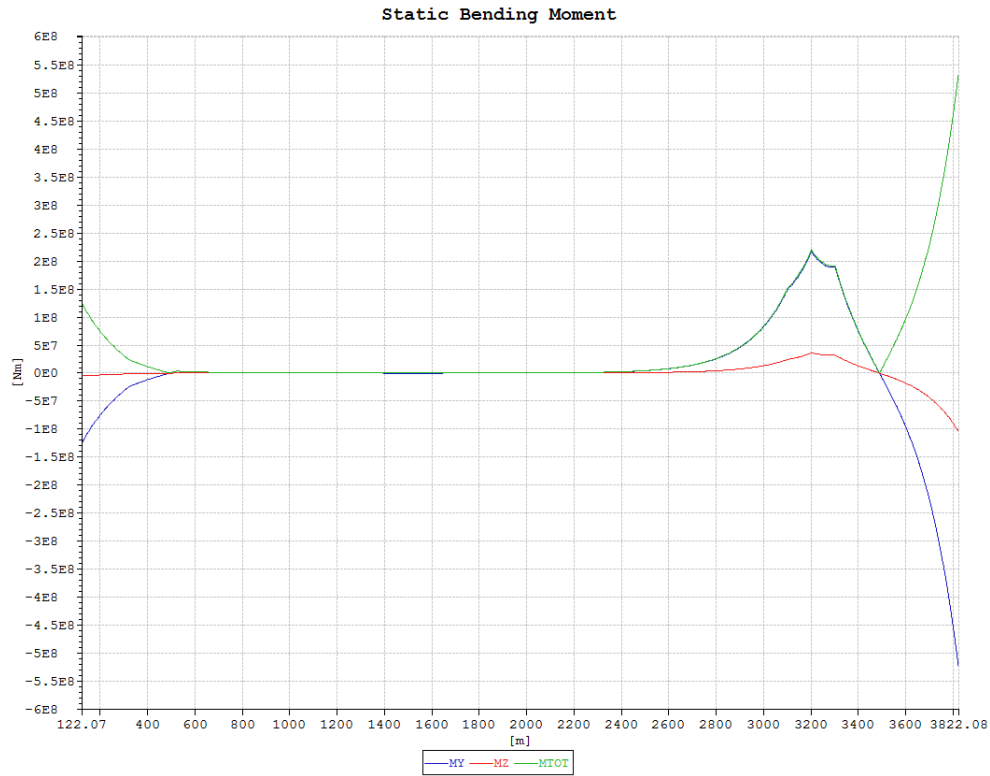
Figure 7.23: Static bending moment

Table 7.3 shows the ten eigenvalues given in both frequency and period. The graphical representation for the eigenmodes can be found in the appendix C.2.2. The modes for X-displacement appear as regular mode shapes, while the ones for Y- and Z-displacement differs more from the regular half circles.

Table 7.3: Eigenvalues for the bundle, Scenario 2 of installation

Mode	Frequency [1/s]	Period [s]
1	0.0040	250.00
2	0.0052	192.31
3	0.0080	125.00
4	0.0107	93.46
5	0.0123	81.30
6	0.0167	59.88
7	0.0175	57.14
8	0.0233	42.92
9	0.0234	42.74
10	0.0286	34.97

The dynamic displacement seen in figure 7.24 below shows that the maximum displacement is in the Z-direction. This displacement is over 2 m, which is large compared with previous results. The remaining displacements are not that large, although the Y-displacement have a sudden peak of 2 m at the towed end point.
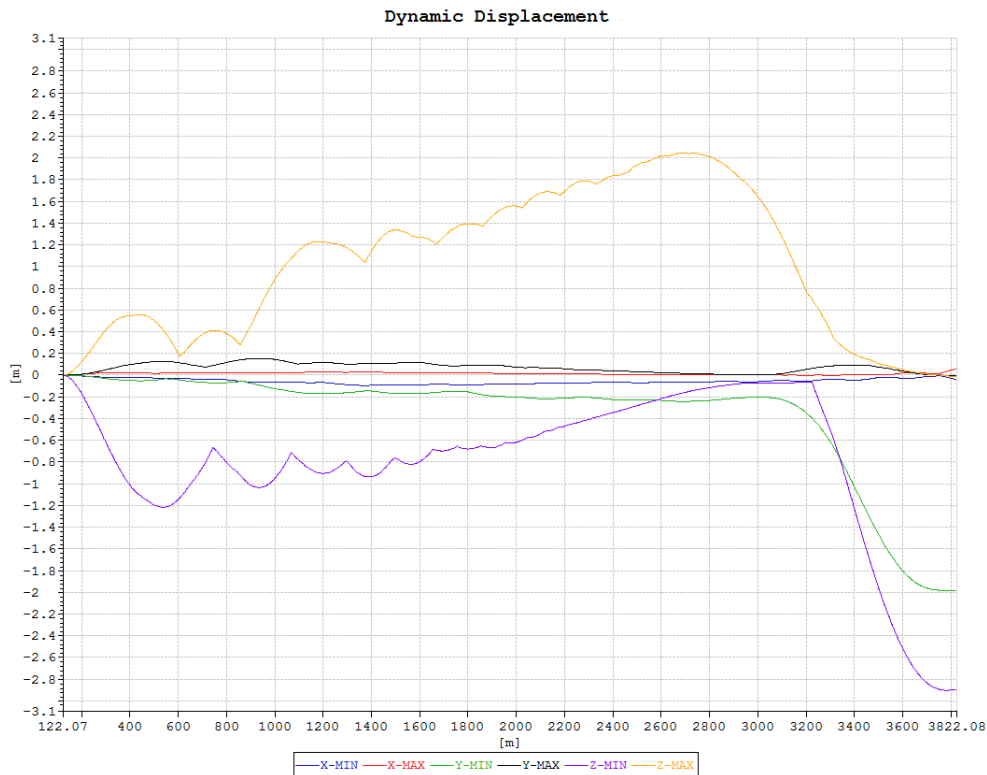
Figure 7.24: Dynamic displacement

The dynamic moment seen in figure 7.25 below has got a similar shape as the static bending moment, with peaks at the fixed end point. The maximum value is found to be approximately 5.5E+08 Nm.
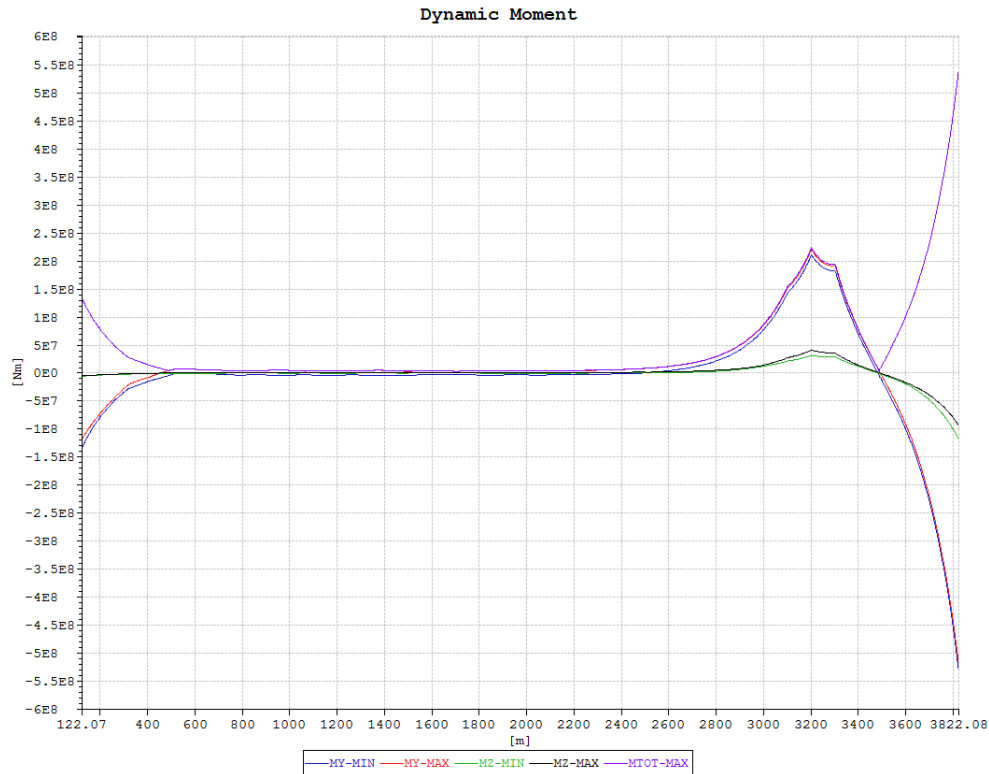
Figure 7.25: Dynamic moment

The dynamic torsional moment is given in Appendix C.2.2. The torsional moment is seen as quite stable, but is slightly deviating along the length of the bundle. The maximum moment is found to be 2.9E+06 Nm.

7.2.3 Scenario 3: Both Horizontal and Vertical Plane

The results for the two parts of this scenario are presented in the following sections. The parameter studies were conducted for both parts, and are thus shown separately in each section. The results from Part 1 should have the most impact when considering the results. This is because the static and dynamic analyses will be run for the configurations with different depths on the final node being installed. This is in contrast to Part 2, where the static and dynamic analyses will be run for the final configuration of the bundle, which means that all the

runs are for a bundle end -30 m below the sea surface. Thus is it only the initial configuration in part that 2 causes the different stress states for the final configuration.

Part 1 - Parameter Study

In the graphs below, the development of the bending moment and the dynamic displacement are seen for increased depth of the free end of the bundle. For the moments, figure 7.26, it is seen a clear connection between increased depth and increased magnitude. However, the differences do not vary significantly, with 2,38E+07 Nm as the smallest moment compared with 2.70E+07 Nm for the largest. For the dynamic displacement in figure 7.27 however, the bundle situated closer to the sea surface will obtain the largest motions.
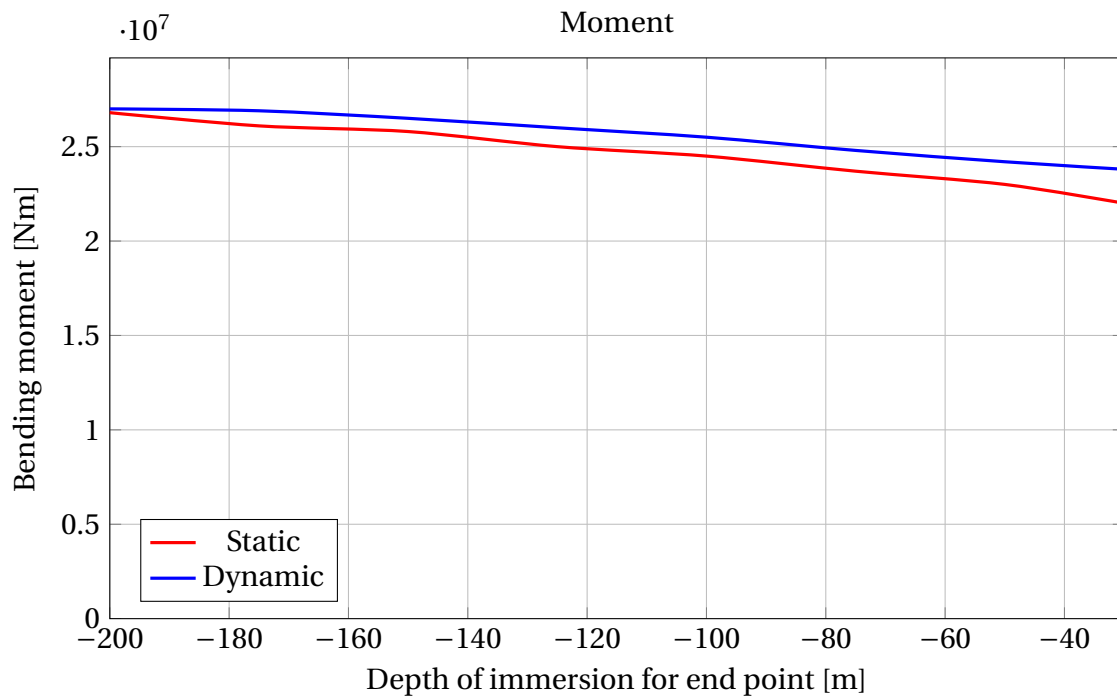
Figure 7.26: Parameter study for Part 1, Moment
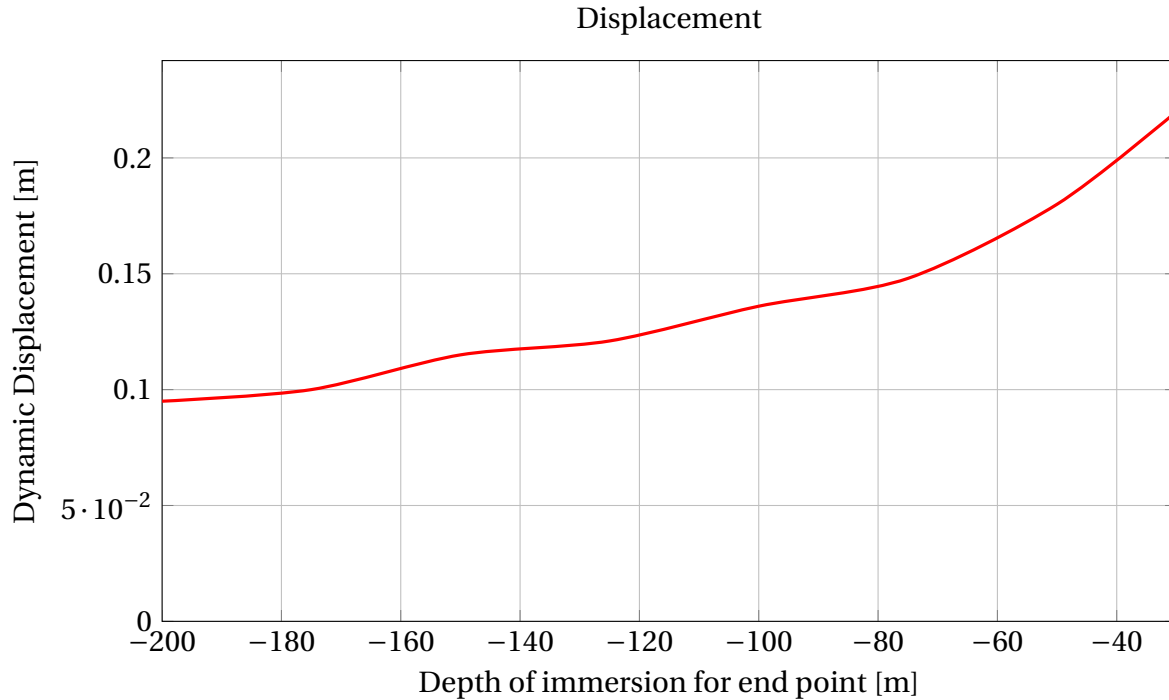
Figure 7.27: Parameter study for Part 1, Displacement

Part 1 - Detailed Results

The largest responses for the moment are observed for a depth of -200 m, and these results will thus be presented here. Figure 7.28 show the static bending moment. The positions of the towing tugs are clearly observed as the peaks that appear on the moment. The maximum value is found to be 2.65E+07 Nm, compared with 2.2E+07 Nm for the bundle submerged -30 m. Thus is the difference not that large. The static torsional moment can be found in Appendix C.2.3. It is observed that it follows a constant value over the length, with a maximum of 4.9E+05 Nm.
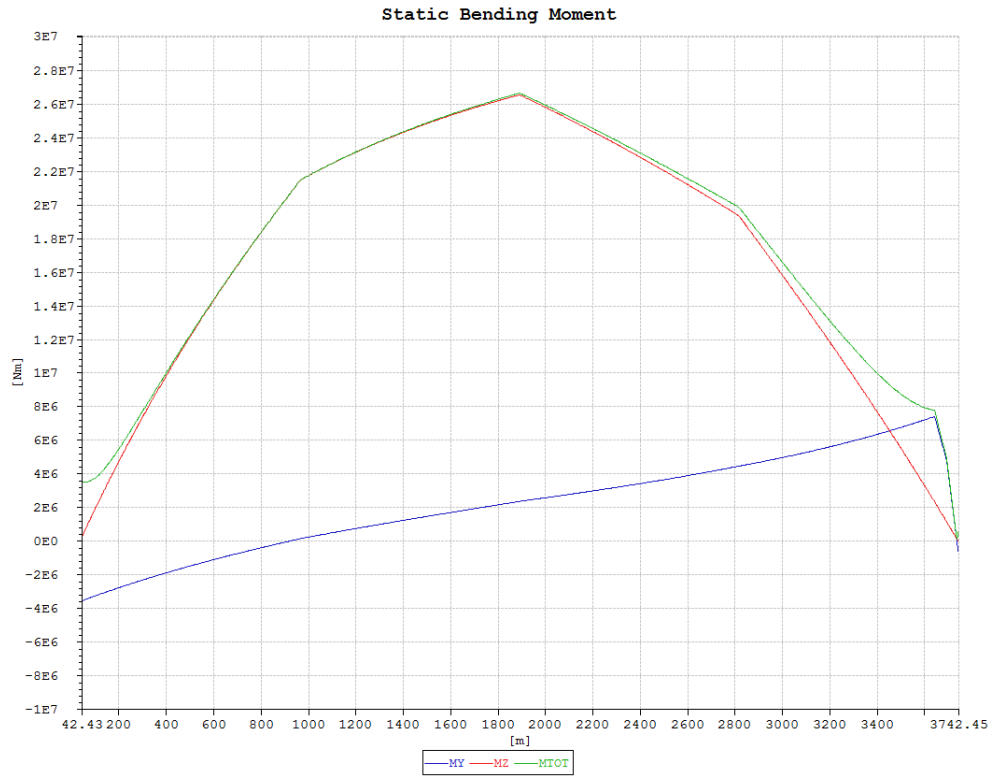
Figure 7.28: Static bending moment, Z=-200 m

The eigenvalues can be seen in table 7.4 given for both frequency and period, for a depth of -30 m and -200 m. The two depths give different eigenmodes and values. The eigenmodes can be found in the appendix C.2.3. The modes for both depths appear to take the shape of regular mode shapes, with an increasing number of half circles for a larger mode number.

Table 7.4: Eigenvalues for the bundle, Scenario 2 of installation

	Depth = -30 m		Depth = -200 m	
Mode	**Frequency** $[1/s]$	**Period** $[s]$	**Frequency** $[1/s]$	**Period** $[s]$
1	0.0010	1000	0.0008	1250
2	0.0014	714.29	0.0009	1111.11
3	0.0023	434.78	0.0019	526.32
4	0.0025	400.00	0.0022	454.55
5	0.0044	227.27	0.0029	344.83
6	0.0046	217.39	0.0035	285.71
7	0.0058	172.41	0.0054	185.19
8	0.0071	140.85	0.0058	172.41
9	0.0093	107.53	0.0082	121.95
10	0.0103	97.09	0.0094	106.38

The dynamic displacement, figure 7.29, show large values at both end points. The motions in between are observed to be not that large. The largest displacement is found to be 0.095 m, compared with 0.22 m for a depth of -30 m. Thus is the displacement for less submerged bundle significantly larger.
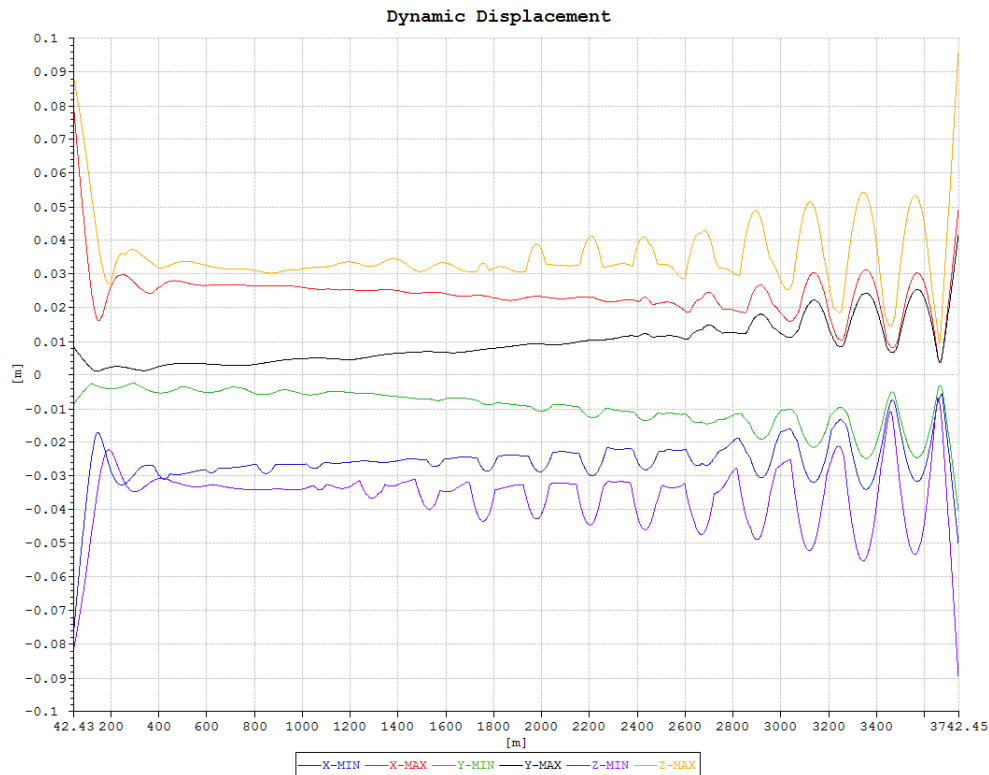
Figure 7.29: Dynamic Displacement, Z=-200 m

The dynamic moment, figure 7.30, are seen to be similar to the static moment. The variations are larger for this moment, especially at the end points. The maximum moment is 2.7E+07 Nm compared with 2.38E+07 Nm for -30 m. The dynamic torsional moment can be found in Appendix C.2.3. It is found to develop as a straight line, with largest value corresponding to 1.97E+06 Nm.
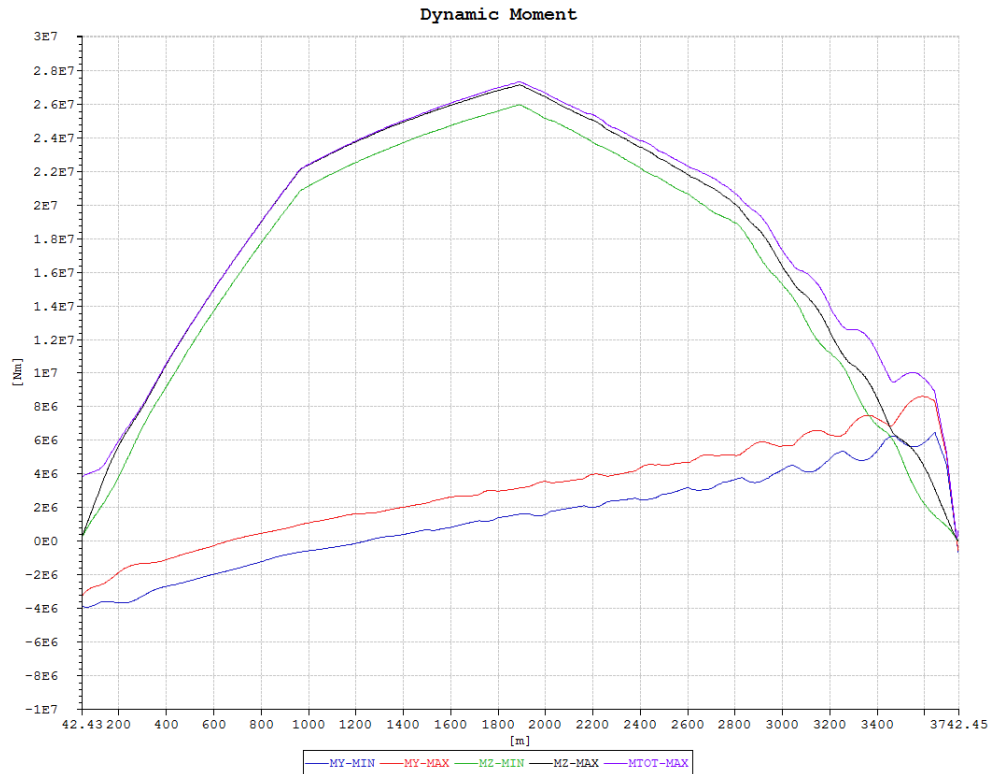
Figure 7.30: Dynamic moment, Z=-200 m

Part 2 - Parameter Study

The parameter study was conducted for this part as well, for the same parameters as for Part 1. The graph for the moments, figure 7.31 do not show any clear correspondence between bending moment and depth. Rather, a varying result that is slowly decreasing is seen. It is likely to believe that these variations are due to small differences between the analyses, although several analyses were run to verify the given results.

The graphs for the displacement, 7.32 show that the depth for the initial configuration will not have a large impact on the dynamic displacement in the final configuration. However, a large increase in displacement is seen for the results of -200 m.
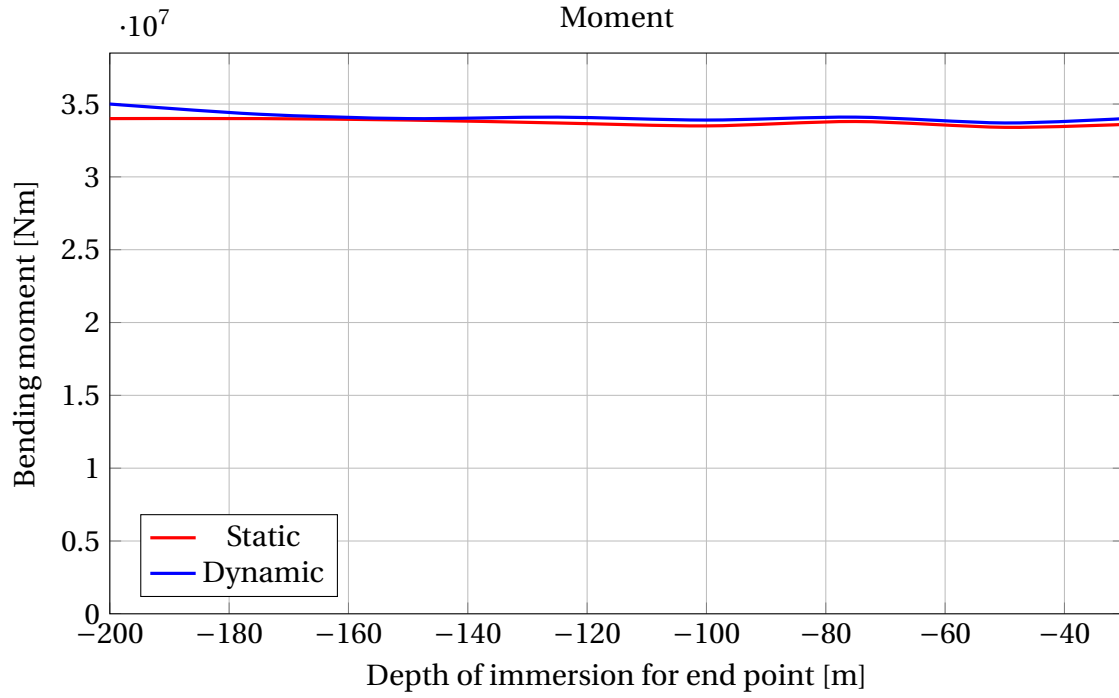
Figure 7.31: Parameter study for Part 1, Moment
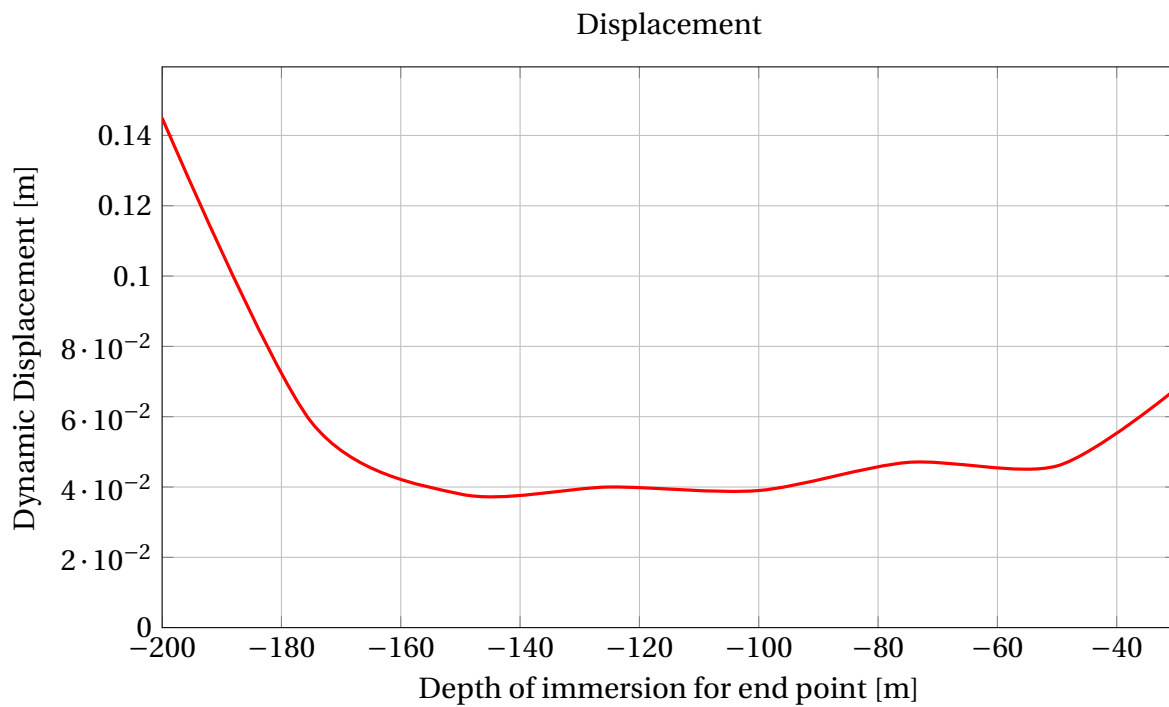
Figure 7.32: Parameter study for Part 2, Displacement

Part 2: Detailed Results

The results for a depth of -200 m are presented here. The static bending moment is seen in figure 7.33. The effect of the increased pull of the tugs is observed in this moment, as the three peaks representing the tugs are larger than for previous results.
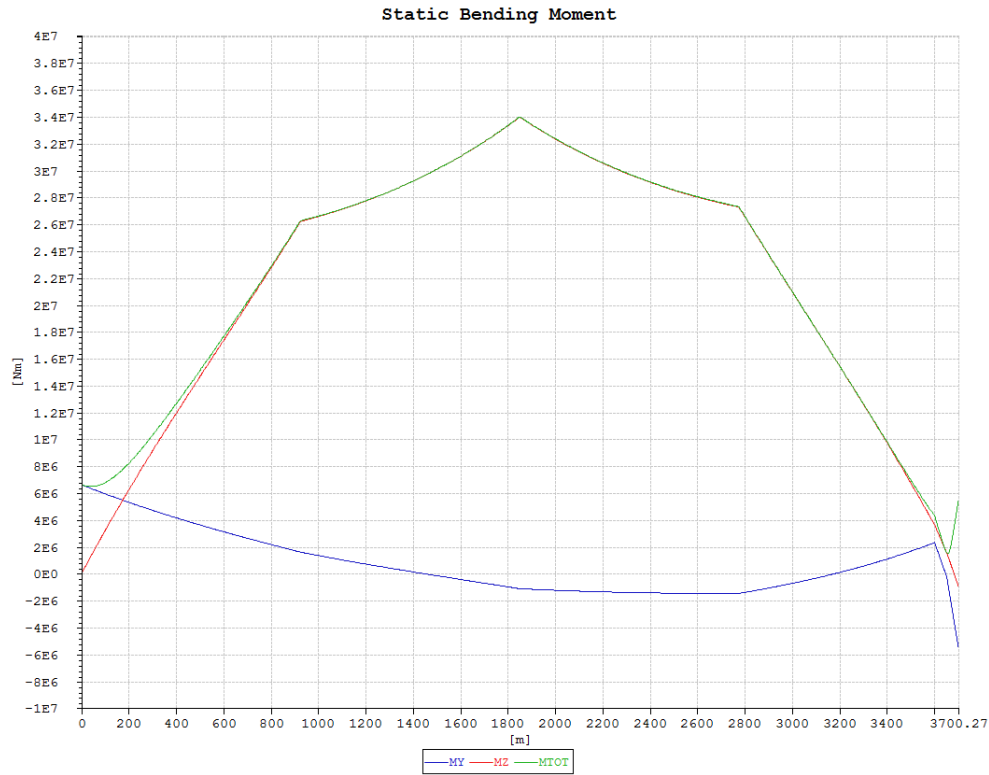
Figure 7.33: Static bending moment, Z=-200 m

The static torsional moment is illustrated in the Appendix C.2.4. The graph shows constant values of the torsional moments, with the largest value being 1.95E+06 Nm.

The eigenvalues are calculated for the final configuration, which is equal for all depths for this part of the scenario. Based on this, only one set of eigenvalues and modes are shown in this section. The table below contains the eigenvalues given in both frequency and period. It is observed that the frequency is very small for the first modes, and that some frequencies are multiplications of previous ones. The eigenmodes can be found in Appendix C.2.4 for displacements in X-, Y- and Z-direction. The modes appear to be regular half circle modes for X- and Z-displacement, with larger deviations for the Y-displacement.

Table 7.5: Eigenvalues for the bundle, Scenario 2 of installation

Mode	Frequency $[1/s]$	Period $[s]$
1	0.0011	909.09
2	0.0022	454.54
3	0.0025	400.00
4	0.0032	312.5
5	0.0050	200
6	0.0062	161.29
7	0.0081	123.46
8	0.0103	97.09
9	0.0118	84.75
10	0.0154	64.94

In order to describe the dynamics of the bundle during installation, more eigenvectors were necessary. Therefore, three additional eigenvectors are presented here. For the displacement in X-direction, eigenvector number 69 is shown below in figure 7.34. The frequency of this mode is 0.6074 $1/s$, which corresponds to 1.65 s.
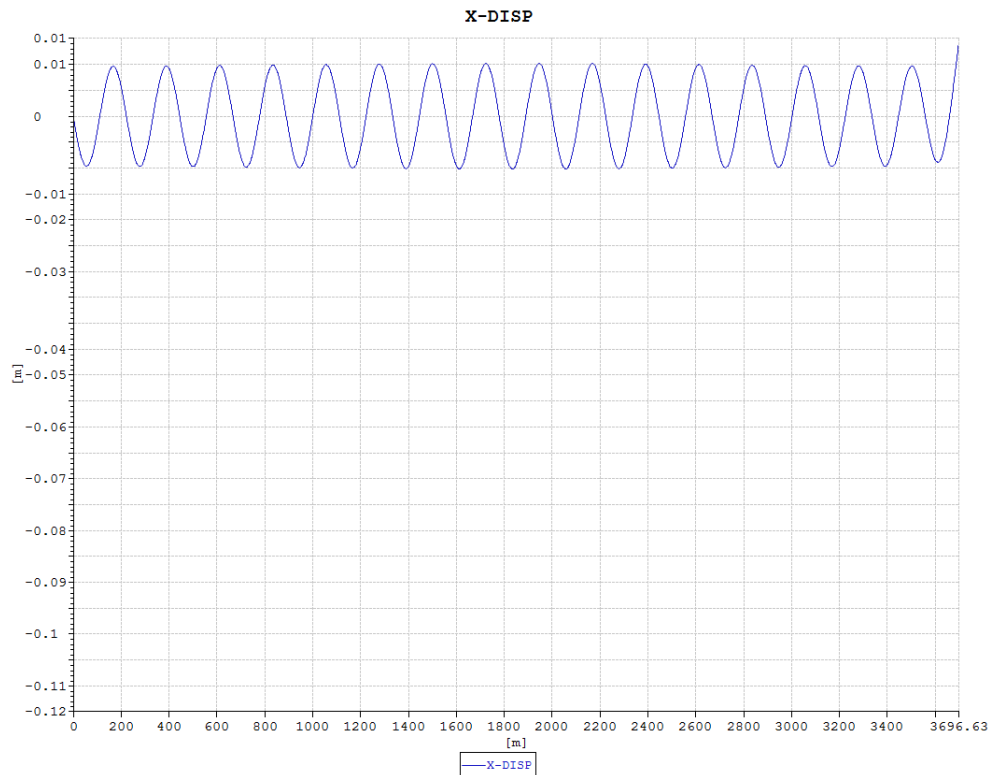
Figure 7.34: Eigenvalue in Z-direction for final configuration Scenario 3, Part 2

Mode number 66 is shown in figure 7.35 for displacement in Y-direction, and figure 7.36 for Z-direction. The frequency is 0.5456 1/s, corresponding to a period of 1.83 s.
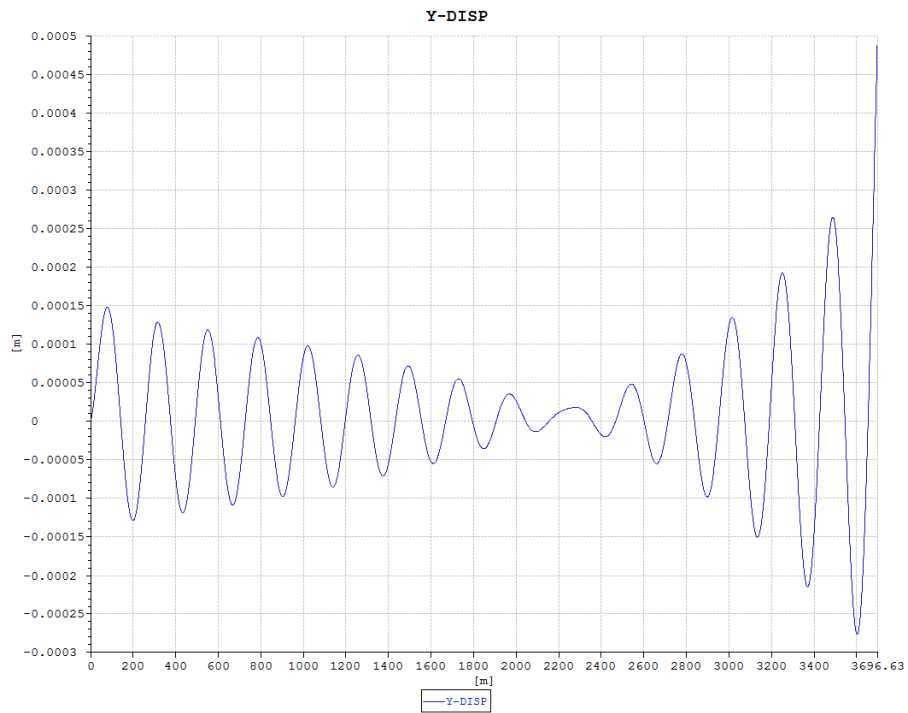
Figure 7.35: Eigenvalue in Y-direction for final configuration Scenario 3, Part 2
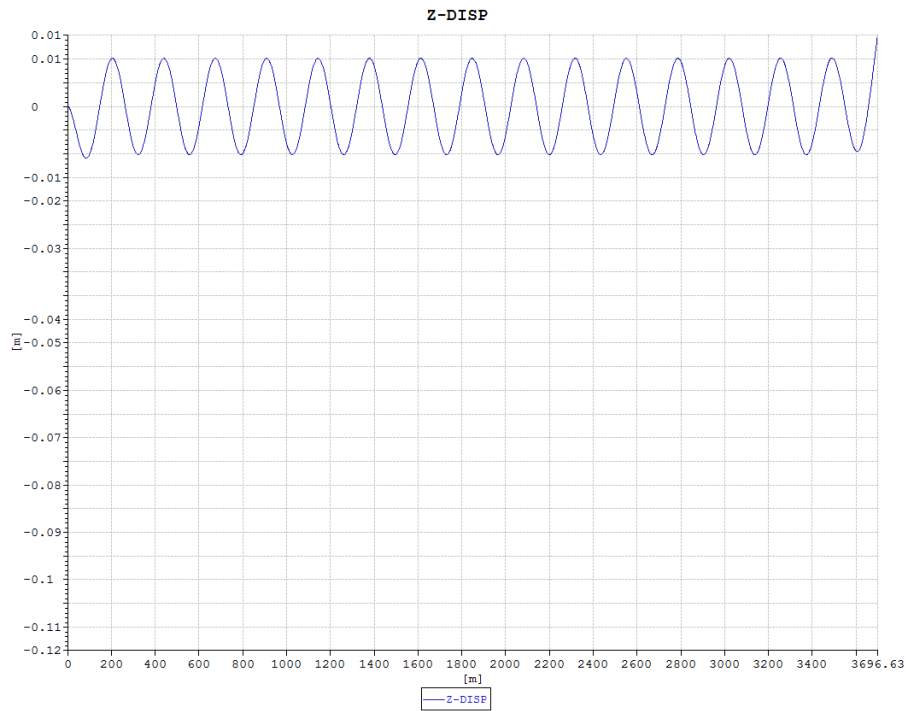
Figure 7.36: Eigenvalue in Z-direction for final configuration Scenario 3, Part 2

The dynamic displacement is seen in figure 7.37 below, and shows large displacements for the towed end point in Z-direction. The maximum value is 0.145 m, compared with 0.07 m for -30 m. However, the responses on the other parts of the bundle are not that large, with approximately 0.03 m as mean.
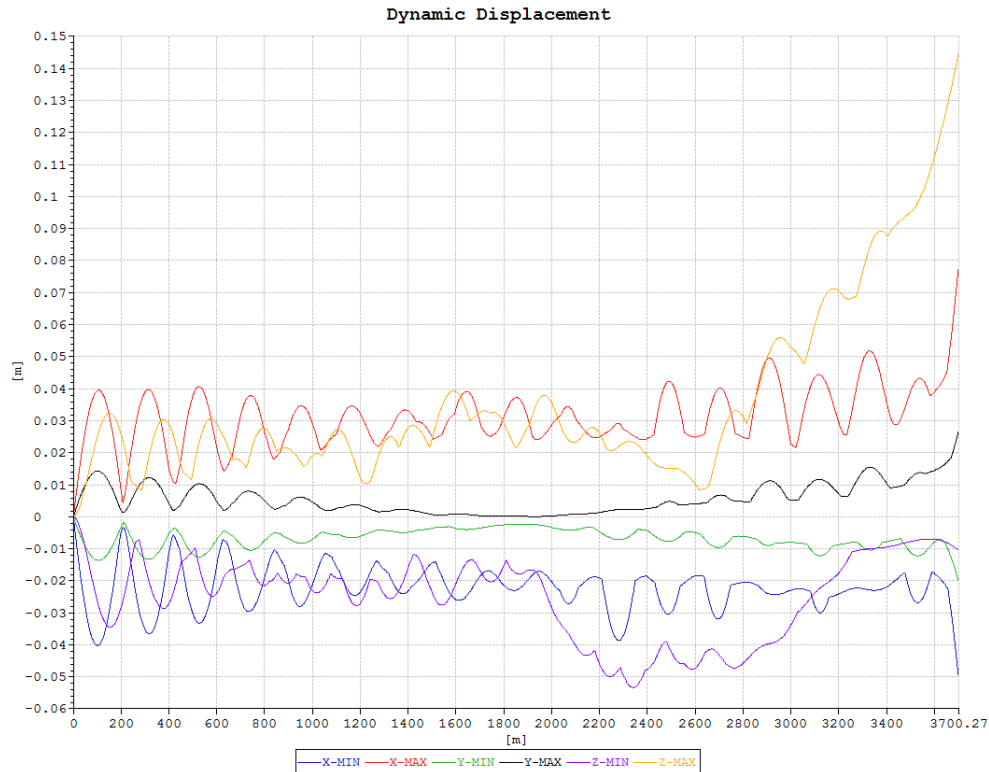
Figure 7.37: Dynamic Displacement, Z=-200 m

Also for the dynamic bending moment, figure 7.38, the locations of the towing tugs are clearly seen as the peaks. The largest moment is seen to be approximately 3.5E+07 Nm. The dynamic torsional moment can be found in appendix C.2.4, and reveal a close to constant value over the length. On some locations it is observed small deviations from the straight line. The maximum value is 5.3E+05 Nm.
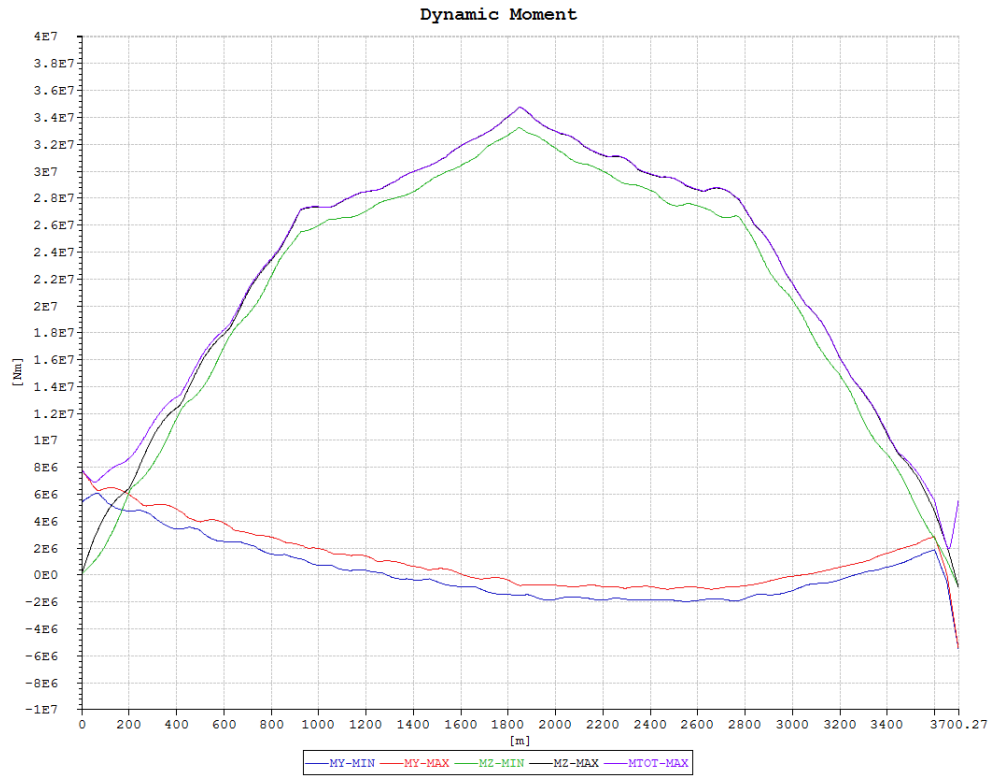
Figure 7.38: Dynamic moment, Z=-200 m

For this scenario as well, snapshots of the displacement during a 100 s dynamic analysis is taken out. The snapshots were taken at 50 s (blue) and 70 s (red). Figure 7.39 shows the snapshots for displacements in X-direction. It is seen that it has approximately 16 peaks for both lines, which corresponds to mode 69 shown previously. Figure 7.40 shows the Y-displacement for time instants 50 s and 70 s. It is seen that this develops as a curve with approximately 15 peaks, corresponding to the number of peaks and shape of the eigenmode number 66 shown previously.
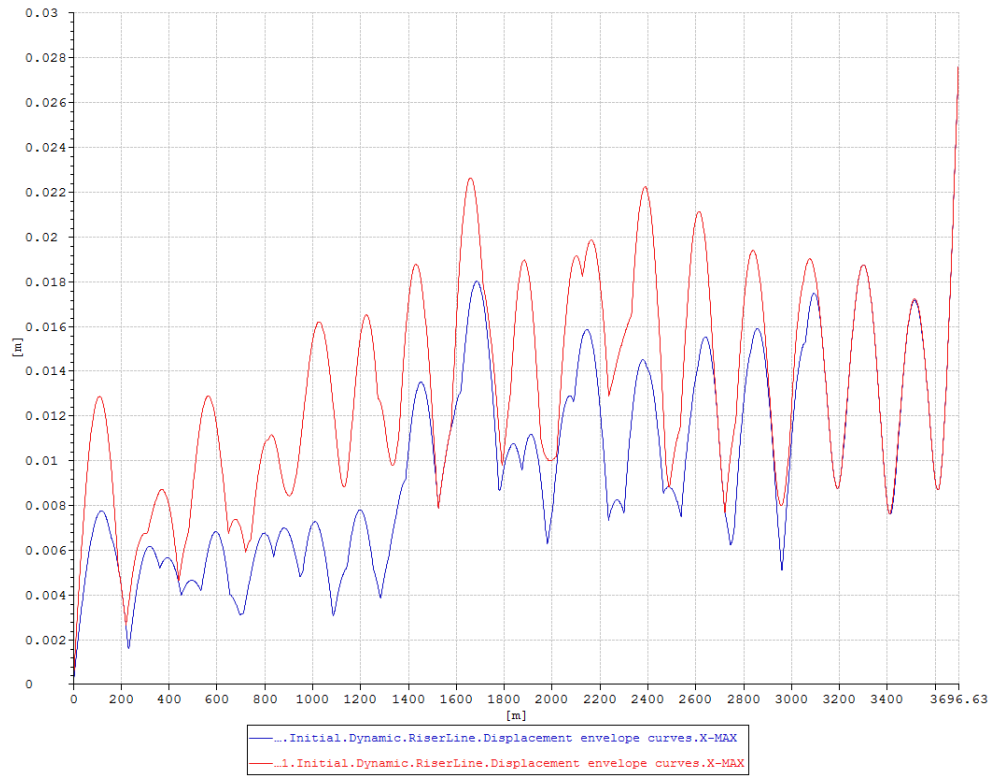
Figure 7.39: Snapshot of X-displacement at time instants 50 s and 70 s
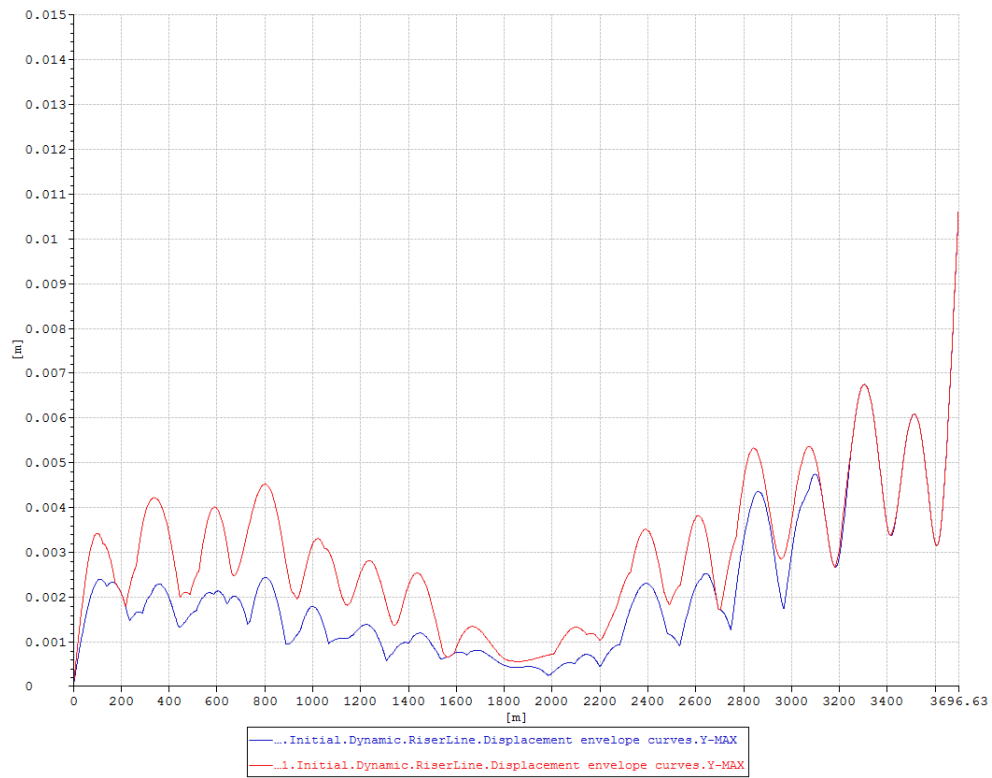
Figure 7.40: Snapshot of Y-displacement at time instants 50 s and 70 s

Below is the illustration of the Z-displacement for time instants 50 s and 70 s, figure 7.41. It is observed that this shape is close to that of eigenmode 66 for Z-displacement shown above, with the same number of approximately 15 peaks.
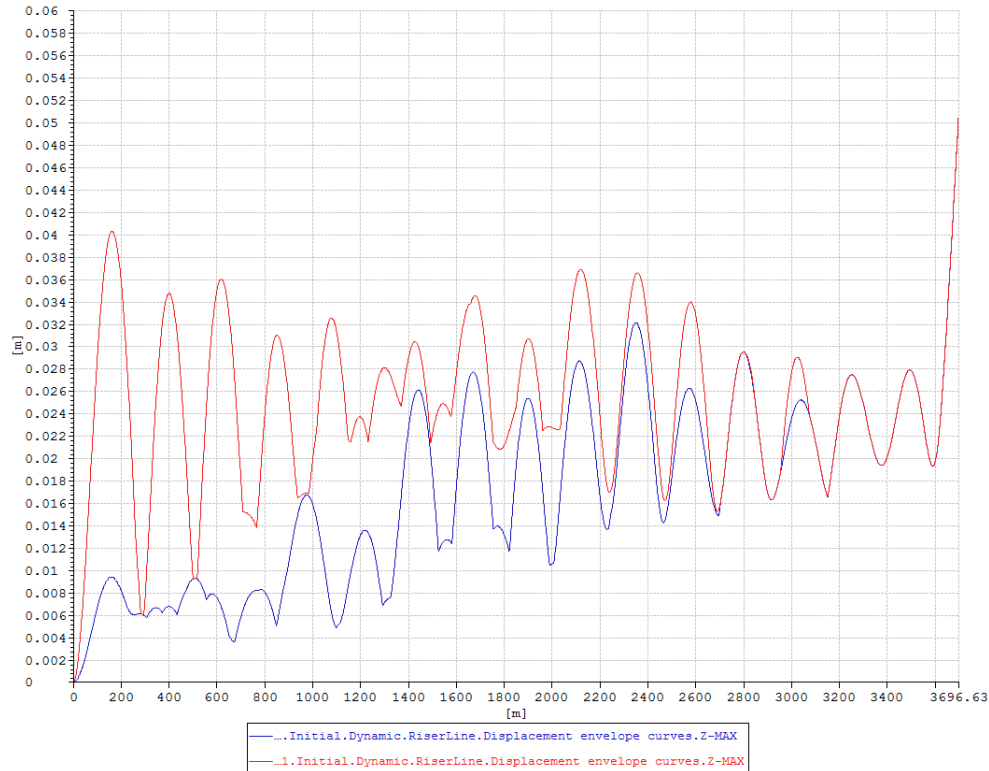
Figure 7.41: Snapshot of Z-displacement at time instants 50 s and 70 s

7.2.4 Assessment of the Scenario - Depth of Sognefjorden

In order for any of the scenarios to be feasible to conduct, the installation must be conducted without interacting with either the seabed or the edges of the shoreline. Therefore it is necessary to study the undersea borders of the fjord.

From the illustrations in Chapter 2, it is seen that at the side of Lavik the depth falls to -300 m just 600 m outside of the shore. 2600 m outside of the shoreline, the depth is -1000 m. So this side has a rapid drop down to approximately -550 m, then a slower drop down to -1000 m.

On the side of Oppedal the depth outside the shoreline drops much slower. After 200 m the depth is only -100 m, after 600 m the depth is only -200 m. However, after 1600 m the depth has reached -1000 m.

Based on this information it seems to be most appropriate to install the first end at the side of Oppedal. For Scenario 3 the submerged end point is positioned 200 m outside of the shore. According to the illustration below, 7.42, it is seen that 200 m outside of the shoreline of Lavik, the depth is in between -200 and -150 m. Therefore the scenarios that immerse the end point more than -150 m are not possible to use.
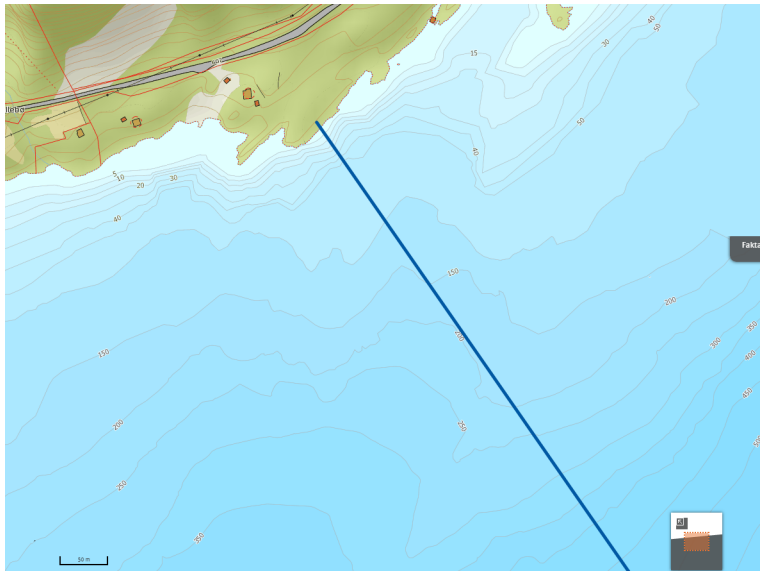
Figure 7.42: Depth at the installation point at Lavik (Norgeskart)

7.3 Statistical Response

In order to assess the results properly, the statistical responses are determined for both transportation and installation. For the transportation, the scenario with a straight bundle exposed to the environmental condition of the Sognefjord is analyzed (Hs = 2.34 m, P=4.8 s). For the installation, Scenario 3 is chosen. Of the two parts in this scenario, part 2 gives the largest responses with respect to bending moment and torsional moment. Part 2 is on this basis considered as the most critical sequence, and is therefore chosen for finding the statistical response. For part 2, end 2 will be submerged to a depth of -75 m. This choice is described in detail in chapter 8.

For both towing and installation, 10 simulations were run for different seeds generating random numbers for the irregular waves. The time domain analyses were run for 30 minutes, because it was decided that 3 hour simulations would be too time consuming for this part of

the study (Leira, 2016). One set of results for is presented in Appendix C.3 for both transportation and installation.

7.3.1 Results of the Gumbel plot

The extreme values for each run were linearized to be plotted in a Gumbel probability paper, as shown in chapter 3.5. Figure 7.43 show the Gumbel probability paper for the dynamic moment for the transportation phase. It is observed that the sample points follow the regression line evenly. There are no large deviations from the regression line, which indicate consistent results.
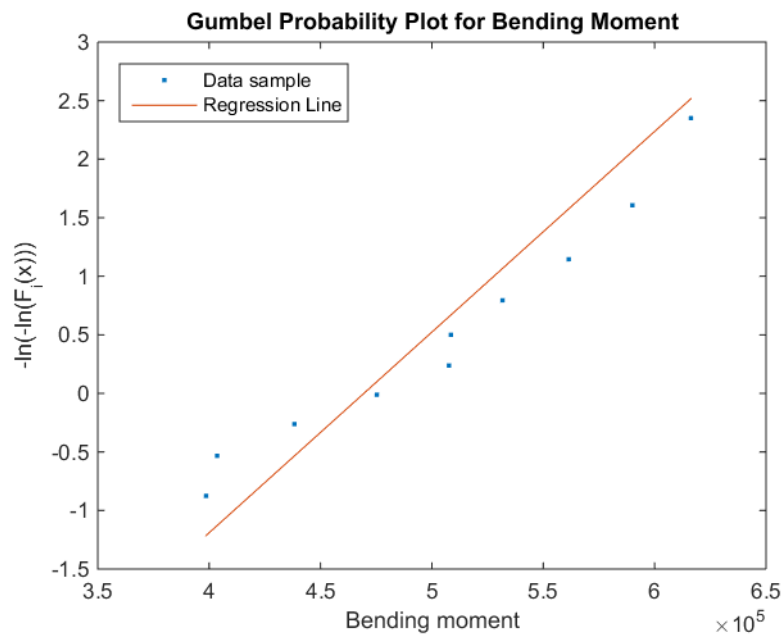
Figure 7.43: Gumbel probability paper for moment, transportation

The plot of the Gumbel probability for the axial force and displacement for the transportation are given in figures 7.44 and 7.45 below. For the axial force, it is seen that most of the sample points are spread around the middle part of the regression line, with a few points in the upper and lower tails. In other words, there are two sample points that show relatively large deviations. It is observed that the maximum axial force that is reached is $1.65E + 04N$. Compared with the maximum allowed stress of 192 MPa, which correspond to approximately $5.86E + 08N$, it is seen that this is well inside of the limit. For the displacement, the sample points are observed to follow a typical spread for a Gumbel plot, with sample points above the regression line for low values, and below the line for high values. The distribution for the

bending moment and the displacement are observed to be comparable with respect to spread of sample points, while the one for axial forces deviate from this.
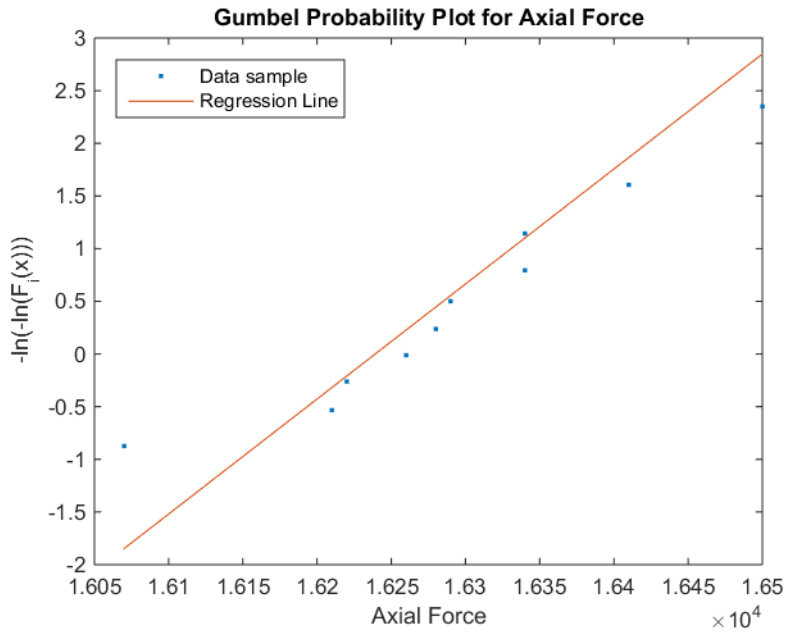
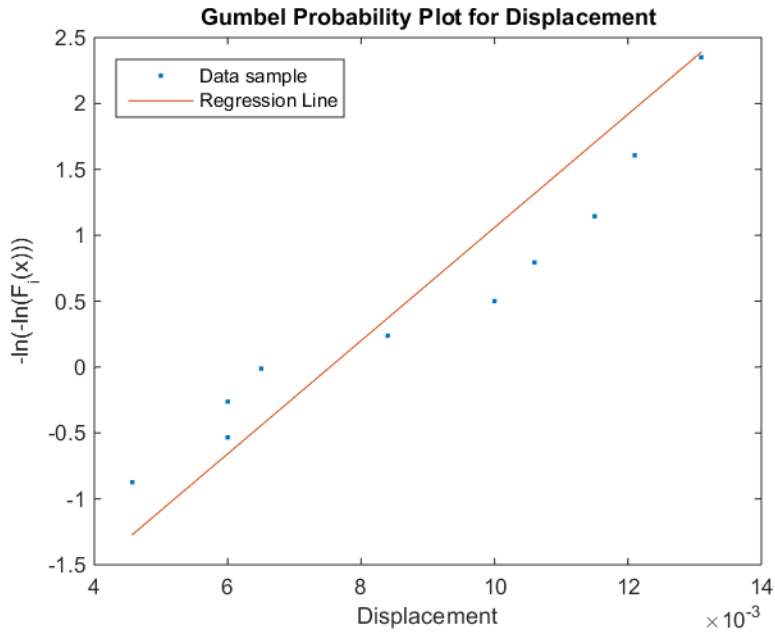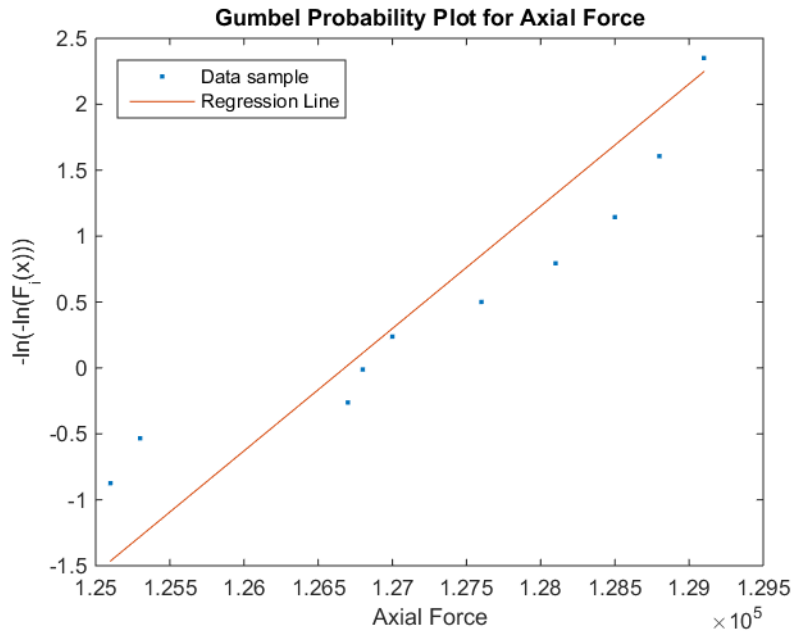**Figure 7.44:** Gumbel probability paper for axial force, transportation

Figure 7.45: Gumbel probability paper for displacement, transportation

Figure 7.46 gives the Gumbel probability plot for the dynamic bending moment for the installation procedure. It is seen that the data sample follow the regression line as in a typical

Gumbel probability plot. The sample points for the lower values follow the line closely, while there are deviations for the largest sample points.
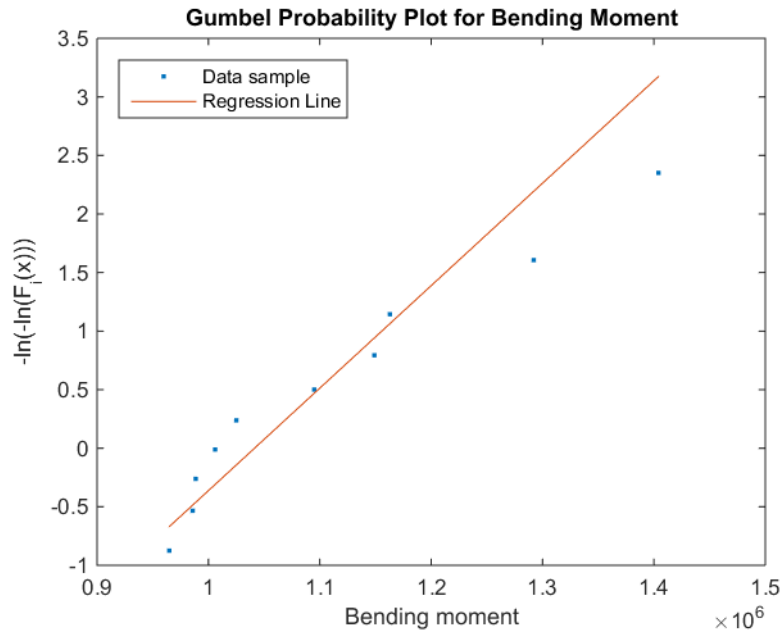
Figure 7.46: Gumbel probability paper for moment, installation

The Gumbel probability plot for the axial force and the displacement are given in figures 7.47 and 7.48. For the axial force, it is seen that most sample points are below the regression line, except for three points that show larger deviations above the regression line. Also for the installation it is observed that the maximum axial force of $1.5E + 06$ is well within the limit of $5.86E + 08$. The Gumbel probability plot for the displacement, figure 7.48, shows that the sample points are mostly positioned around the middle part of the regression line, with only two sample points in the upper and lower tails.

Figure 7.47: Gumbel probability paper for axial force, installation
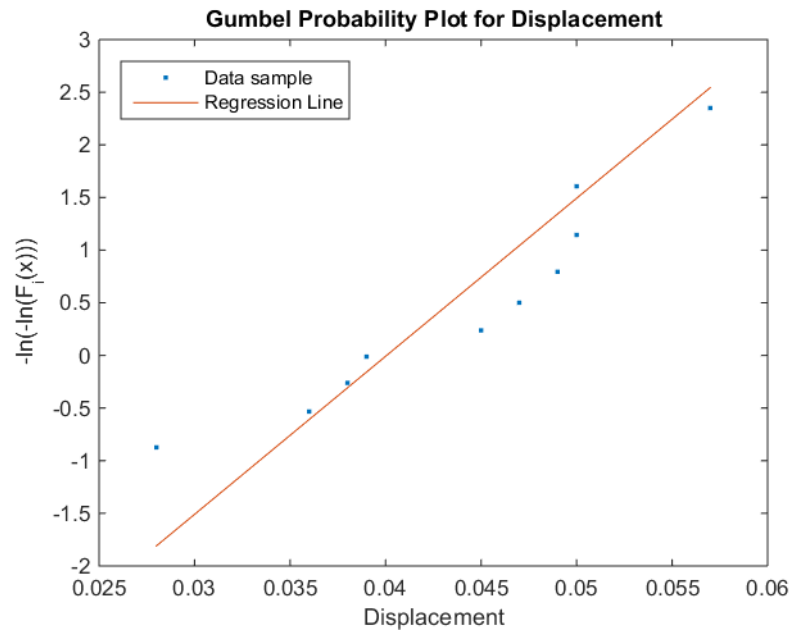
Figure 7.48: Gumbel probability paper for displacement, installation

It is seen that the sample points mostly follow the regression line properly. This might indicate that the Gumbel distribution chosen for the samples is correct. However, 10 sample points are not enough to be certain of the distribution, so it is necessary to create a larger samples in order to find the correct distribution.

7.4 Verification of Model and Results

In order to verify that the modeling and results became correct and realistic, a few simple methods were applied. These are explained shortly in this section.

Verification of Vessel Motion

In order to verify that the ships were actually moving in the dynamic analyses conducted in Sima Riflex, the peak period of the waves were modified. For the towing phase, the ships are exposed to following waves. These cause responses in heave and pitch for the vessels. The peak period from the environmental condition in the Sognefjord gives little response of the vessels, because this period is outside of the response areas in the transfer functions of the given vessels. Therefore, a peak period of 7 s were chosen to generate large motions of the vessels, because this period coincides with the largest responses from the vessels transfer functions. This test proved that the vessels are moving in the dynamic analysis.

Torsional Moments Compared to Number of Towing Tugs

For Scenario 3 of the installation, the analyses performed with only one additional towing tug resulted in large torsional moments. These torsional moments proved to be rapidly changing as well. By separating the towing force on several tugs, the torsion of the bundle became more evenly disturbed over the length of the bundle, and also significantly smaller. After discussions with my supervisor at Deep Ocean Group, Martin Hasle (Hasle, 2016), the decision fell upon three towing tugs. This is used consistently throughout scenario 3 of the installation.

Verification of Torsional Moments

For installation, Scenario 3, the torsional moments prove to be relatively large, with increasing torsional moments for larger depths. It was decided to run an analysis of a bundle that is straight from the horizontal plane, thus no immersed parts, to verify if this could be correct. The results revealed lower torsional moments, but still significant results. It can thus be concluded that the torsional moment probably increase due to coupling effects between the horizontal force and torsion, but that this effect will not cause the main part of the torsional moment.

Chapter 8

Discussion of Results

The results need to be considered critically, in order to find their credibility and impact. This chapter covers the discussions about the results, parameters and methods for this study.

8.1 Discussion of Results

8.1.1 Transportation

Scenario 1 of the transportation will give results that show how the bundle will behave when exposed to severe environmental conditions. It is observed that for increasing peak period, the dynamic displacement will increase significantly. This is because the wave motion will move deeper into the sea for larger peak periods, as shown in chapter 3.2.3. Additionally this also causes significantly increased dynamic moment. The results indicate that in the case of severe environmental conditions, the bundle should be towed at a deeper level than -30 m, to avoid direct wave loads.

For Scenario 2, the bundle's response to bending is being studied for a towing phase. The results revealed that a plateau is reached for bending between 200 m and 750 m, where the moment do not increase for increased bending. However, after 750 m the moment increase significantly, indicating that 750 m is the limit for bending during transportation. Scenario 3 gives the bending of the bundle for the environmental conditions inside of the Sognefjord. Similar results are observed as for Scenario 2, also indicating that the limit is 750 m for bending.

Structures with low natural frequencies can be exposed to slowly-varying motions (Faltinsen, 1990), as explained in chapter 3.2.2. The bundle is found to have low natural frequencies for the first ten modes, meaning it can be exposed to these effects. This might be what is observed in the bundle during tow, a slowly varying motion. Although VIV is highlighted as an issue for long slender structures (DNV GL, 2007), this will not be an issue for the bundle during tow, because it meets the current head on.

However, during transportation the results reveal that the displacement in X-direction is activated by eigenvector number 29, with period 11.59 s. For the displacement in Z-direction it is found that mode number 56 is active, with period 2.8 s. The period of 2.8 s is in the wave period band, and the motion is thus caused by waves. As explained in Section 3.2.2, a wave-frequency motion occur in the same frequency range as the significant wave energy in the sea spectrum. The bundle response is in the same range as the waves, indicating that they could be caused by direct wave loads or by the motion of the tugs. It has been shown for the sea state of Scenario 3 that the wave motion is extinguished for the depth of the bundle. From this it can be concluded that the response is not caused by direct wave loads on the bundle, but because of the motion of the tugs. The results for Scenario 1 and 2 show larger responses than for Scenario 3. Additionally are the wave motions for these scenarios not totally extinguished for the given depths. Therefore it can be concluded that these responses are caused by a combination of direct wave loads and the motion of the tugs. In other words, the responses do not seem to arise due to slowly varying forces, but due to direct or indirect wave forces.

According to da Cruz and Davidson (da Cruz and Davidson, 2006), the minimum water depth that can be used when towing with CDTM is 60 m. This is not an issue for this transportation phase, because the depth will never be this shallow. As shown in Chapter 3.4 it is the sideways displacement that is of concern. The results prove that these motions will not be that large, and should not be an obstacle for this operation. The displacements during transportation are observed to be small, with the largest value from the extreme value distribution being approximately 13 mm. Jacobsen and Næss stated that it is important to consider the fatigue in relation to the distance the structure is towed (Jacobsen and Naess, 2014). The period is quite small, indicating that the bundle will move rapidly. It is therefore important to study the fatigue during tow, although the forces acting might not be that large.

To summarize, the study conducted shows that the towing of the bundles will cause shifting dynamic displacement and bending moment over the length. These variations are likely caused by the motion of the tugs for the sea state inside of Sognefjord, and by direct wave loads for severe environmental conditions. The concern should be fatigue during tow, and this should be studied closer. The dynamic torsion is negligible for the towing phase, thus is the bundle not that exposed to current forces when towed in a straight line. The torsional moment increase for a bent bundle, and this is important to keep in mind if considering to use this method. Furthermore, for the bent bundle will the dynamic moment about the Z-axis give the largest responses, compared with the straight bundle that has largest responses about the Y-axis. The moment about the Y-axis will still be shifting for the bent bundle, but not as rapidly varying as for the straight bundle. Regarding the implementation of the towing, neither the sideways displacement or the depth seem to be of concern.

8.1.2 Installation

Scenario 1 for Installation, which bends the bundle only in the horizontal plane, is seen to give the second largest responses of bending moment. This scenario is very close to the modeling of Scenario 3, part 2 for a depth of -30 m, however the results differ somewhat due to different modeling.

Scenario 2 tries to install the bundle by submerging it downwards, but the results show that this will not be a feasible solution. This is due to the large forces the bundle is exposed to when forced into this configuration. The amount of additional weight and buoyancy indicate how much extra force that needs to be utilized in order to be able to install the bundle by this approach. The resulting bending moment causes the largest responses seen in this study, and the dynamic displacements are large as well. Thus is this method considered inappropriate for installing the bundle.

For Scenario 3 it is Part 1 that will give the most important results. This is first and foremost because the final configuration of Part 2 is equal for all of the parameter studies. The differences are mostly caused by different static stress states. Secondly is the towing line of different lengths for each analysis in Part 2, due to simplifications as explained previously. This might cause deviations that occur because of the modeling. Part 1 show a gradually increasing

bending moment and torsional moment for increased depth. However, the dynamic displacement increases with decreasing depth. The displacement is smaller for larger depths because the current will be reduced with increasing depth.

For Scenario 3 the feasibility of this installation is dependent on the depth being large enough. In this analysis, the end point of the bundle is immersed to a maximum of -200 m while the end point is situated 200 m outside of the shore lines. At this distance from shore, the depth is between 150-200 m, dependent on the exact position of the bundle. Thus is it not appropriate to use the scenarios for immersion larger than 125 m. After the end point has been lowered to its respective depths, it is gradually pulled upwards and approaches its installation point at -30 m depth. In accordance with the maps of the site, the decrease in depth will be dependent on the exact position of the bundle. However, it is of high relevancy to keep a good distance from the undersea borders of the fjord.

As a conclusion, a depth in between the two extremes of -125 and -30 m might be appropriate for installation by this approach. Therefore the choice fell upon -75 m. This will give slightly increased moment, but reduced dynamic displacements, as well as good distance to the undersea borders. Approximately 75 m will be between the bundle and the seabed, which will reduce any risks related to collision with the seabed. -75 m is used for the statistical response studies for the installation.

It is stated by da Cruz and Davidson (da Cruz and Davidson, 2006) that specific directions of the wave loading can cause resonance of long slender structures. The structure is still exposed for the same environmental loading as towing in Scenario 3, and direct wave loads are thus likely avoided. As a conclusion, the direction of the waves will probably not affect the bundle in this sea state directly, only indirectly by the tugs.

In this configuration the bundle will be exposed for current entering from the side. This may cause vertical resonance, which will increase the bending moment. When comparing the bending moment for the bundle submerged -30 m to the one submerged -200 m, it is observed that the one most submerged will experience slightly larger moments. This might be caused by coupling between horizontal current force and torsional moment. However, the difference is not that large. What is observed, on the other hand, is that the bending moment for the bundle submerged -30 m have more varying moments than for the one submerged -200 m. This might

indicate that direct current loads affect the bundle more than the effect of the coupling. Additionally, the bundle will experience torsional effects during installation, which it will not experience during transportation.

From the results it is found that the modes that are active have periods in the range between 1-2 s. This indicates that the bundle during installation will move more rapidly than during transportation. Thus is the effect of fatigue important to consider for the installation procedure as well, although this procedure lasts shorter than the transportation procedure. It was found that the vortex shedding period will be 19.5 s for the bundle during installation. This is based on assumptions that the bundle can be considered as a fixed cylinder in steady flow. The assumption about the fixed cylinder will weaken the credibility of the calculated vortex shedding period, as the results show that the bundle will have significant displacements during installation. Thus it can not be considered as fixed. However, if the vortex shedding period is considered as correct, it is observed that the active periods of the bundle are far away from the vortex shedding period, and thus will VIV not be an issue. The active periods of the bundle are in the range of the wave band, which indicate that also for this part the response of the bundle will be due to the motion of the towing tugs.

Feasibility of Installation Procedure

The installation procedure need to obtain full control of the bundle at all times. During the study of Scenario 3, part 2, it was observed that the end point being towed by a tug did move very easily. This will make the implementation of the installation more difficult. In order to keep this end point as stable as possible, one idea is to connect another tug to this end point. During installation these tugs can be connected on either side of the bundle. This is likely to reduce the displacements in the positive and negative X-directions. The figure below, 8.1, illustrates an example of how this idea can be conducted.
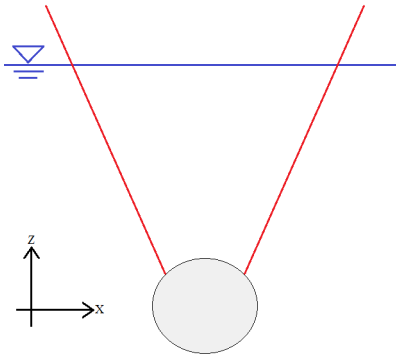
Figure 8.1: Illustration of installation with additional tug connected at end point

The ship motions will still cause some movement of the bundle. However, if the winch have a system for counteracting the tug responses, the installation will be easier implemented.

With additional tugs connected with equal distances along the bundle, there appear to be no issues related to bending the bundle in the wanted configurations. This will not, according to the results from this study, cause responses that exaggerate the critical response. In order to lower parts of the bundle to the wanted depth, additional weights are necessary to add to the bundle. The weights used for the analyses in Scenario 3 are constant for the different analyses. In other words, they are not customized to one specific depth. Therefore it is likely to believe that if conducting this operation with an immersion of -75 m, it will not be necessary to use as much additional weight as shown in this study.

8.2   Method and Modeling

In this study the towing line is not simulated as being pulled in by a winch. This means that when the bundle is changing its immersed depth, the towing wire end point is situated above the water line. This is necessary to keep the wire in tension. This can for instance cause the motion in the YX-plane to be larger due to the increased towing line length. This is illustrated in installation Scenario 3, Part 2, where the bundle is pulled up from different depths. Thus is the final configuration supposed to be equal for all analyses, while the initial configuration differs. The results reveal that for an initial depth of -30 m, the dynamic displacement of the bundle end point is not that large. However, for the situation with an initial depth of -200 m, the displacement at the bundle end point is twice that of -30 m. This might be caused by the

differences in towing wire lengths. The one submerged to -200 m will have a longer towing wire than for -30 m, enabling larger motions in all directions. On the other side, the dynamic moment differ for the two configurations, which is caused by different initial configurations. This might have an effect on the dynamic displacement as well, although it is unlikely that a small difference in moments can cause the large differences in dynamic displacement.

The RAO file of the towing tugs used is of default values. The responses of the towing tugs will be of large importance when towing the bundles. If the RAO file deviates vigorously from the tugs that are to be used in the operation, the responses of the bundle might change significantly. However, this study is conducted in order to find which responses and effects that are likely to appear, thus will changes of the RAO file probably not cause other effects.

In this study, the Scenario 3 of the installation phase is separated into two parts. By doing so, the initial configuration for part 2 is not the same as the final configuration in part 1. Although the analyses were modeled to make these two as close to each other as possible, certain limitations in the computer program made the two parts deviating from each other. By this approach, the stress state caused by part 1 will not influence part 2 in the same way as for a real operation. It could be considered as the stress state is reset between the two parts. Thus might this approach lead to smaller stress states than for the real operation. However, the bundle is still being moved the correct displacement, which will lead to tension forces in the bundle. Although these forces might be smaller than for the real case, they are still present, and thus is this effect not totally neglected.

8.3 Parameters

When modeling the bundle, a simplification to use a circular shape instead of three pipes connected to each other was decided upon. The properties of the original bundle were applied to the simplified model. Thus it is likely to believe that the results given in this study are comparable to the results that will come of the original shape of the bundle. However, some deviations may exist. These deviations may be due to errors in calculation of stiffness, or lack of information about the construction of the original shape.

The bundle is found to be in the force regimes of large inertia with contributions from drag,

see Section 6.3.6. Based on this classification, the mass forces will be the dominating response. It is additionally found that the structure has active eigenfrequencies that are in the energetic wave frequency band. Therefore, it is important to consider the multiplications of the frequencies, as explained in 3.3.2. The active frequency can move towards the frequency of the waves, although the natural frequency is far away. It is likely to believe that this is the reason mode number 56 is activated for the displacement in the Z-direction, as it might be a multiplication of one of the first modes. Since the bundle in this study has activated modes with low periods during tow, it will move rapidly. With respect to fatigue, it would be beneficial if the period increased, leading to fewer cycles completed during transportation. The eigenfrequency is shown in section 5.3, and can be changed by altering the stiffness or the mass of the structure. This could lead to lower modes being active, and thus fewer fatigue cycles completed during transportation through Songefjord.

Chapter 9

Conclusions

The active modes of the bundle during transportation have eigenperiods of 2.8 s, which is in the energetic wave period band. It is found that the wave motion is extinguished at -30 m for the sea state inside of Sognefjord. Thus will the motion and moments on the bundle during tow inside of the fjord be caused by the motions of the tugs, and not direct wave loads. It is therefore important that the tugs chosen for the operation have small responses for the given sea state. For the towing through Sognesjøen, it is found that for more severe sea states than those inside of the Songefjord, the bundle is exposed to direct wave loads in combination with tug motions. These wave loads will increase the dynamic displacements and moments to a large extent. It is therefore important to reduce these loads, either by avoid towing in the more severe sea states, or by towing at a larger depth where the wave motion is reduced further.

According to literature, the normal approach for installing long slender marine structures is to conduct the operation in off-bottom mode. This is not possible in the Sognefjord, and the operation must thus be performed with the bundle floating in water. It is found that the best approach for installing the bundle is to utilize the ocean space in both the horizontal and vertical directions. For the chosen installation procedure it is observed that increase in dynamic displacement and moment is caused by the current, which is now affecting the bundle from the side. The horizontal force from the current couples with torsional moment on the bundle, and thus increasing the forces. However, it appears that direct loads from current are larger than the effect of the coupling. The active eigenperiods are not near the period of the vortex shedding, thus is it likely to believe that the effect of VIV is avoided. Therefore, by lowering parts of the

bundle during the installation, the effect of the current on the free end will be reduced, leading to less displacements during installation. It is found from parameter studies that a depth of -75 m will leave excessive distance between the undersea borders of the fjord, as well as lower displacements without increasing the moments radically.

For the practical implementation of the installation procedure, it is observed that the motion of the end points will move during the fixing of the ends. By connecting two tugs to the end points, the motion of these points will be reduced. This will make the installation more simple and secure. The use of a motion compensation system would also decrease the responses of the bundle, both during transportation and installation.

As a conclusion, it has been found that the towing through the fjord is feasible, but that direct wave loads should be avoided. For the installation, a procedure that exploits both the horizontal and the vertical plane will be most suitable. The responses both during transportation and installation remain below the critical limit, but fatigue damage is of concern and should be studied closer.

9.1 Recommendations

For further work on this project, the following topics should be assessed:

1. Run analyses with RAO files corresponding to the tugs used for the operation

2. Model the tugs situated along the bundle as tugs; not as horizontal forces as in this study

3. Identify the fatigue damage during both transportation and installation, and compare this with the DNV-RP-H103 limit of 10 % allowable fatigue damage (see section 4.2.4)

4. Perform parameter studies of an altered mass, to avoid responses in the energetic wave frequency band

5. Perform an analysis of the installation with two tugs connected at the end point, to study if this will reduce the motion

Bibliography

(2015). Ryfast. https://no.wikipedia.org/w/index.php?title=Ryfast&oldid=14293494.
    Accessed: 2015-09-30.

Aas-Jakobsen (2005). Nordhordland bridge. http://www.aaj.no/bruer/pdf/Nordhordland_
    flyt_eng.pdf. Accessed: 2016-02-17.

Askheim, S. and Thorsnæs, G. (2015). Sognefjorden. https://snl.no/Sognefjorden.
    Accessed: 2016-03-14.

Bai, Y. and Bai, Q. (2005). *Subsea Pipelines and Risers*. Oxford: Elsevier.

Cengel, Y. A. and Cimbala, J. M. (2010). *Fluid Mechanics, Fundamentals and Applications*. Mc
    Graw Hill.

Chandler, N. How floating bridges work. http://science.howstuffworks.com/
    engineering/structural/floating-bridge4.htm. Accessed: 2016-02-17.

da Cruz, I. C. P. and Davidson, J. D. (2006). Deepwater installation of pipelines and risers by
    towing. In *Offshore Technology Conference, Houston, Texas, USA*.

DNV GL (2007). DNV-RP-C205 Environmental Conditions and Environmental Loads.
    Recommended Practice.

DNV GL (2011a). DNV-OS-C301 Stability and Watertight Integrity. Offshore Standard.

DNV GL (2011b). DNV-OS-H101 Marine Operations, General. Offshore Standard.

DNV GL (2011c). DNV-RP-H103 Modelling and Analysis of Marine Operations. Recommended
    Practice.

DNV GL (2015). DNV-OS-H202 Sea Transport Operations. Offshore Standard.

eFunda (2016). Radius of Gyration Formula. http://www.efunda.com/math/areas/radiusofgyration.cfm. Accessed: 2016-03-31.

Engineering Department, Deep Ocean (2014). Kunstig Sjøbunn. Technical report, Deep Ocean Group.

Engineering Department, Deep Ocean (2015). GAP Analyse Marine Operasjoner. Technical report, Deep Ocean Group.

Faltinsen, O. M. (1990). *Sea Loads on Ships and Offshore Structures*. Cambridge: Cambridge Ocean Technology Series.

Fjeld, A. (2013). Mulighetsstudie for kryssing av Sognefjorden - Neddykket rørbru. Technical report, Reinertsen, Olav Olsen Group.

Gisvold, M. (2015a). Bjørnafjorden kan få verdens lengste flyte- eller rørbru. *Teknisk ukeblad*, 162(5):26. http://www.tu.no/samferdsel/2015/03/10/bjornafjorden-kan-fa-verdens-lengste-flyte--eller-rorbru.

Gisvold, M. (2015b). Verdens første rørbru kan stå ferdig i 2025. *Teknisk ukeblad*, 162(13):60–61. http://www.tu.no/samferdsel/2015/09/23/verdens-forste-rorbru-kan-sta-ferdig-i-2025.

Gracewski, S. M. (2009). Chapter 3: Real eigenvalue analysis. Applied Vibrations, University of Rochester, New York. http://www.me.rochester.edu/courses/ME443/NASTRAN/Chpt3RealEigenvalueAnalysis.pdf.

Grevstad, S. (2015). Vortex Induced Vibrations on an "Artificial Seabed" for Support of a Floating Bridge. Master's thesis, Norwegian University of Science and Technology, Department of Marine Technology, Trondheim.

Hasle, M. (2016). Review of MSc Projects. Meeting 03.05.2016.

Haver, S. K. (2011). Prediction of Characteristic Response for Desing Purposes (PRELIMINARY VERSION). Technical report, Statiol.

Ingerslev, C. (2010). Immersed and floating tunnels. *Procedia Engineering*, 4:51–59.

Irgens, F. (2010). *Formelsamling mekanikk*. Tapir akademisk forlag.

Jacobsen, T. and Leira, B. J. (2012). Numerical and experimental studies of submerged towing of a subsea template. In Incecik, A. and Collette, M., editors, *Ocean Engineering Volume 42*, pages 147–154. Elsevier.

Jacobsen, T. and Naess, T. B. (2014). Installation of subsea structures using mid-size construction vessels in harsh environments. In *Offshore Technology Conference, Kuala Lumpur, Malaysia*.

Jøssang, T. I. (2005). Høgsfjord-drømmer. *Stavanger Aftenblad*, 162(13):60–61. http://www.aftenbladet.no/nyheter/lokalt/Hogsfjord-drommer-2585101.html.

Kelley, B. S. (2009). Lecture notes and readings, Section 16: Neutral Axis and Parallel Axis Theorem. https://cnx.org/resources/c8a2e4f16c9fc4944e4186c4ba328fb4faa2425b/16-Slides%20-%20Advanced%20Stress.pdf. Accessed: 2016-03-29.

Kjelsaas, C. (2015). Structural Response of Submerged Floating Tunnels Exposed to Current and Waves. Project Thesis, Norwegian University of Science and Technology, Department of Marine Technology, Trondheim.

Langen, I. and Sigbjörnsson, R. (2007). *Dynamisk Analyse av konstruksjoner*. Fagbokforlaget.

Lankhorst Ropes, Offshore Division (2013). Lankhorst Ropes - Offshore Steel Wire Ropes Brochures. http://www.lankhorstropes.com/files/uploads/Offshore/brochures/Steel_Wire_Rope_brochure__100dpi__April_2013.pdf. Accessed: 2016-03-31.

Larsen, C. M. (2014). *Kompendium TMR4182 Marin Dynamikk*. Trondheim: Akademika Forlag.

Larsen, C. M. (2015). Vortex Induced Vibrations (VIV). Its Learning - Dynamic Analysis Module, NTNU, Trondheim.

Larsen, K. (2016). Towing Operations. Its Learning - TMR4225 Marine Operations, NTNU, Trondheim.

Leira, B. J. (2015). Lecture Notes in TMR4235 Stochastic Theory of Sea Loads. Its Learning. NTNU, Department of Marine Technology.

Leira, B. J. (2016). Guidance MSc. Meeting 01.05.2016.

Lothe, E. A. and Brørs, B. (2011). Mulighetsstudie for Kryssing av Sognefjorden Opedal - Lavik, Estimat på Bølger og Strøm. Technical report, Sintef.

Lundby, L. e. (2013). *Havromsteknologi - Et hav av muligheter*. Trondheim: NTNU.

Marintek (2015). RIFLEX Theory Manual. No. 46, Rev. 0.

Moan, T. (2003). *TMR4190 Finite Element Modelling and Analysis of Marine Structures*. Trondheim: Akademika Forlag.

Moxnes, S. (2011). SIMA - The New Graphical Interface for RIFLEX and SIMO. http://www.ktf.no/fileadmin/Dokumenter/Kursdokumenter/2011/3_subsea_lifting_operations/11-sima-the-new-graphic-interface.pdf. Accessed: 2016-03-20.

Myrhaug, D. and Lian, W. (2014). *Irregular Waves*. Trondheim: Akademika Forlag.

Norgeskart. Sognefjorden. https://www.norgeskart.no/#10/-22773/6809535/-land/+sjo. Accessed: 2016-03-02.

Øderud, H. T. (2009). Bergsøysundet bru. https://snl.no/Bergs%C3%B8ysundet_bru. Accessed: 2016-02-17.

Orcina Ltd. (2015). Orcaflex - Line Types: Structure Data. http://www.orcina.com/SoftwareProducts/OrcaFlex/Documentation/Help/Content/html/LineTypes,StructureData.htm. Accessed: 2016-04-04.

Ottosen, N. and Petersson, H. (1992). *Introduction to the Finite Element Method*. Suffolk: Pearson / Prentice Hall.

Reinertsen (2014a). Kunstig Sjøbunn - Kvalifiseringsstudie for nytt forankringskonsept. Technical report, Reinertsen.

Reinertsen (2014b). Kunstig Sjøbunn - Transport, Installasjon og kostestimering. Technical report, Reinertsen.

Reinertsen (2014c). Visualisering Kunstig Sjøbunn - Dimensjoner og Størrelser. . PowerPoint Presentation.

Rooduyn, E. G. (1985). Transportation of pre-fabricated pipelines with the controlled depth tow method (cdtm). In *Advances in Underwater Technology and Offshore Engineering Vol. 2*, pages 127–144. Graham and Trotman Ltd.

Skorpa, L., I. B. B. K. S. J. H. E. M. K. L. O. . G. O. E. (2012). Ferjefri E39 - Hovedrapport, Delprosjekt Fjordkryssinger. Technical report, Statens Vegvesen.

Skorpa, L. and Østlid, H. (2001). Owners experience with the pilot project høgsfjord submerged floating tunnel. In Krogeborg, J., editor, *Proceedings of the 4th Symposium on strait crossings 2001, Strait Crossings*, pages 547–550. A. A. Balkema.

Supratik, D. (2014). Computing stiffness of linear elastic structures: Part 1. https://www.comsol.no/blogs/computing-stiffness-linear-elastic-structures-part-1/. Accessed: 2015-10-15.

Sævik, S. (2015). Advanced structural analysis week 45 2015. Its Learning - TMR4305/4505, Department of Marine Technology, NTNU.

Villoria, B. (2015). Floating bridge - when is the technology ready? http://www.vegvesen.no/Vegprosjekter/ferjefriE39/Konferanse/teknologidagene2015/_attachment/1023747?_ts=14ff497c800&fast_title=10+Coastal+Highway+Route+E39+-+floating+bridge+-+Bruno+Villoria+NPRA.pdf. Accessed: 2016-02-17.

Watanabe, E. and Utsunomiya, T. (2003). Analysis and design of floating bridges. In *Progress in Structural Engineering and Materials Volume 5*, pages 127–144. John Wiley and Sons, Ltd.

Appendix A

Detailed Calculations of Bundle Properties

The detailed calculations were conducted in an Excel sheet. The results are shown in this chapter of the Appendix.

A.1 Calculations on Bundle Structure

A.1.1 Area Calculations

Table A.1: Area Calculations

Parameter	Value
Inner Diameter [mm]	853.4
Outer Diameter [mm]	914.4
Tot. area one pipe [m^2]	0.65669
Int. area one pipe [m^2]	0.57199
Tot. area 3 pipes [m^2]	1.97007
Int. area 3 pipes [m^2]	**1.71599**
Radius of circle around bundle [m]	0.98512
Corresponding diameter [m]	1.97025
Ext. area of circle [m^2]	**3.04885**

A.1.2 Buoyancy and Weight

Table A.2: Calculation of Buoyancy and Weight

Parameter	Value
Sea Water Density [kg/m^3]	1005
Buoyancy [kg/m]	3064.0949
Weight [kg/m]	3065.254

A.1.3 Moment of Inertia and Radius of Gyration

Table A.3: Calculation of regular and polar moment of inertia

Parameter	Value
I of one pipe [m^4]	0.00828
Dist. X-O [m]	0.52792
I one pipe with Steiner [m^4]	0.19130
Tot. MOI [m^4]	**0.57392**
J of one pipe [m^4/rad]	0.01656
Dist X-O [m]	0.52792
J one pipe with Steiner [m^4]	0.19958
Tot. polar MOI [m^4]	**0.59876**

Table A.4: Calculation of Radius of Gyration

Parameter	Value
Tot. MOI [m^4]	0.57392
Radius of Gyration [m]	0.43386

A.1.4   Strength Properties of Bundle Structure

Table A.5: Calculation of strength properties

Parameter	Value
Yield stress [MPa]	480
Elastic Modulus, E [N/m^2]	2.07E+11
Poissons Ratio [$-$]	0.3
Shear Modulus, G [N/m^2]	7.96E+10
Axial Stiffness [N]	6.31E+11
Bending Stiffness [Nm^2]	1.19E+11
Shear Stiffness [N]	2.43E+11
Torsional Stiffness [Nm^2/rad]	4.77E+10

A.1.5   Drag Coefficients and Added Mass

Table A.6: Drag coefficient and added mass for circle

Parameter	Value
Kinematic Viscosity [m^2/s]	1.52E-06
Reynolds Number [$-$]	6.22E+05
Roughness [m]	0.001
C_D from table [$-$]	0.85
C_A from table [$-$]	1
A_R calc. from table [m^2]	3.04885
$A_{ij}[kg/m]$	3064.0949

Table A.7: Drag coefficient and added mass for triangle

Parameter	Value
Kinematic Viscosity [m^2/s]	1.52E-06
Reynolds Number [$-$]	6.22E+05
Roughness [m]	0.001
C_D from table [$-$]	2
C_A from table [$-$]	0.67
A_R calc. from table [m^2]	3.04885
$A_{ij}[kg/m]$	2052.9436

Table A.8: Drag coefficient and added mass for bundle from experiments

Parameter	Value
Kinematic Viscosity [m^2/s]	1.52E-06
Reynolds Number [$-$]	6.22E+05
Roughness [m]	0.001
C_D [$-$]	0.5
C_A [$-$]	0.7
$A_R[m^2]$	3.04885
$A_{ij}[kg/m]$	2144.8665

A.1.6   Calculation of Wave Theories

Table A.9: Calculation of Validity area for wave theory

Parameter	Value
Significant Wave Height [m]	2,34
Period [s]	4,8
Wave length [m]	35,97
Standard Gravity [m/s^2]	9,81
Wave Steepness Parameter [$-$]	0,06505421
Shallow Water Parameter [$-$]	5,56018905
Ursell Number [$-$]	0,00037845
d/T^2 [m/s^2]	8,68055556
H/T^2 [m/s^2]	0,1015625

Table A.10: Calculation of Wave Force Regime

Parameter	Value
H/D	1,18766161
piD/lambda	0,17208086
lambda >5D	9,85129086
lambda/D	18,2564907

A.2 Calculations of Towing Wire Properties

Table A.11: Calculation of Towing Wire Properties

Parameter	Value
Diameter [mm]	102
Weight [kg/m]	43
Axial Stiffness [N]	7.26E+06
External Area [m^2]	0.00817
MOI [m^4]	5.31338E+06
Radius of Gyration [m]	0.0255

A.3 RAO for Towing Tugs
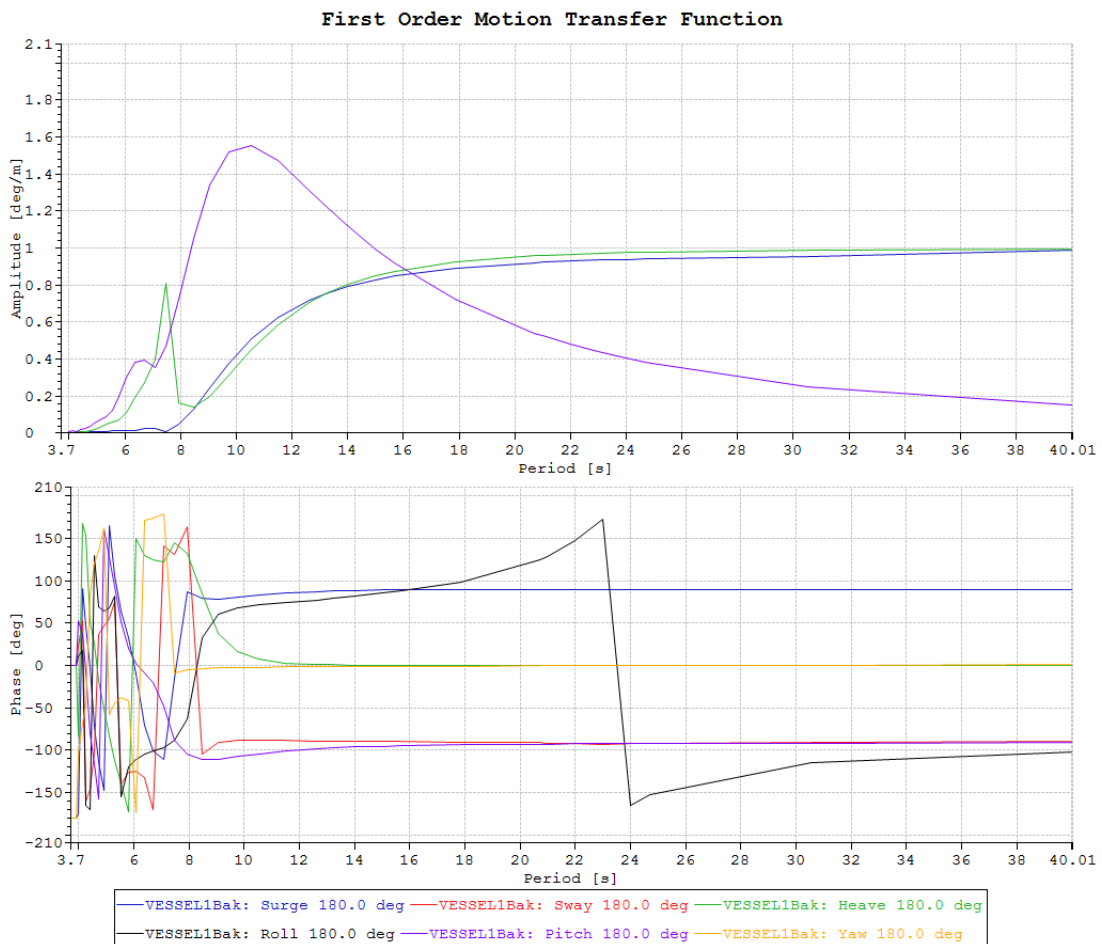
Figure A.1: Transfer functions for towing tugs

Appendix B

Detailed Results from Parameter Studies

B.1 Results from Parameter Studies for Towing

B.1.1 Scenario 1: Peak Period Variations

Table B.1: Parameter study of peak period variations

Peak Period	Bending Moment	Torsional Moment	Displacement
6	2,23E+06	3,59E-05	0,17
5,75	1,48E+06	1,36E-05	0,089
5,5	1,47E+06	1,35E-05	0,089
5	1,29E+06	1,15E-05	0,072
4,5	5,30E+05	4,60E-06	0,027
4	2,60E+05	2,70E-06	0,012

B.1.2 Scenario 2: Studies of Degree of Bending

Table B.2: Parameter study of degree of bending, Scenario 2

	Static		Dynamic		
Disp. Node 1	Bending Mom.	Torsional Mom.	Bending Mom.	Torsional Mom.	Disp.
0	5,80E+04	1,88E-06	4,90E+06	2,80E-05	0,65
250	1,25E+07	-750	1,30E+07	6,00E+03	0,8
500	1,38E+07	285	1,49E+07	1,20E+04	0,89
750	1,45E+07	-2580	1,60E+07	1,24E+04	0,89
1000	2,20E+07	-2800	2,55E+07	3,45E+04	1,11

B.1.3 Scenario 3: Studies of Degree of Bending

Table B.3: Parameter study of degree of bending, Scenario 3

	Static		Dynamic		
Disp. Node 1	Bending Mom.	Torsional Mom.	Bending Mom.	Torsional Mom.	Disp.
0	5,80E+04	1,88E-06	1,75E+05	2,17E-06	0,0118
250	1,23E+07	-780	1,23E+07	-1080	0,012
500	1,38E+07	285	1,39E+07	830	0,024
750	1,45E+07	-2580	1,45E+07	-3250	0,011
1000	2,20E+07	-2800	2,25E+07	2,48E+05	0,22

B.2 Results from Parameter Studies for Installation

B.2.1 Scenario 3, Part 1

Table B.4: Parameter study of immersion of end point, Part 1 of installation

	Dynamic		Static		
Depth	Bending Mom.	Torsional Mom.	Disp.	Bending Mom.	Torsional Mom.
-30	2,38E+07	4,39E+05	0,22	2,20E+07	2,90E+05
-50	2,42E+07	4,57E+05	0,18	2,30E+07	3,42E+05
-75	2,48E+07	4,78E+05	0,148	2,37E+07	3,85E+05
-100	2,55E+07	4,93E+05	0,136	2,45E+07	4,15E+05
-125	2,60E+07	5,04E+05	0,121	2,50E+07	4,38E+05
-150	2,65E+07	5,15E+05	0,115	2,58E+07	4,55E+05
-175	2,69E+07	5,21E+05	0,1	2,61E+07	4,75E+05
-200	2,70E+07	5,30E+05	0,095	2,68E+07	4,90E+05

Table B.5: Parameter study, Part 1, results for middle element

Depth	Axial Force	Mom.	Torsional Mom.	Shear Force
-30	1,14E+05	2,37E+07	4,35E+05	-3,40E+04
-50	9,20E+04	2,42E+07	4,57E+05	-2,75E+04
-75	7,55E+04	2,48E+07	4,79E+05	-2,40E+04
-100	6,85E+04	2,55E+07	4,95E+05	-2,18E+04
-125	6,35E+04	2,60E+07	5,10E+05	-2,05E+04
-150	5,94E+04	2,64E+07	5,20E+05	-1,85E+04
-175	5,61E+04	2,68E+07	5,30E+05	-1,65E+04
-200	5,35E+04	2,70E+07	5,35E+05	-1,58E+04

B.2.2 Scenario 3, Part 2

Table B.6: Parameter study of immersion of end point 2, part 2 of installation

	Dynamic			Static	
Depth	Bending Mom.	Torsional Mom.	Disp.	Bending Mom.	Torsional Mom.
-30	3,40E+07	7,75E+05	0,068	3,36E+07	7,49E+05
-50	3,37E+07	8,95E+05	0,046	3,34E+07	8,80E+05
-75	3,41E+07	1,10E+06	0,047	3,38E+07	1,09E+06
-100	3,39E+07	1,25E+06	0,039	3,35E+07	1,24E+06
-125	3,41E+07	1,42E+06	0,040	3,37E+07	1,44E+06
-150	3,40E+07	1,61E+06	0,038	3,39E+07	1,60E+06
-175	3,43E+07	1,76E+06	0,0585	3,40E+07	1,75E+06
-200	3,50E+07	1,95E+06	0,145	3,40E+07	1,95E+06

Table B.7: Parameter study, Part 2, results for middle element

Depth	Axial Force	Moment	Torsional Mom.	Shear Force
-30	1,38E+05	3,41E+07	7,85E+05	-1,87E+04
-50	1,32E+05	3,39E+07	9,00E+05	-1,75E+04
-75	1,25E+05	3,40E+07	1,10E+06	-1,65E+04
-100	1,24E+05	3,39E+07	1,25E+06	-1,59E+04
-125	1,18E+05	3,40E+07	1,45E+06	-1,60E+04
-150	1,15E+05	3,41E+07	1,62E+06	-1,61E+04
-175	1,20E+05	3,48E+07	1,77E+06	-2,01E+04
-200	1,32E+05	3,50E+07	1,97E+06	-2,70E+04

Appendix C

Additional Results

This Appendix include the results that are not showed in the main text of the report.

C.1 Transportation

C.1.1 Scenario 1

The static and dynamic torsional moments are presented for peak periods 4 s and 6 s.
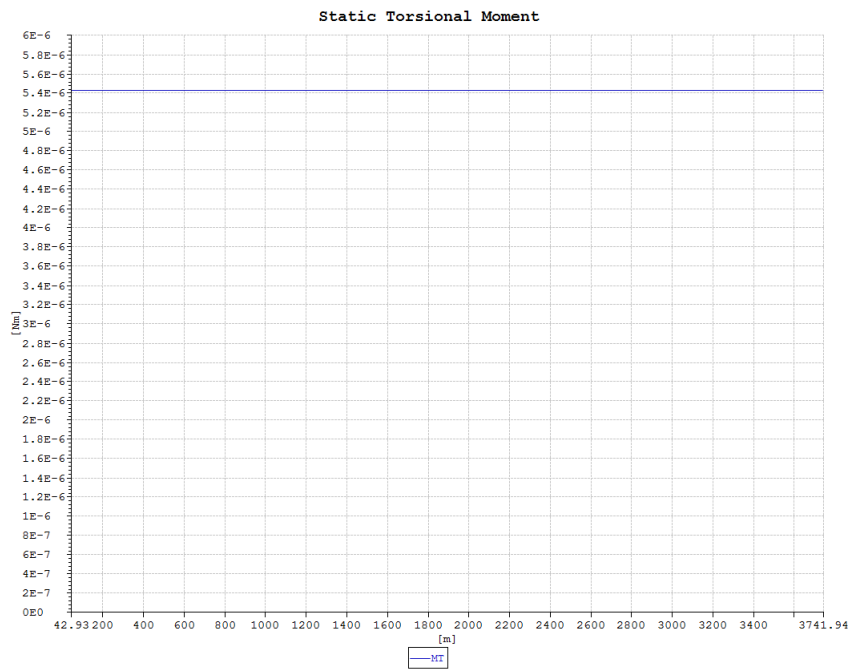
Figure C.1: Static torsional moment
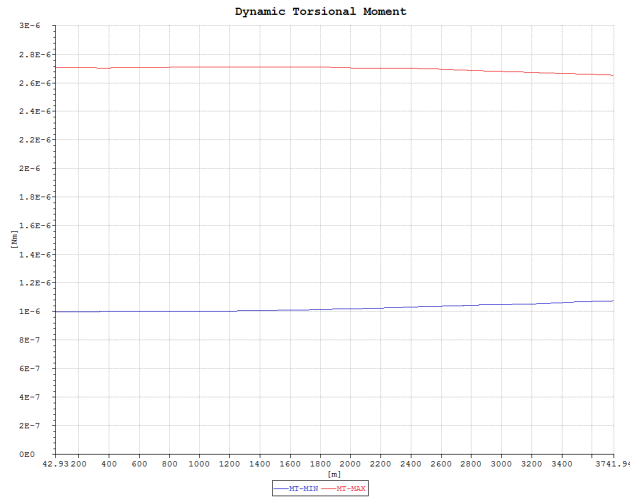
Figure C.2: Dynamic torsion, $T_P = 4$ s
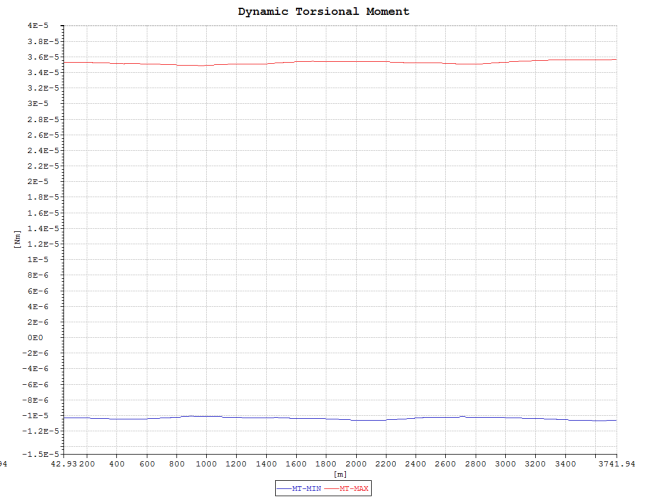
Figure C.3: Dynamic torsion, $T_P = 6$ s

C.1.2 Scenario 2

The static and dynamic torsional moments are presented for a straight bundle and for the most bent bundle. Additionally are the eigenmodes for both presented as well.
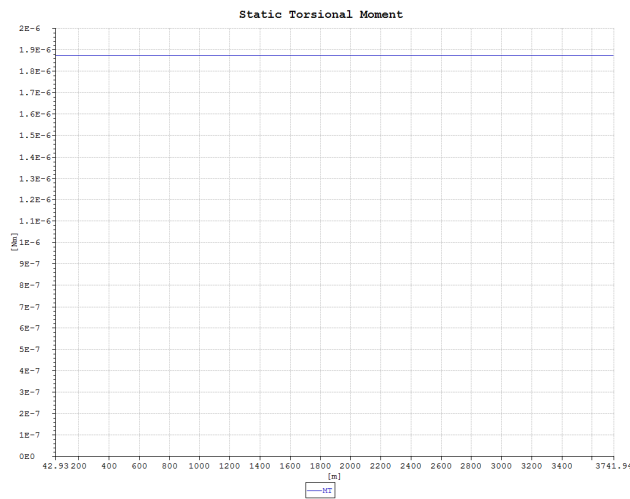
Figure C.4: Static torsional moment, X=0
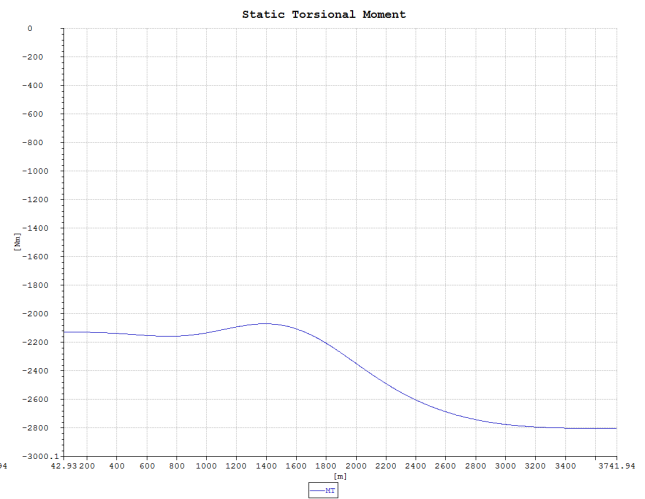
Figure C.5: Static torsional moment, X=1000
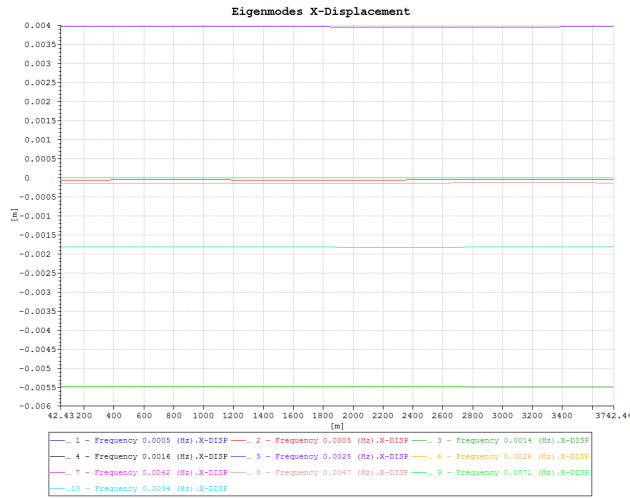
Figure C.6: Eigenmodes X-displacement, X=0
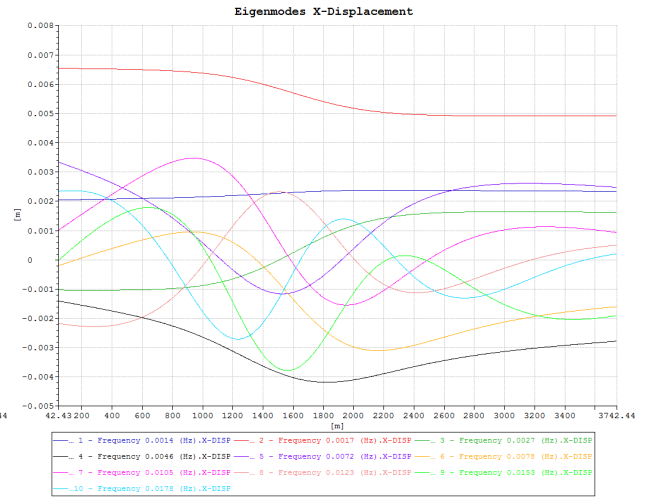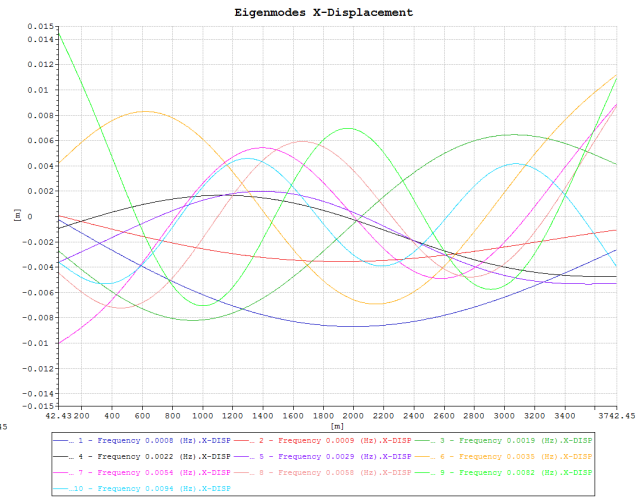

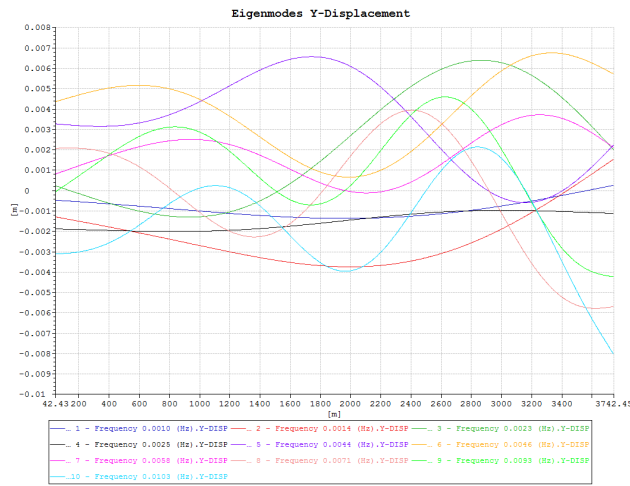**Figure C.7:** Eigenmodes X-displacement, X=1000
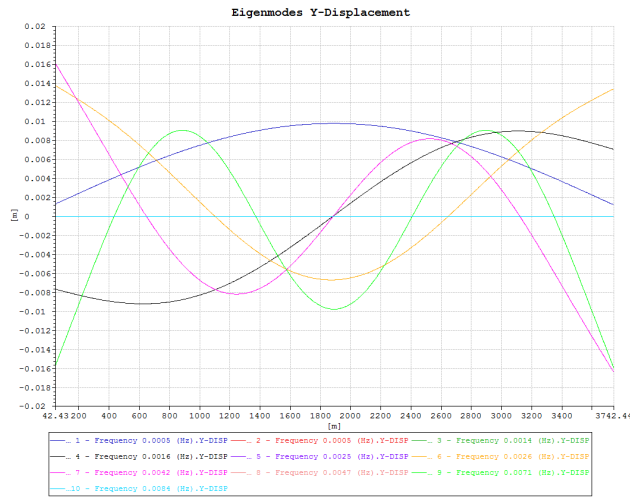
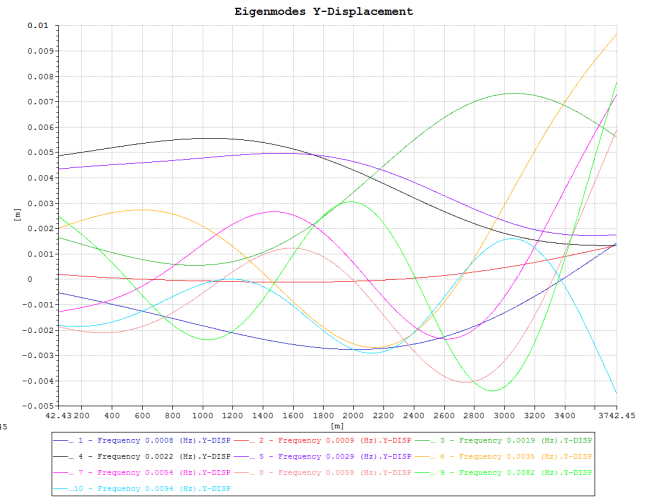**Figure C.8:** Eigenmodes Y-displacement, X=0
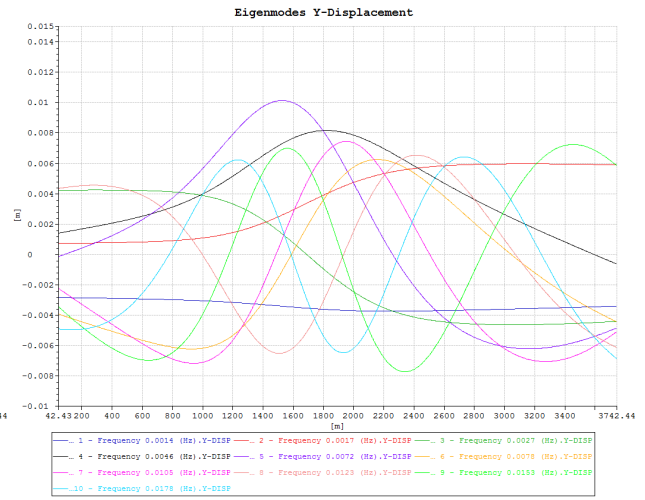
Figure C.9: Eigenmodes Y-displacement, X=1000
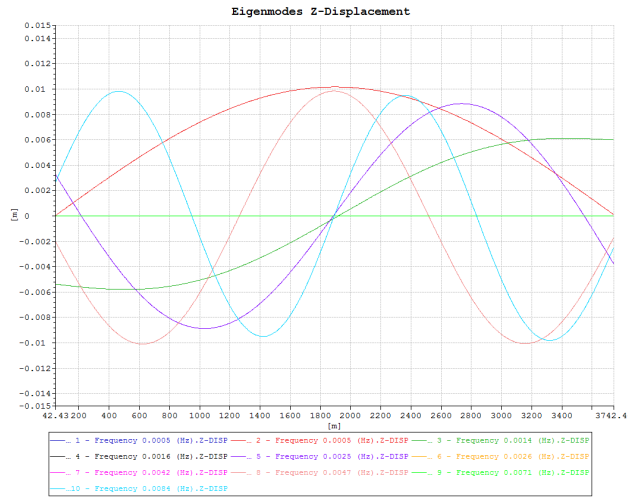
Figure C.10: Eigenmodes Z-displacement, X=0
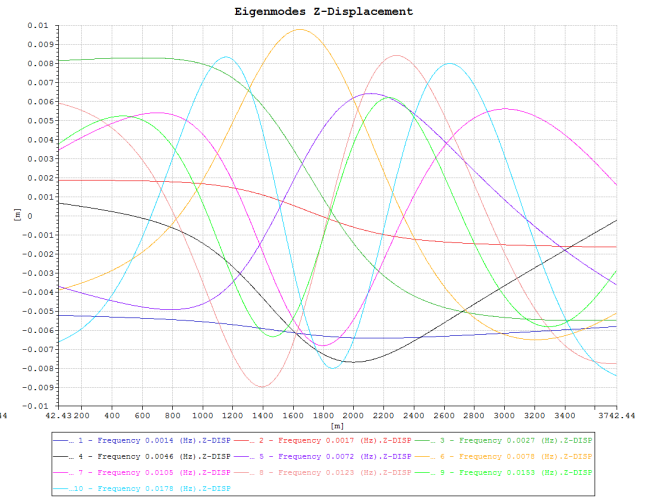
Figure C.11: Eigenmodes Z-displacement, X=1000
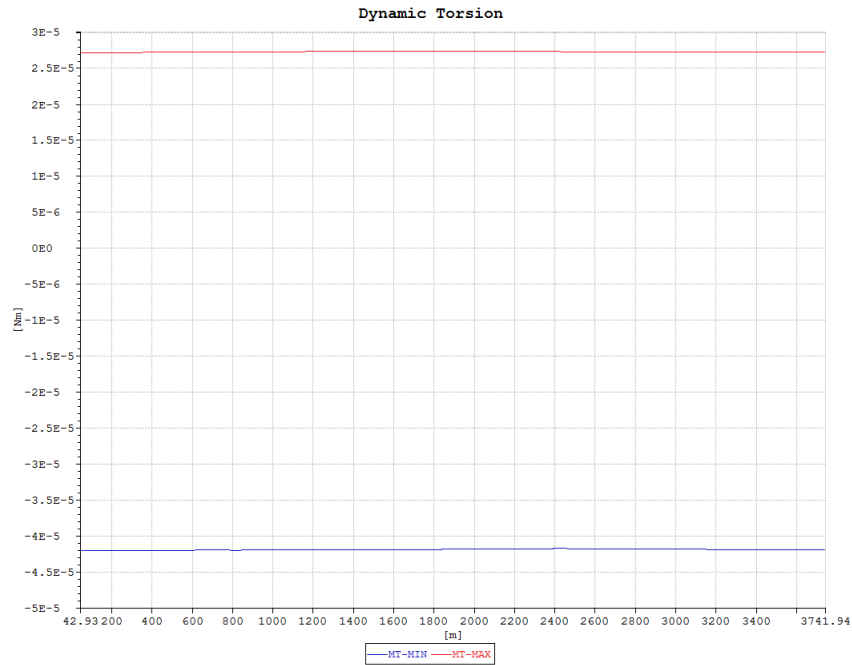
Figure C.12: Dynamic torsional moment for a straight bundle, X=0
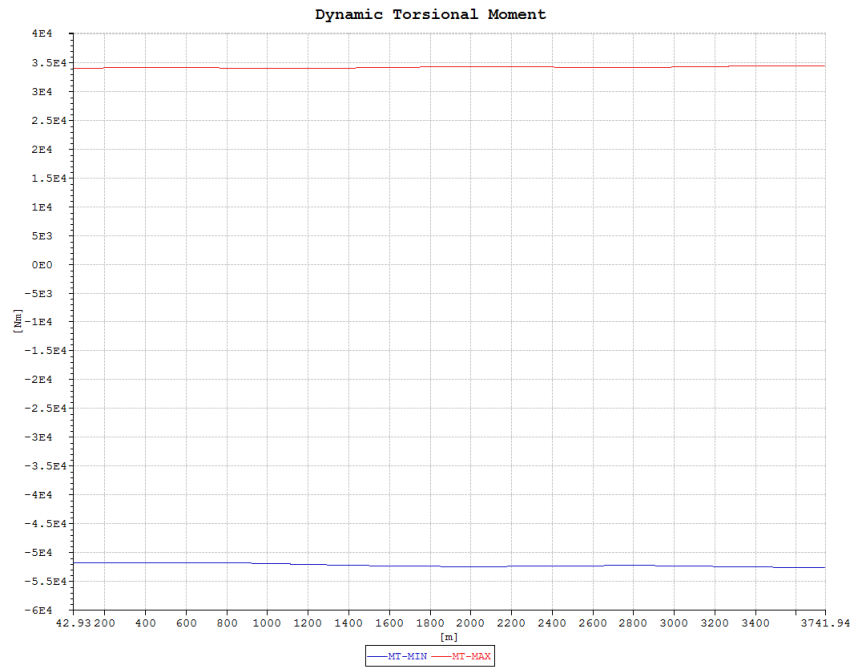
Figure C.13: Dynamic torsional moment for a curved bundle, X=1000

C.1.3   Scenario 3

In addition to the torsional moments, the static results are also shown for this scenario.

Figure C.14: Static moment for straight bundle, X=0
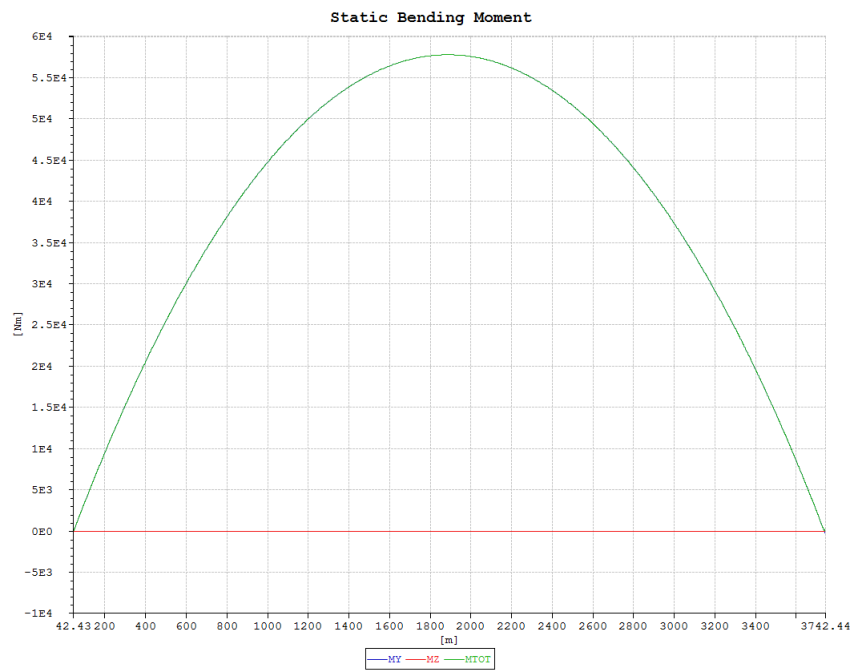
Figure C.15: Static Moment for curved bundle, X=1000
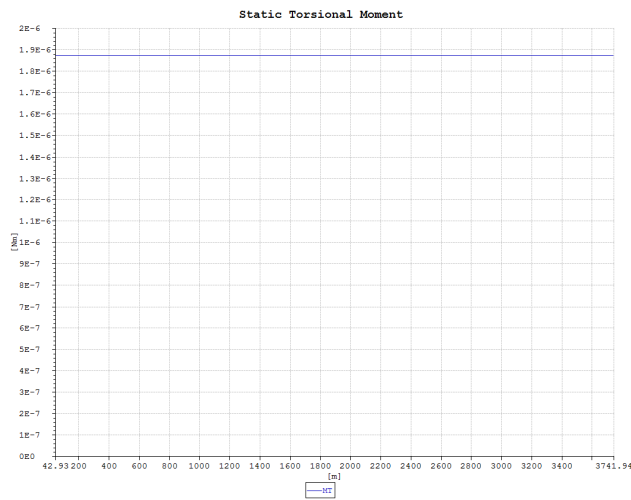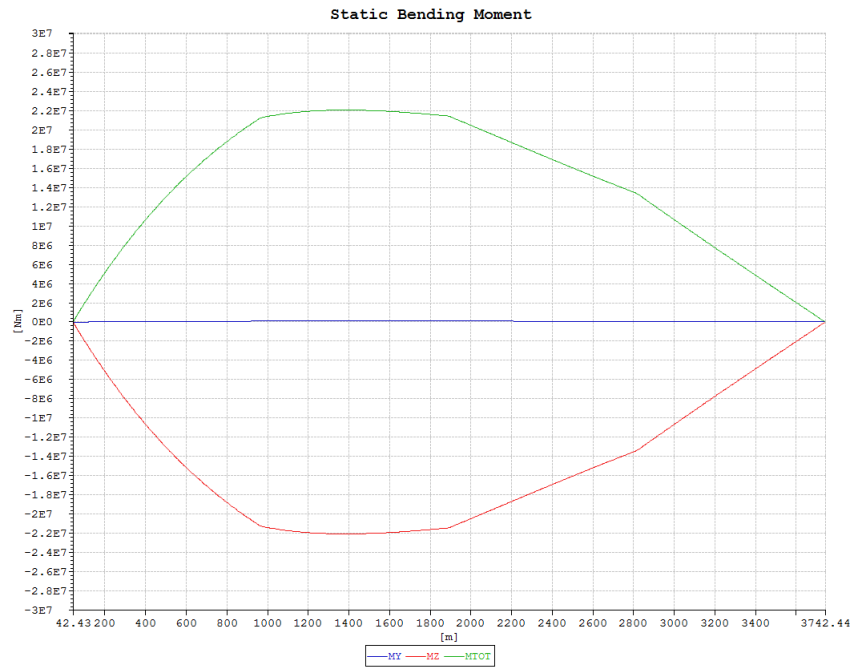
Figure C.16: Static torsional moment, X=0 **Figure C.17:** Static torsional moment, X=1000
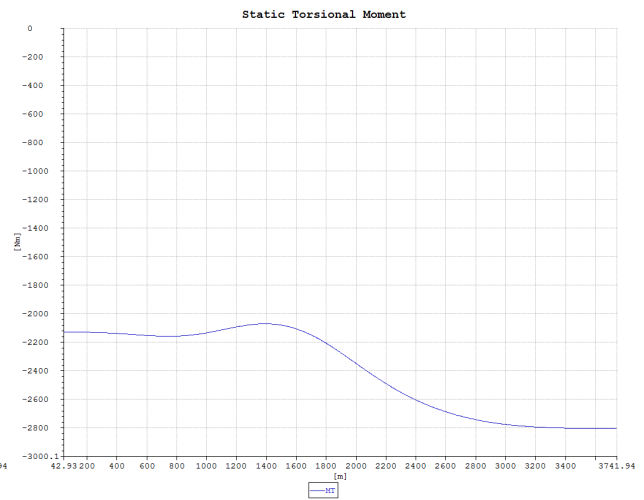
Figure C.18: Dynamic torsional moment for a straight bundle, X=0
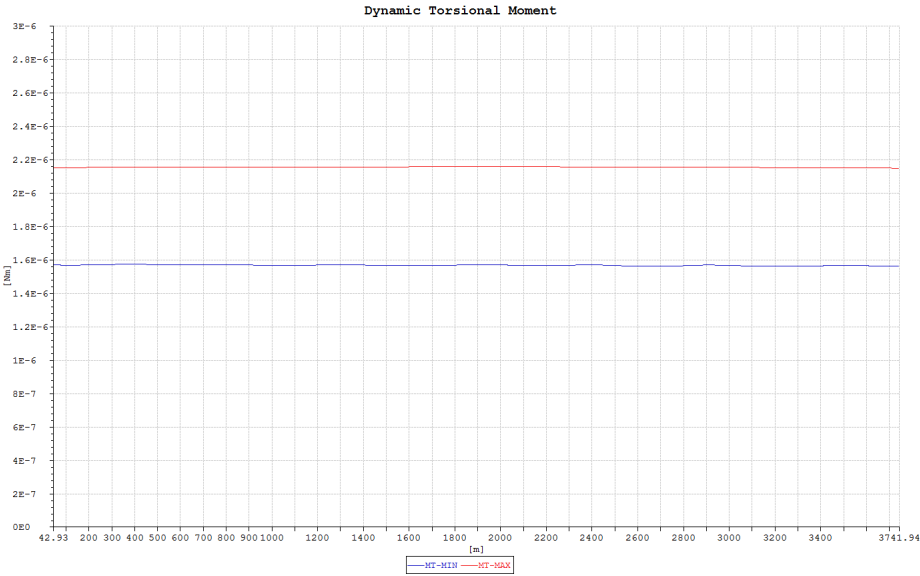
Figure C.19: Dynamic torsional moment for a curved bundle, X=1000
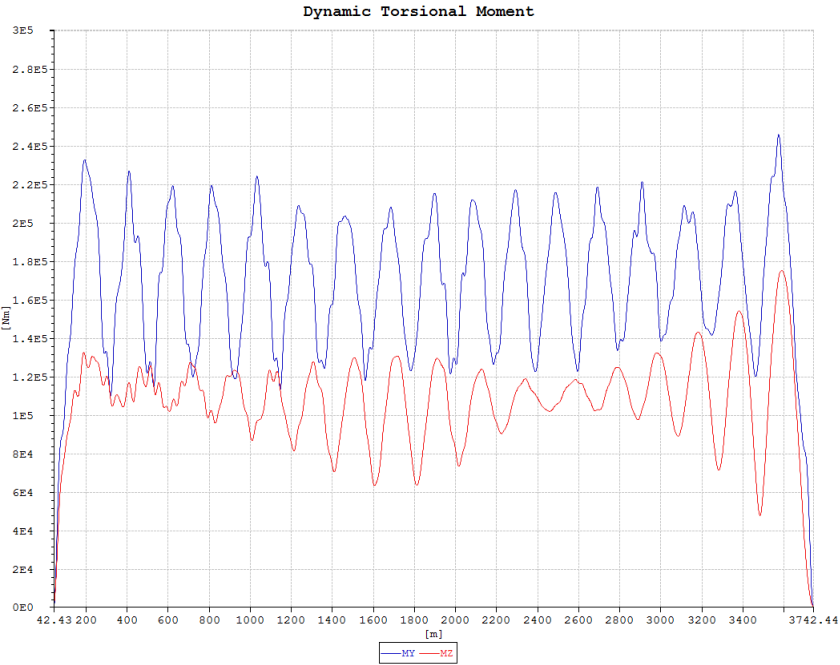
C.2   Installation

C.2.1   Scenario 1

The static displacements are shown in the figures below, followed by static and dynamic torsional moments and eigenmodes.
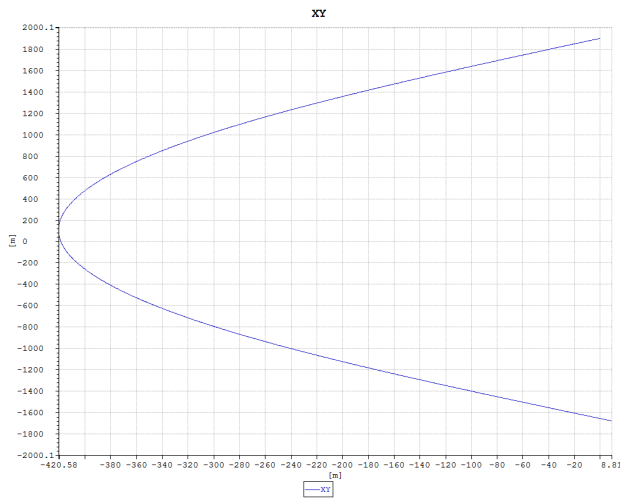
Figure C.20: Static displacement in XY-direction
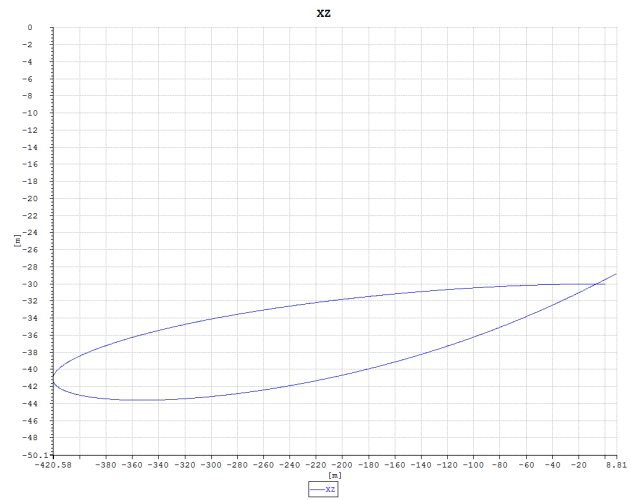
Figure C.21: Static displacement in XZ-direction
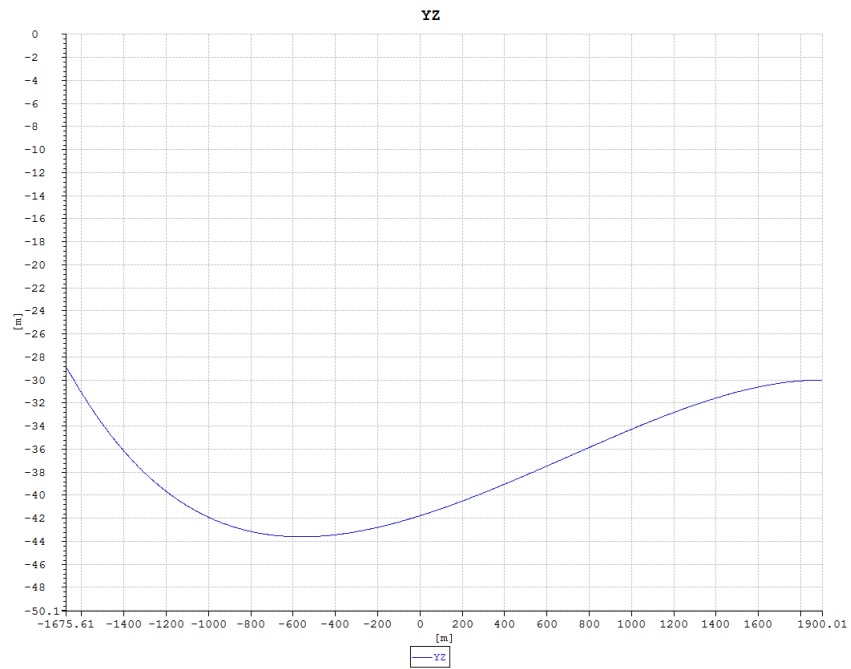
Figure C.22: Static displacement in YZ-direction
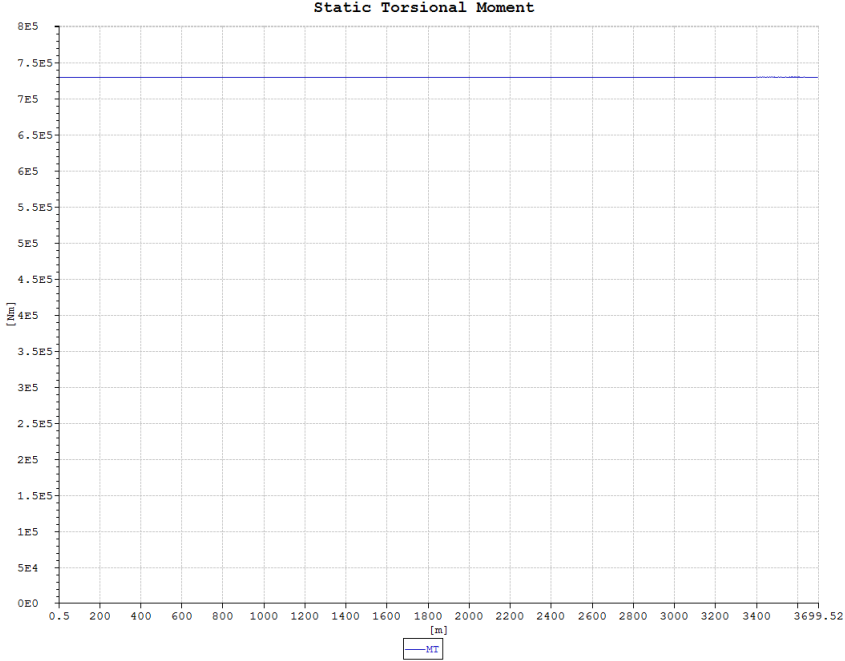
Figure C.23: Static Torsional Moment
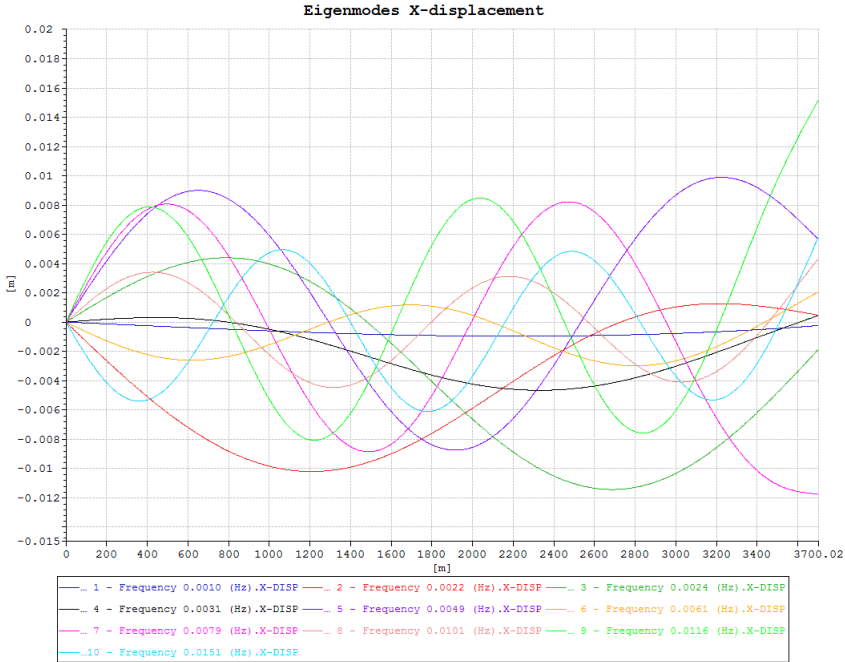
Figure C.24: Eigenvalues for displacement in X-direction for Scenario 1 of Installation
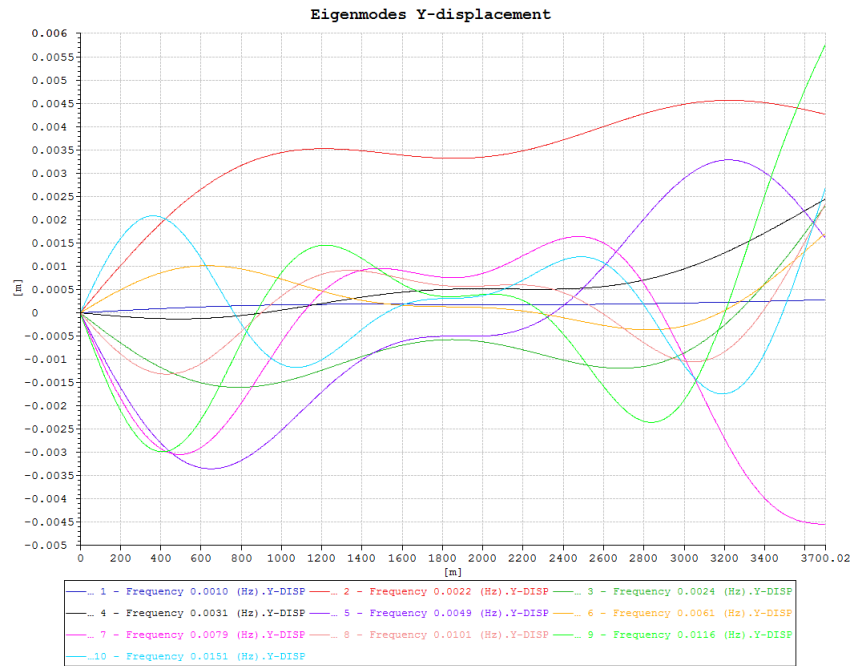
Figure C.25: Eigenvalues for displacement in Y-direction for Scenario 1 of Installation
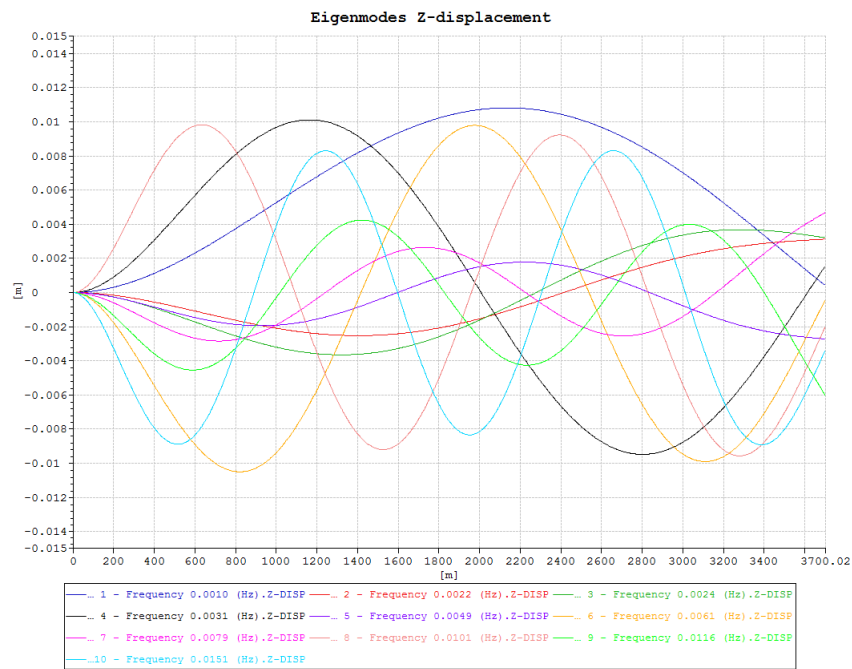
Figure C.26: Eigenvalues for displacement in Z-direction for Scenario 1 of Installation
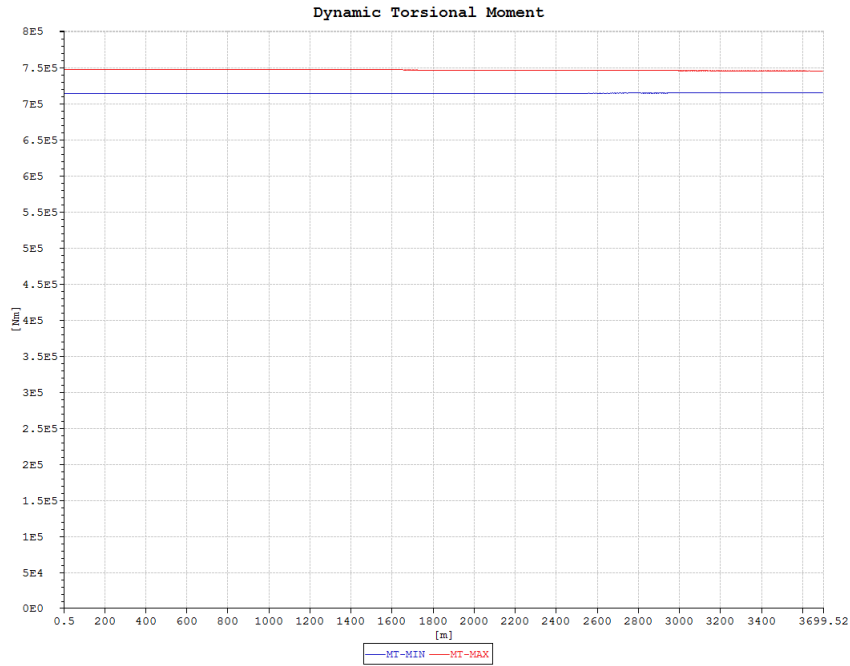
Figure C.27: Dynamic Torsional Moment

C.2.2   Scenario 2
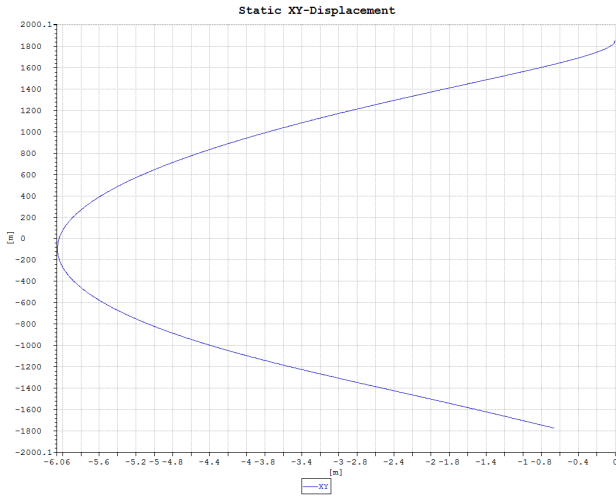
Figure C.28: Static displacement in XY-direction
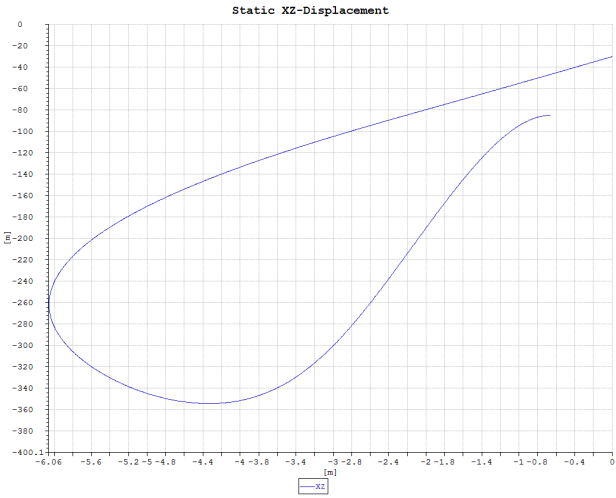
Figure C.29: Static displacement in XZ-direction
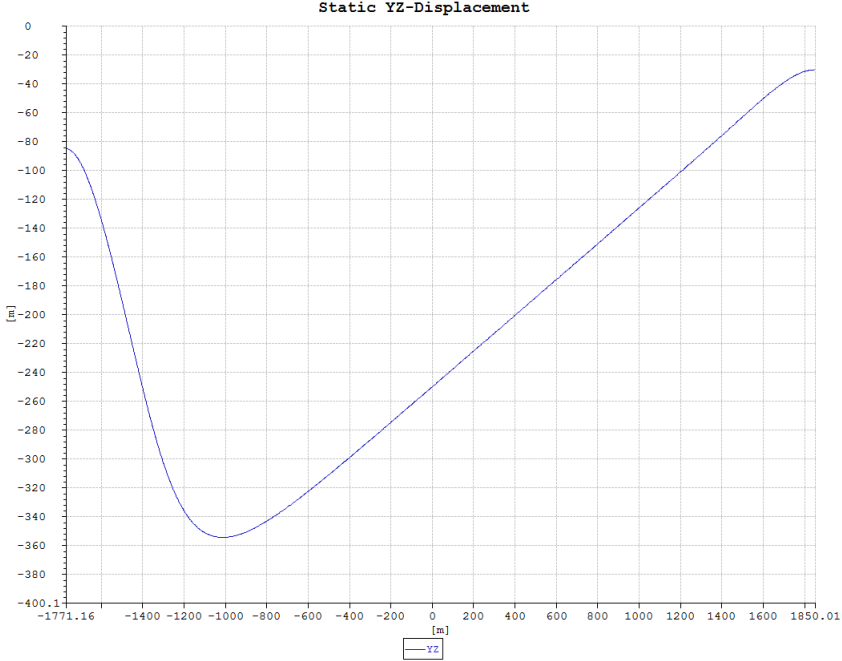
Figure C.30: Static displacement in YZ-direction
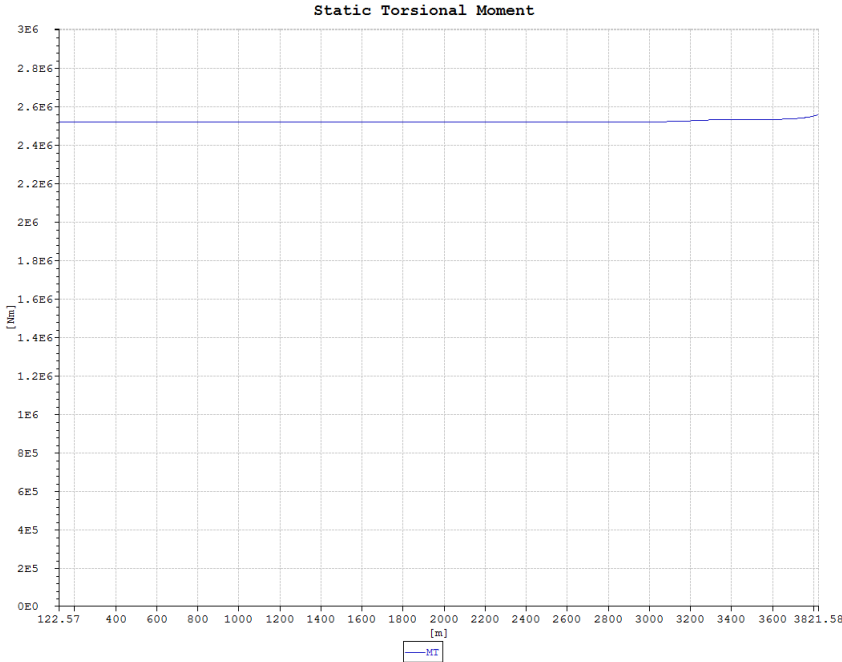
Figure C.31: Static torsional moment
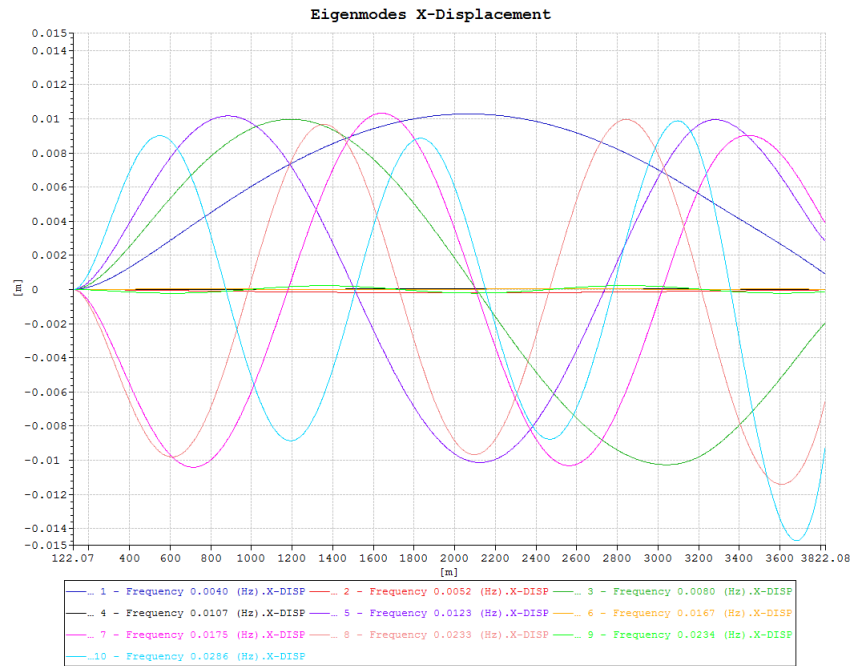
Figure C.32: Eigenvalues for displacement in X-direction for Scenario 2 of Installation
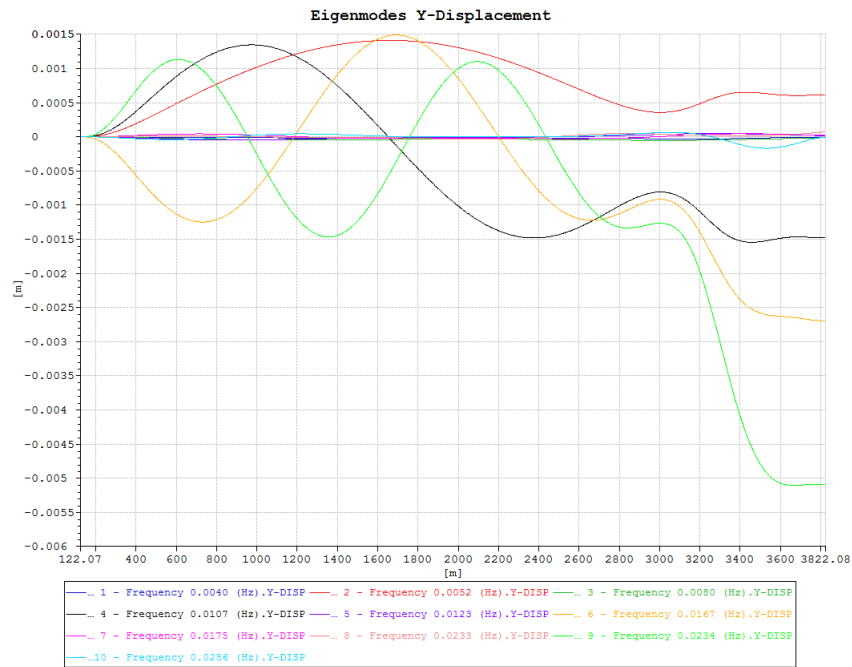
Figure C.33: Eigenvalues for displacement in Y-direction for Scenario 2 of Installation
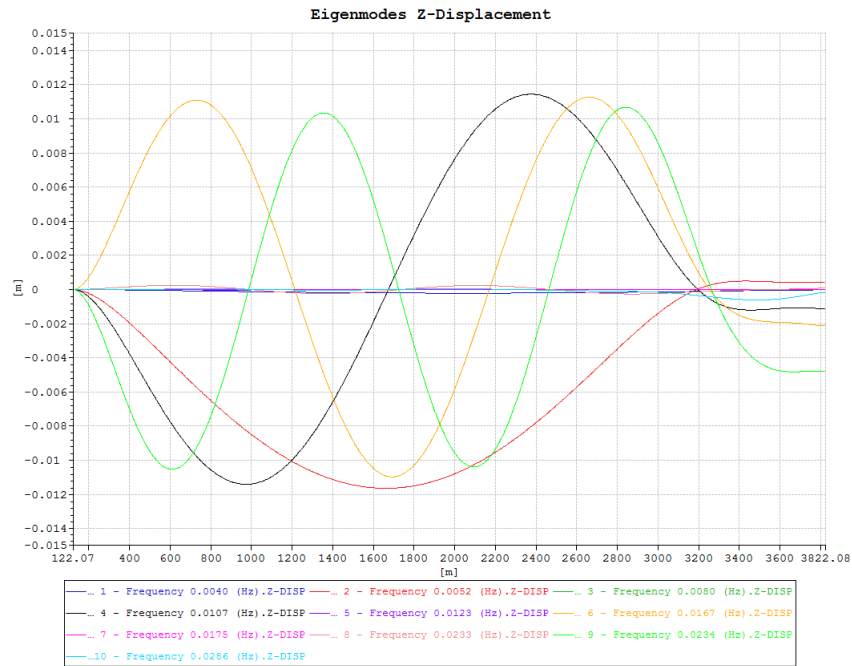
Figure C.34: Eigenvalues for displacement in Z-direction for Scenario 2 of Installation
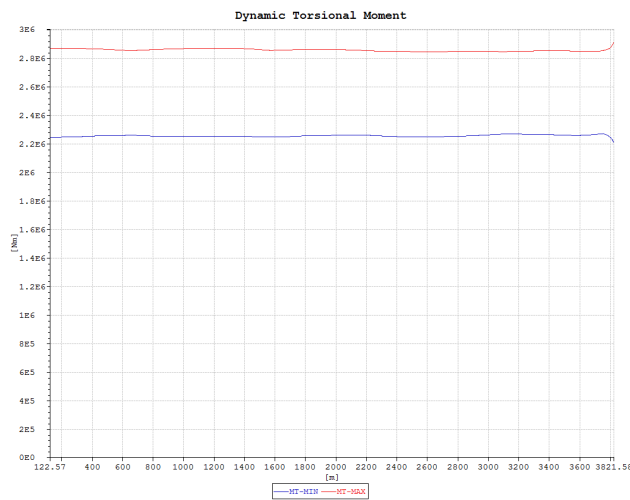
Figure C.35: Dynamic torsional moment
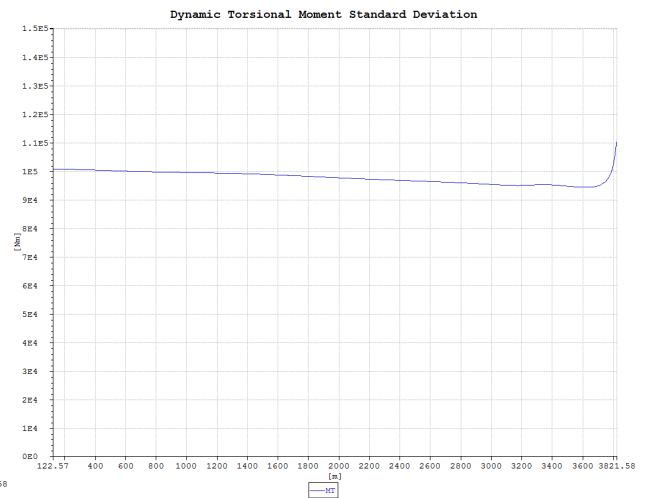
Figure C.36: Dynamic torsional moment, standard deviation

C.2.3 Scenario 3 - Part 1
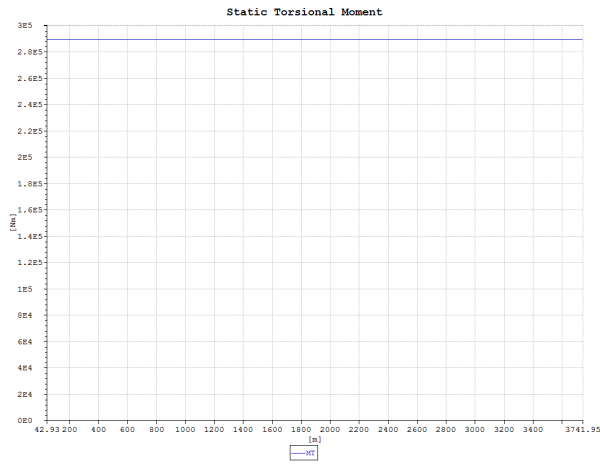
Figure C.37: Static torsional moment, Z=-30 m
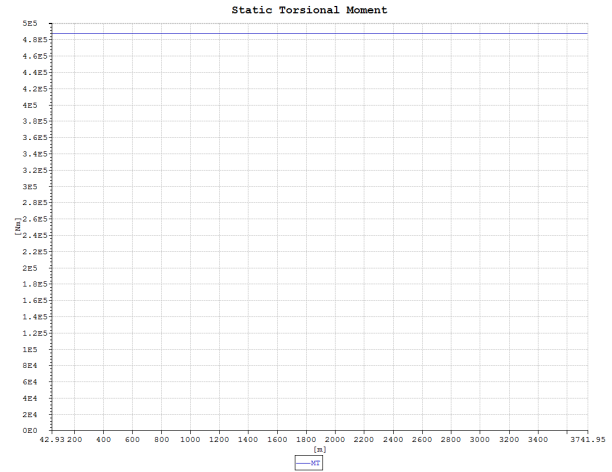
Figure C.38: Static torsional moment, Z=-200 m
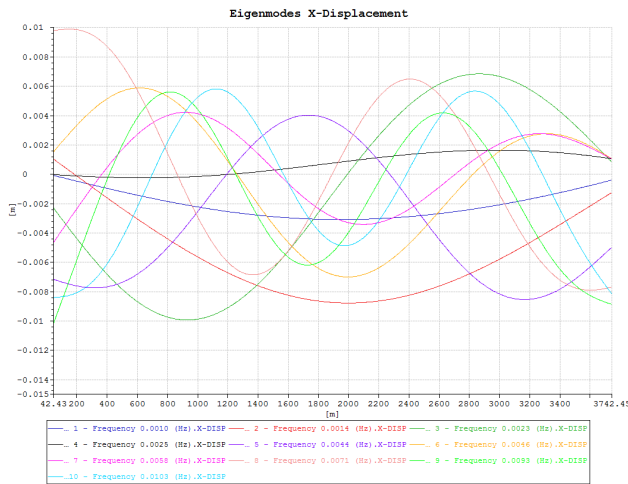
Figure C.39: Eigenmodes X-Displacement, Z=-30 m

Figure C.40: Eigenmodes X-Displacement, Z=-200 m

Figure C.41: Eigenmodes Y-Displacement, Z=-30 m

Figure C.42: Eigenmodes Y-Displacement, Z=-200 m
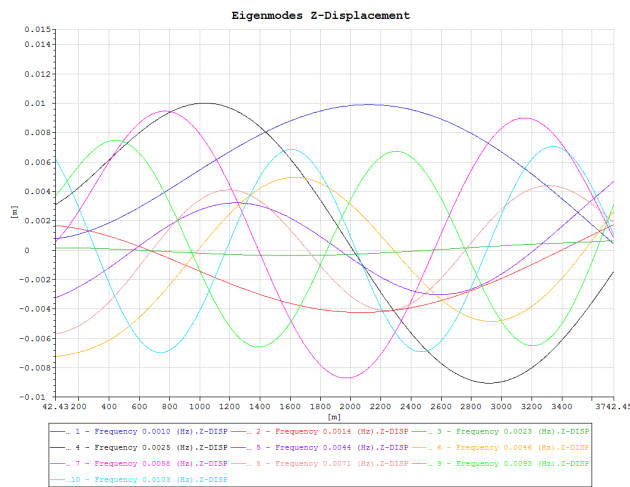
Figure C.43: Eigenmodes Z-Displacement, Z=-30 m
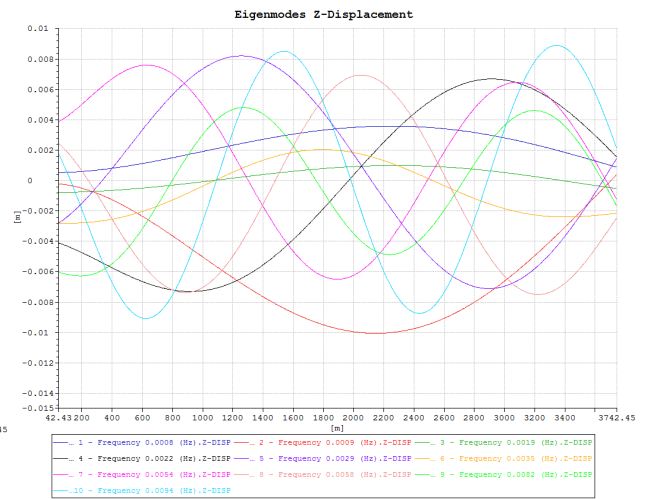
Figure C.44: Eigenmodes Z-Displacement, Z=-200 m
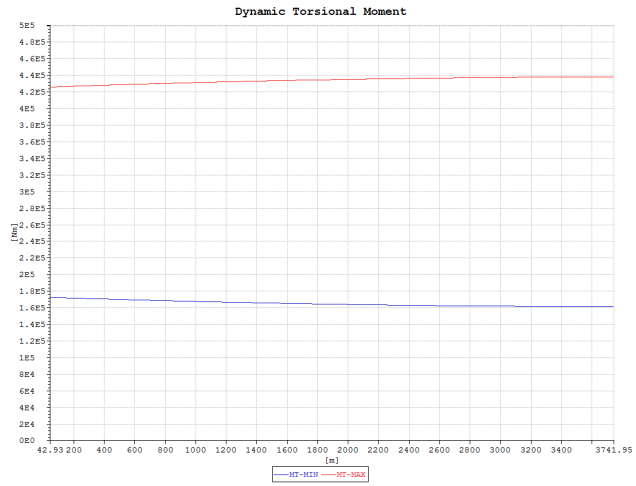
Figure C.45: Dynamic Torsion, Z=-30 m
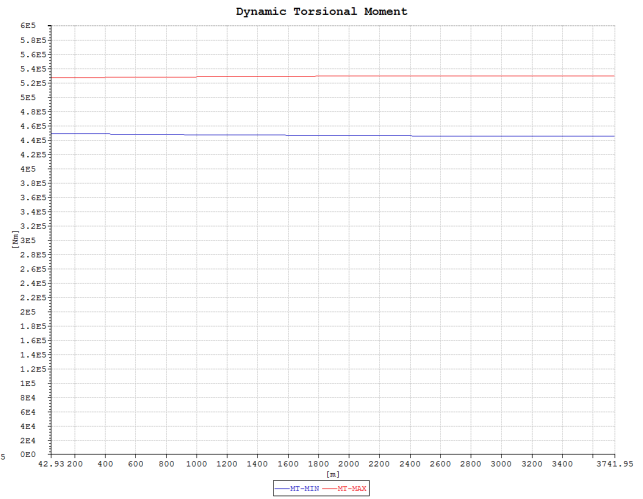
Figure C.46: Dynamic Torsion, Z=-200 m

C.2.4   Scenario 3 - Part 2
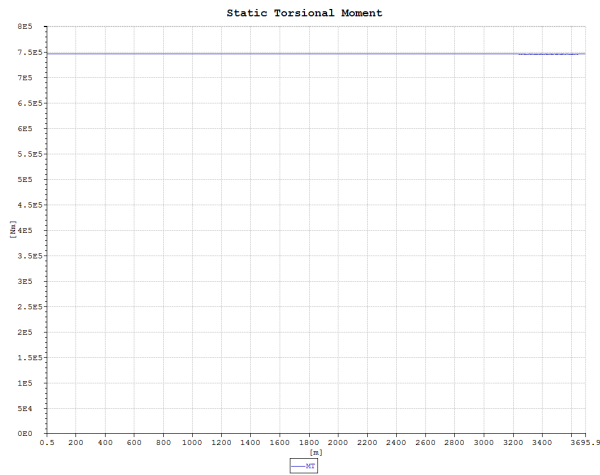
Figure C.47: Static torsional moment, Z=-30 m
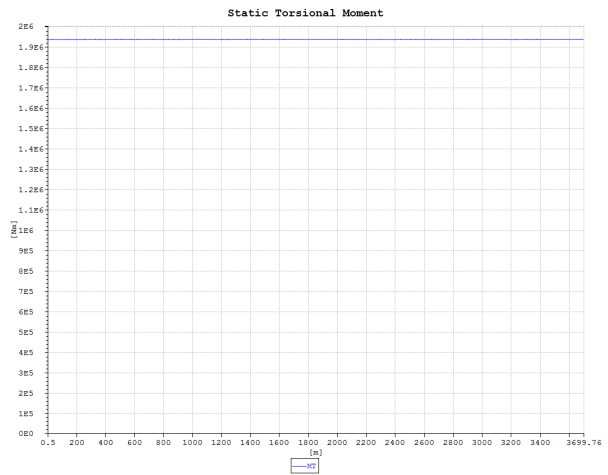
Figure C.48: Static torsional moment, Z=-200 m
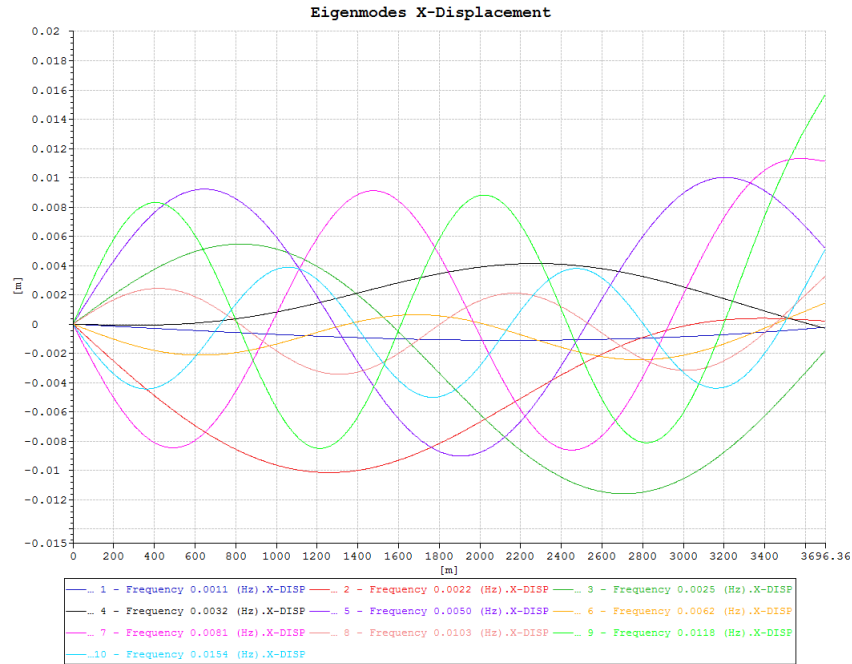
Figure C.49: Eigenvalue in X-direction for final configuration Scenario 3, Part 2
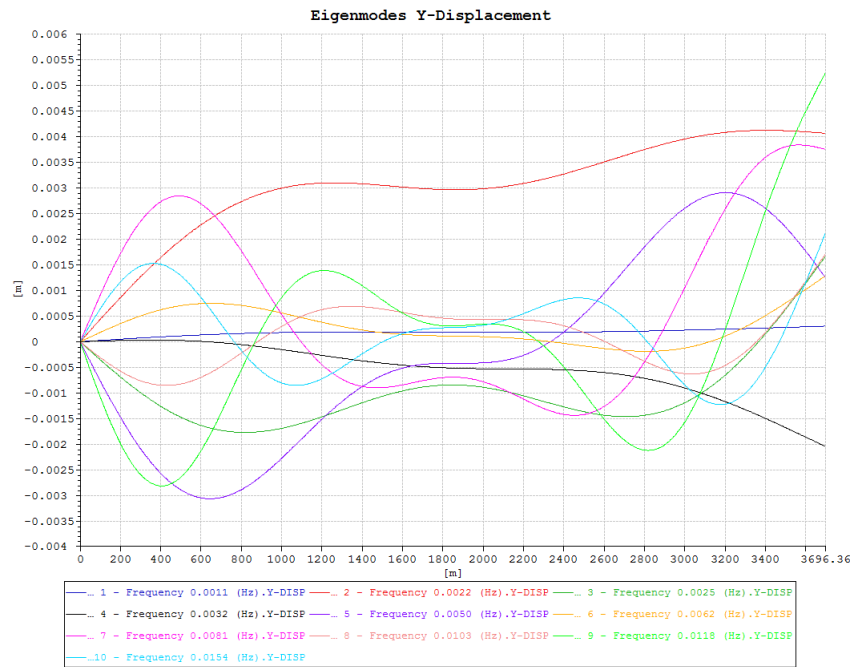
Figure C.50: Eigenvalue in Y-direction for final configuration Scenario 3, Part 2
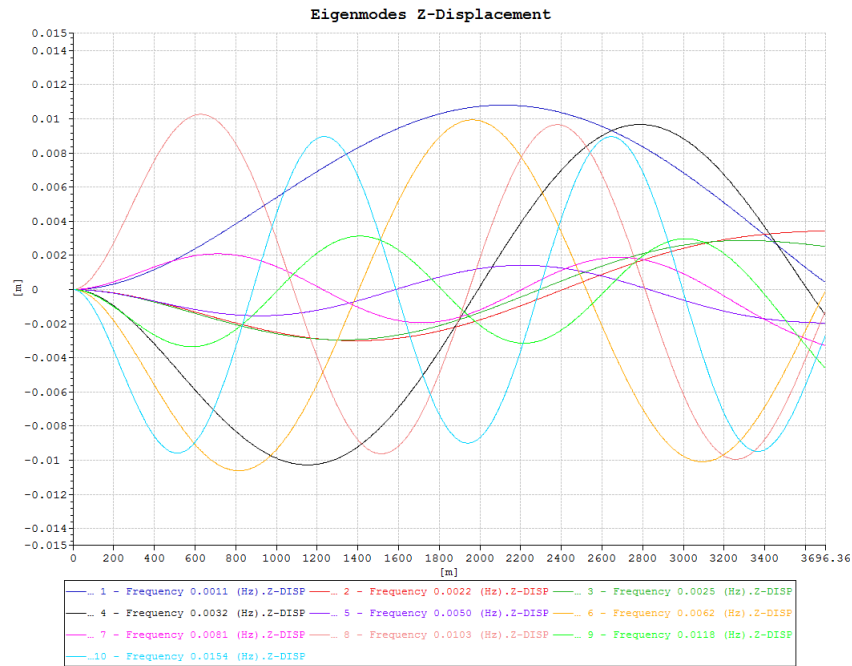
Figure C.51: Eigenvalue in Z-direction for final configuration Scenario 3, Part 2
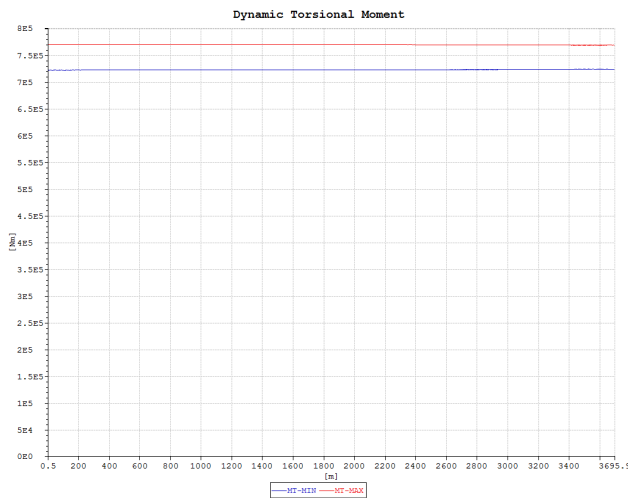
Figure C.52: Dynamic Torsion, Z=-30 m
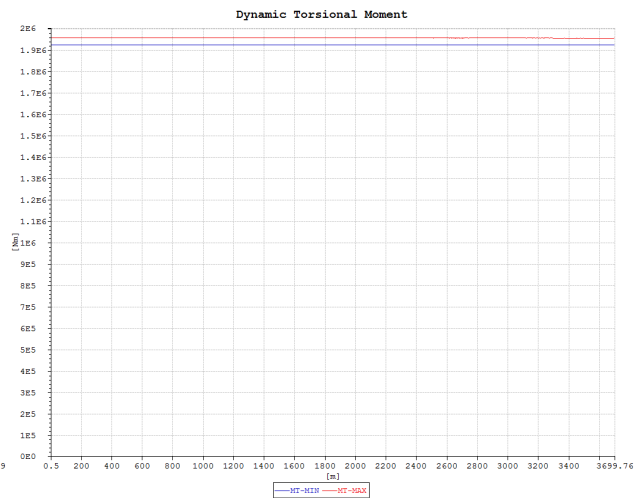
Figure C.53: Dynamic Torsion, Z=-200 m

C.3 Statistical Results

Some of the statistical results are shown in this section of the appendix. Although 10 analyses were run for both transportation and installation, only one analysis for each part will be shown in this appendix, in order to keep the amount of information on a reasonable level.

C.3.1 Transportation

The results for seed 29852 are shown below.

Figure C.54: Displacement for 30 min dynamic analysis of transportation
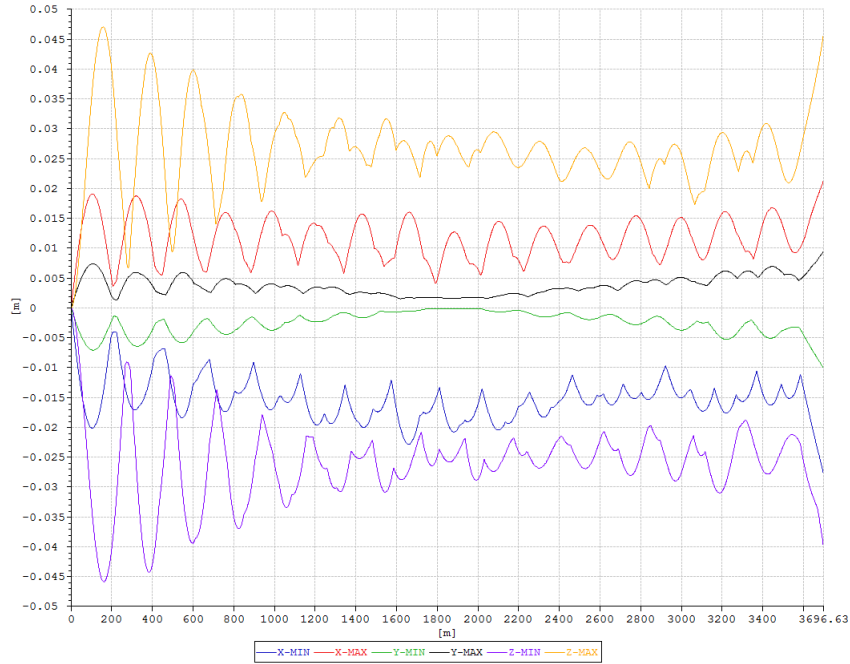
Figure C.55: Moment for 30 min dynamic analysis of transportation
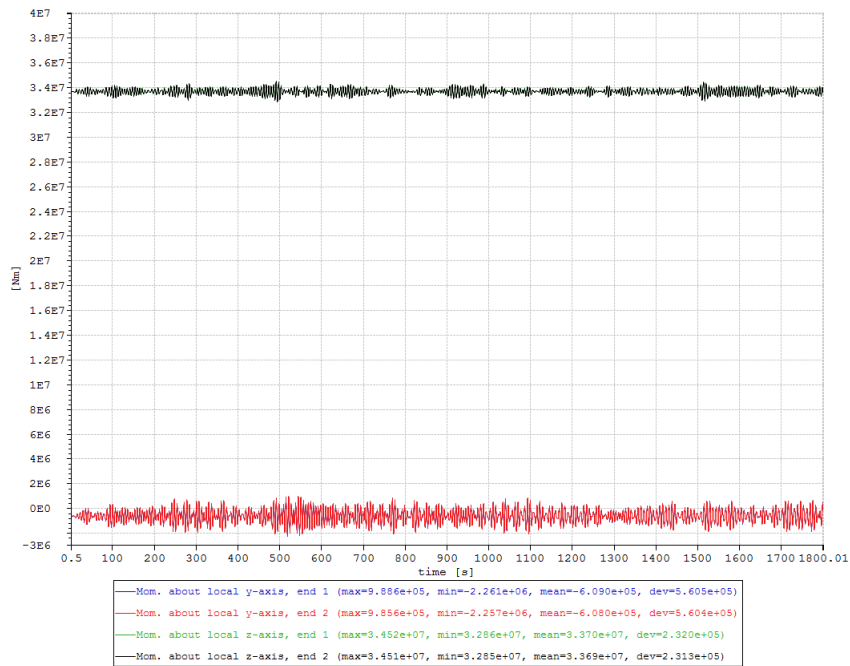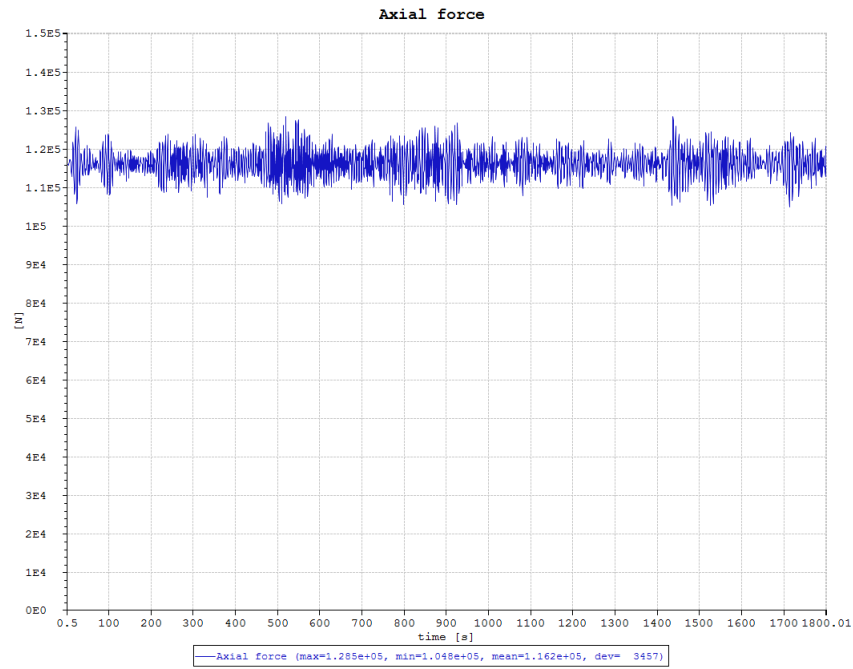
Figure C.56: Axial force for 30 min dynamic analysis of transportation

C.3.2 Installation

The results for seed 19852 are shown below.

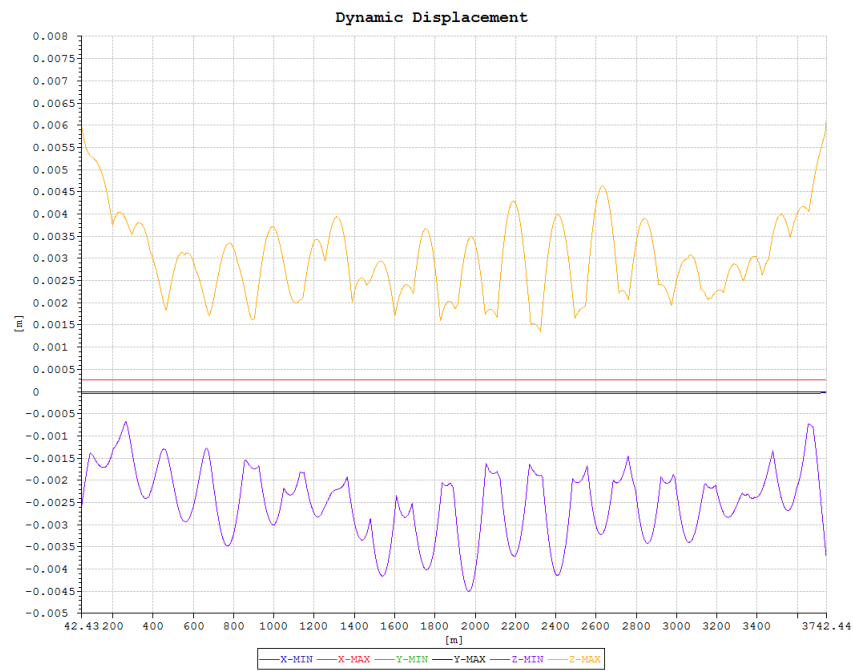**Figure C.57:** Displacement for 30 min dynamic analysis of installation

Figure C.58: Moment for 30 min dynamic analysis of installation
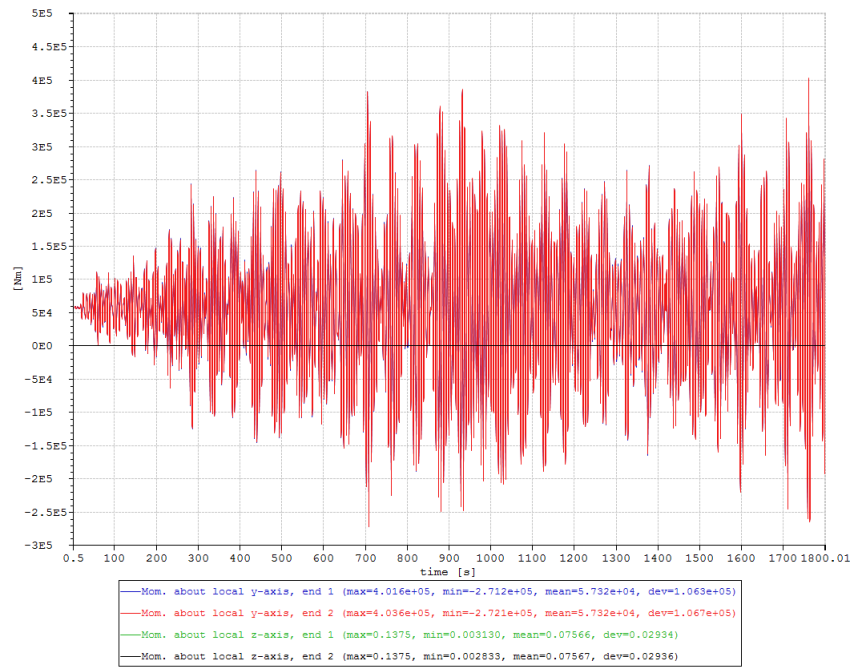

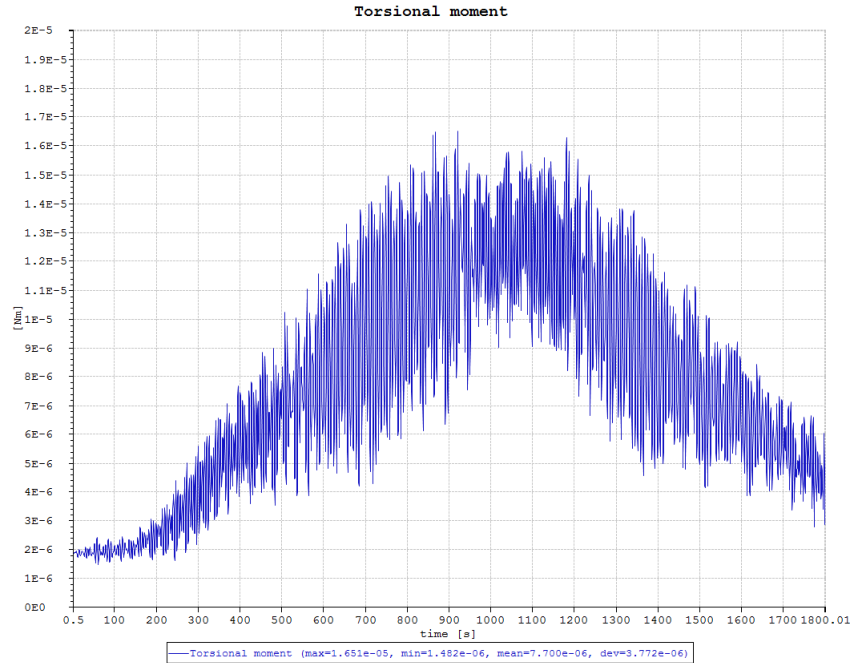**Figure C.59:** Torsional moment for 30 min dynamic analysis of installation

Figure C.60: Axial force for 30 min dynamic analysis of installation